Quantitative description of the metabolic capabilities of *Streptomyces clavuligerus* for clavulanic acid production: A combined constraint-based modeling approach and experimental testing

By

Howard Diego Ramirez Malule

A dissertation submitted in partial fulfillment of

the requirements for the degree of

DOCTOR IN CHEMICAL ENGINEERING

UNIVERSITY OF ANTIOQUIA
Faculty of Engineering
June 2016
Colombia

To the Faculty of Engineering of University of Antioquia:

The members of the Committee appointed to examine the dissertation of HOWARD DIEGO RAMIREZ MALULE find it satisfactory and recommend that it be accepted.

_____

Chair

_____

_

_____

_

_____

_

This Thesis is dedicated to:
To Diego Jose, Calixta Isabel, Diego Fernando, Rina and my family.

Dedicado a:
A Diego Jose, Calixta Isabel, Diego Fernando, Rina y mi familia.

ACKNOWLEDGEMENTS

I would like to express my deepest gratitude to my supervisor Professor Rigoberto Rios Estepa for giving me the opportunity to perform my doctoral project under his supervision. I appreciate his gigantic support and smart guidance, as well as, for trusting me during the whole doctoral research.

I'm also very thankful to Prof. Dr. Peter Neubauer for giving me the opportunity to carry out all my experimental work in his group, for his fruitful suggestions to the design of the experimental work and for his willingness to share his knowledge.

I'm especially thankful to Dr.-Ing. Stefan Junne for his invaluable support during the design, set up of the experimental work, and smart discussion of the results. Thanks a lot for the diverse and always useful conversations.

I owe to thank to Professor Silvia Ochoa for her notorious collaboration during my process formation as Doctor in Chemical Engineering.

Many thanks to all BVT members for great atmosphere during my two doctoral stays in the Neubauer's group, specially Sergej, Robert, Anna maria, Erick, Eva, Nico, Anika, Juan Antonio, Anja and Elvis.

Thank you very much to Brigitte, Erick and Thomas for the training and helps in HPLC quantification, and Irmgard for activation of the strain.

I also owe thank to Victor Lopez for productive discussion of Flux Balance Analysis and set up of simulations procedures.

I want to thank to Professors Wilson Cardona, Albeiro Restrepo, Julian Zapata, Carlos Lopez, Felipe Otalvaro and Alex Saez for huge support at different topics of my doctoral research.

I would like to express my deepest thankfulness to god and my family for their support in every phase of my life.

Finally, I want to thank to my girlfriend, Rina, for her love, encouragement and for joining me at this stage of my life.

Quantitative description of the metabolic capabilities of *Streptomyces clavuligerus* for clavulanic acid production: A combined constraint-based modeling approach and experimental testing

Abstract

By Howard Diego Ramirez Malule, Ph.D.

University of Antioquia

June 2016

Chair: Prof. Rigoberto Rios Estepa

Clavulanic acid (CA) is produced by *Streptomyces clavuligerus (Sc)* as a secondary metabolite; it exhibits pharmaceutical interest due to its potential to inhibit β-lactamase enzymes secreted by bacteria as a defense mechanism against β-lactam antibiotics. Because of its low antibacterial effectiveness, CA is co-formulated with a broad-spectrum of antibiotics, thus increasing production costs. CA is produced by fermentative processes; however, titers are commonly low. Besides bioprocessing strategies, further studies of *Sc* metabolism are required so as to improve the understanding of CA biosynthesis. Therefore, metabolic studies certainly provide tools for bioprocess development that would eventually contribute with a feasible solution to high-quality cheaper-drug availability.

In this dissertation, a successful combination of metabolic modeling approaches and experimental testing was used as a promising strategy for understanding the metabolic

capabilities of *Sc*. In the first chapter, a brief overview of *Sc* metabolism (special emphasis on the clavam pathway), and a discussion about flux balance analysis (FBA) and kinetics studies in *Sc*, is presented. Next, an HPCL-DAD method is presented; the method used a gradient elution approach, and was successfully validated for CA quantification in samples from fermentation broths of *Sc*.

In order to represent the complexity of *Sc* metabolic pathways, a genome scale metabolic model was developed and validated; this model was used for simulation purposes. Furthermore, in a fourth chapter, the accelerostat technique (A-stat) was implemented with the aim of evaluating metabolic patterns and the possible accumulation of TCA cycle intermediates during CA biosynthesis. A combined FBA and A-stat approach showed a strong association between the accumulation of succinate, oxaloacetate, malate and acetate with CA production. Besides, the simultaneous accumulation of CA and acetate led to propose a reaction mechanism - based on a computational simulation approach - for the acetylation of N-glycyl-clavaminic acid to form N-acetyl-glycyl-clavaminic acid.

Moreover, due to the well-known limitations of the traditional FBA approach, an alternative methodology, such as the ^{13}C Metabolic Flux Analysis (^{13}C-MFA) technique, was considered for potential upcoming studies. ^{13}C-MFA could provide accurate information of the isotopomer distribution in the metabolic network, thus leading to identify further bottlenecks in the pathway. Hence, a theoretical analysis of the ^{13}C-labeled compound distribution in the CA biosynthetic pathway in *Sc* is presented as a perspective of an isotope labeling study in *Sc*.

Finally, as far as I know, this is the first study to indicate the prevalence of accumulated TCA intermediates and its association with CA biosynthesis.

TABLE OF CONTENTS

Page

LIST OF TABLES

Page

LIST OF FIGURES

Page

Introduction

Clavulanic acid (CA) is produced by *Streptomyces clavuligerus* (*Sc*) (Brown et al., 1976); though it exhibits modest antibacterial activity, it is a potent inhibitor of β-lactamase enzymes secreted by bacteria, bringing about a broad pharmaceutical interest (Brown et al., 1976; Elander, 2003; Hamed et al., 2013; Ozcengiz and Demain, 2013). Since CA was discovered (Brown et al., 1976), an extensive series of studies have been carried out (Arulanantham et al., 2006; Iqbal et al., 2010; Ives and Bushell, 1997; Mellado et al., 2002; Valegård et al., 2013); however, low titers are still acquired during fermentation processes (Bushell et al., 2006; Roubos et al., 2002; Teodoro et al., 2010). Consequently, further studies are needed for a better understanding of the complexity of *Sc* metabolism.

In this dissertation, a successful combination of metabolic modeling approaches and experimental testing was used as a promising strategy for improving the understanding of the metabolic capabilities of *Sc*.

The principal aim of this thesis dealt with the development of a genome-scale metabolic model so as to represent the complexity of *Sc* metabolic pathways. Model validation did consider identification of dead-end metabolites, single-connected metabolites, zero-flux reactions and, robustness and phenotypic phase plane analysis. Concurrently, a set of chemostat and accelerostat (A-stat) cultivations was performed to generate experimental constraints under different environmental conditions. The constrained model was used to perform computer simulations that would help to explain experimental results related to diverse CA accumulation profiles, and its relationships with intermediate metabolite accumulation and/or depletion. In this endeavor, potential metabolic targets were identified for further genetic manipulation so as to attain a desired CA-overproducer strain.

This thesis represents a summary of six manuscripts, a so-called compilation thesis. The thesis was divided into two parts: the first part deals with the fundamentals of CA biosynthesis, a description of the HPLC quantification method, and a brief discussion about CA instability. In the second group, a methodological approach that involves math

modeling and experimental testing is presented. Each chapter is described in detail below.

Chapter 1 describes the importance of CA as a bio-compound of pharmaceutical interest. A brief overview of CA production by fermentation processes is also presented. This information is completed with a record of recent flux balance analysis (FBA) studies in *Sc*.

Chapter 2 contains an improved HPLC-DAD method for CA quantification in samples from fermentation broths of *Sc*. This method, which used a gradient elution approach, was successfully validated. The gradient elution configuration avoids overlapping of new peaks with the CA peak, a case commonly found in isocratic elution. Furthermore, the method was tested using different complex and chemically defined media, and, in each scenario, the CA peak was clearly resolved. The validation process also provided information about CA instability, both free and as clavulanate-imidazole complex.

With the aim of representing the complexity of *Sc* metabolic pathways, a genome scale metabolic model was developed and validated; this model was used for simulation purposes. In **chapter 3**, an *in silico* analysis using FBA and sensitivity analysis showed a trade-off between succinate, acetate and oxaloacetate secretion with CA production and biomass synthesis. Interestingly, for all the analyzed scenarios, a ratio lower than 2 between arginine synthesis, (from the urea cycle) to the net flux of glyceraldehyde-3-phosphate (from both, glycolysis and pentose phosphate pathway) was a necessary condition for CA biosynthesis. Moreover, a phenotypic phase plane (PhPP) analysis showed a positive effect of oxygen greater than that of glycerol on biomass synthesis and CA production.

The accelerostat technique (A-stat) was implemented with the aim of evaluating metabolic patterns and the possible accumulation of TCA cycle intermediates during CA biosynthesis. A combined FBA and A-stat approach showed a strong association between the accumulation of succinate, oxaloacetate, malate and acetate with CA

production. To the best of my knowledge, this is the first work showing such a strong association in CA biosynthesis. In addition, when the strain was exposed to glycerol and phosphate limitation, the activation of the glyoxylate pathway was also observed. Furthermore, the *in silico* identification of the carboxylation of phosphoenolpyruvate (PEP) by PEP carboxylase was consistent with oxaloacetate accumulation and the highest CA production. All the above-mentioned findings were presented in **Chapter 4**.

The simultaneous accumulation of CA and acetate led to propose a reaction mechanism - based on a computational simulation approach - for the acetylation of N-glycyl-clavaminic acid to form N-acetyl-glycyl-clavaminic acid, which is a postulated new step in the clavam pathway. This reaction mechanism consisted of two stages, for which the enzyme-driven reaction was considered to occur just for the second step; in contrast, the first step was thermodynamically feasible. Besides, a complete route for the inversion of the stereochemical configuration of (3S, 5S)-clavaminic acid into (3R, 5R)-clavulanic acid, including a novel alternative of double epimerization using proline racemase (considering the structural-chemical similarities between proline and bicyclic β-lactam ring), was also proposed. Interestingly, this alternative reaction does not require rupture of the bicyclic β-lactam ring. These experimental results were presented in **Chapter 5**.

In the final chapter, the ^{13}C Metabolic Flux Analysis (^{13}C-MFA) technique was considered for potential upcoming studies. ^{13}C-MFA could provide accurate information for the isotopomer distribution in the metabolic network, thus leading to identify further bottlenecks in the pathway. Hence, a theoretical analysis of the ^{13}C-labeled compound distribution in the CA biosynthetic pathway in *Sc* was presented, as a perspective for isotope labeling studies in *Sc*.

Publication List

Papers

Howard Ramirez-Malule, Stefan Junne, Peter Neubauer, Rigoberto Rios-Estepa. A combined FBA and A-stat approach identifies a strong association between the TCA cycle intermediate accumulation and clavulanic acid biosynthesis in *Streptomyces clavuligerus***.** Submitted to *Applied Microbiology and Biotechnology*.

H. Ramirez-Malule, S. Junne, C. López, J. Zapata, A. Sáez, P. Neubauer, R. Rios-Estepa., An improved HPLC-DAD method for clavulanic acid quantification in fermentation broths of *Streptomyces clavuligerus*, J. Pharm. Biomed. Anal. 120 (2016) 241–247. doi:10.1016/j.jpba.2015.12.035

Ramirez-Malule, H., Restrepo, A., Cardona, W., Junne, S., Neubauer, P., Rios-Estepa, R., 2016. Inversion of the stereochemical configuration (3S,5S)-clavaminic acid into (3R,5R)-clavulanic acid: A computationally-assisted approach based on experimental evidence. J. Theor. Biol. 395, 40–50. doi:10.1016/j.jtbi.2016.01.028

Howard Ramirez-Malule, Víctor A. Lopez-Agudelo, Silvia Ochoa, Rigoberto Rios. Sensitivity analysis of clavulanic acid biosynthesis in *Streptomyces clavuligerus*: TCA cycle intermediates as a case study. To be submitted.

Oral Presentations

Howard Ramirez-Malule, Albeiro Restrepo, Wilson Cardona, Stefan Junne, Peter Neubauer, Rigoberto Rios-Estepa. Studies on the clavam biosynthetic pathway: A controlling step for clavulanic acid production. 4th BioProScale Symposium "Bioprocess intensification through Process Analytical Technology (PAT) and Quality by Design (QbD)", April 6 to 8, 2016, Berlin, Germany.

Howard Ramirez-Malule, Víctor A. Lopez-Agudelo, Silvia Ochoa, Rigoberto Rios. Identifying the role of TCA cycle intermediates in the biosynthesis of clavulanic acid by *Streptomyces clavuligerus*: an *in silico* approach. III Congreso Colombiano de Biología Computacional y Bioinformática", Septiembre 16 al 18 2015, Medellín Colombia.

Howard Ramirez, Alex Sáez, Stefan Junne, Peter Neubauer, Rigoberto Rios, Theoretical analysis of 13C-glycerol metabolism in *Streptomyces clavuligerus*, XXVII Congreso Interamericano y Colombiano de Ingeniería Química, Octubre 6 a 8 2014, Cartagena Colombia.
ISBN: 978-958-58438-0-6

Posters

Howard Ramirez, Juan Arzate, Nicolas Cruz-Bournazou, Stefan Junne, Peter Neubauer, Rigoberto Rios, Effect of phosphate concentration and oxygen oscillation conditions on clavulanic acid production in *Streptomyces clavuligerus*. 3rd BioProScale Symposium Inhomogeneities in large-scale bioprocesses System biology and process dynamics, April 2 to 4, 2014, Berlin, Germany.

CHAPTER 1

1. Clavulanic acid: an overview of its biosynthesis and metabolic fluxes

Abstract

Clavulanic acid (CA) is an antibiotic with modest activity, produced by *Streptomyces clavuligerus (Sc)*; it is also a potent inhibitor of β-lactamase enzymes secreted by a wide spectrum of Gram-positive and Gram-negative bacteria. Although CA has been widely studied in submerged culture, low titers (about 1 g/L) are commonly obtained, thus increasing production costs. In this regard, fermentative studies along with metabolic flux analysis would certainly help to improve the understanding of the diverse metabolic phenotypes and CA biosynthesis. This review chapter briefly discusses CA biosynthesis - with special emphasis on the clavam pathway - as well as novel flux balance analysis (FBA) studies in *Sc*.

1.1. Introduction

Pharmaceuticals companies have played a remarkable role in drug development for effective treatments against multidrug-resistant bacteria, e.g., Augmentin® (Elander, 2003). However, an increment of resistant bacteria to antibiotics has been noticeable in the last two decades (Van Boeckel et al., 2014; World Health Organization, 2015).

Clavulanic acid (CA) is produced by *Streptomyces clavuligerus (Sc)* as a secondary metabolite (Fig. 1.1 and 1.2); it exhibits pharmaceutical interest due to its potential to inhibit β-lactamase enzymes secreted by bacteria as a defense mechanism against β-lactam antibiotics (Brown et al., 1976; Ozcengiz and Demain, 2013).

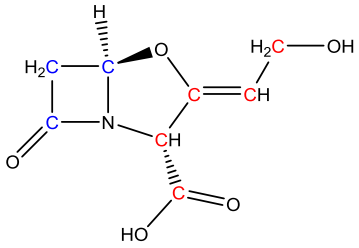

Fig. 1.1. Clavulanic acid structure. Color Code: red and blue C corresponds to carbon atoms from arginine and glyceraldehyde-3-phosphate, respectively.

Because of its low antibacterial effectiveness, CA is co-formulated with a broad-spectrum of antibiotics (Elander, 2003), thus increasing production costs for composed drug. Sales of approximately £140 million were reported for Augmentin® (a combination of amoxicillin and CA) in the first quarter of 2015 (GlaxoSmithKline, 2015). Further studies on *Sc* metabolism are required so as to improve the understanding of CA biosynthesis

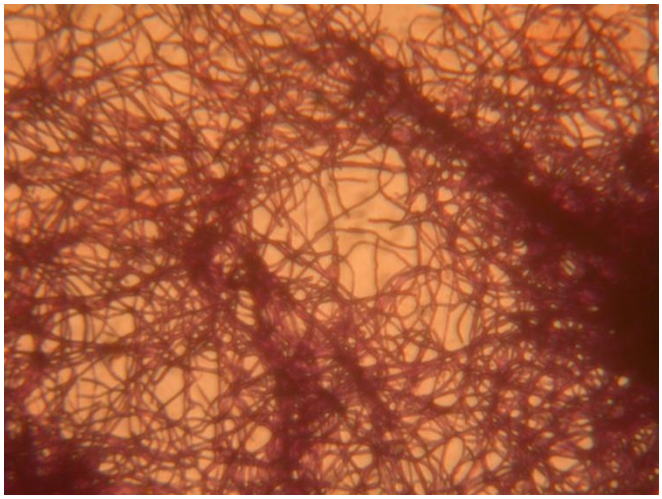

Fig. 1.2. Gram-stain image of *Streptomyces clavuligerus*.

1.2. Clavulanic acid production by fermentation processes

A wide variety of culture media have been used to produce CA in *Sc* (Bellão et al., 2013; Bushell et al., 2006; Roubos et al., 2002; Teodoro et al., 2010). CA is produced by conventional fermentative processes such as batch, fed-batch and continuous cultivation; however, titers are commonly low (Saudagar et al., 2008). Although the highest CA concentration has been attained in fed-batch cultures, continuous cultivations have favored the largest CA productivity (Neto et al., 2005). Thus, continuous culture may be seen as a feasible strategy for *Sc* cell suspension culture for CA production. In this regard, effects of carbon, nitrogen and phosphate sources on CA production have been evaluated (Kirk et al., 2000; Saudagar and Singhal, 2007). Phosphate deficiency has a remarkable positive role on glyceraldehyde-3-phosphate (GAP) availability and, indirectly, on CA synthesis, since it is strongly dependent on GAP (Bushell et al., 2006; Ives and Bushell, 1997). As it will be discussed in the next section, CA biosynthesis strongly depends on arginine and GAP availability. Arginine is restricted under nitrogen limitation, thus affecting CA production, whereas, under carbon limitation, there is a decrease in catabolic activity; hence, a limited production of TCA cycle derivative-compounds is obtained (Ives and Bushell, 1997). This may ultimately cause a reduction in anabolic precursors for CA biosynthesis.

1.3. Biosynthetic clavam pathway

During fermentation processes, glycerol, as carbon source, is preferably used for CA production in *Sc* (Bushell et al., 2006; Ives and Bushell, 1997; Teodoro et al., 2010). GAP, as the first CA precursor, is synthesized from glycerol through three consecutive oxidation reactions (Fig. 1.3). At this point, the metabolic flux splits into three branches: gluconeogenesis, glycolysis and clavam pathway. At the final reaction of glycolysis, pyruvate is synthesized, which produces acetyl-CoA; then, the carbon flux goes through the TCA cycle where two precursors of the urea cycle - alpha-ketoglutarate and oxaloacetate - are obtained. The second CA precursor, arginine, is produced in the urea cycle. In this metabolic scenario, GAP and arginine

are available and, the clavam route is ready for the production of CA and diverse clavam compounds. The clavam pathway is commonly divided into the so-called “early” and “later” steps. The first reaction in the clavam pathway is the condensation of GAP and arginine - a reaction catalyzed by *N*^{2}-(2-carboxy-ethyl) arginine synthase (CEAS1/CEAS2), in a thiamin diphosphate-dependent reaction - to form *L*-*N*^{2}-(2-carboxy-ethyl) arginine (Khaleeli et al., 1999). Then, β-lactam synthetase (BLS1/BLS2), an ATP/Mg^{2+}-dependent enzyme, triggers the formation of deoxyguanidinoproclavaminic acid from *L*-*N*^{2}-(2-carboxy-ethyl) arginine (Bachmann et al., 1998); the previous reaction allows the cellular systems to form the β-lactam ring. This is followed by the synthesis of guanidinoproclavaminic acid by clavaminate synthase (CAS1/CAS2) with alpha-ketoglutarate dependent dioxygenase, a hydroxylation of deoxyguanidinoproclavaminic acid (Zhang et al., 2002). Subsequently, proclavaminate amidino hydrolase (PAH1/PAH2) catalyzes the reaction for proclavaminic acid formation, where a guanidine group is released as by-product (Wu et al., 1995). The next two reactions are driven by (CAS1/CAS2), where dihydroclavaminic acid and clavaminic acid are obtained in an oxidative ring closure and a desaturation, respectively (Zhang et al., 2002); the latter two compounds contain a bicyclic ring (a β-lactam ring fused to the oxazolidine ring). This type of compounds, including CA, is called clavams. Up to now, the biosynthesis of CA and 5s clavam share all of these well-characterized reactions; this fraction of the clavam pathway is usually called the “early” steps (Ozcengiz and Demain, 2013). At this point, there is a bifurcation and two routes appear: one for CA production and another for 5s clavam biosynthesis; both pathways constitute the so-called “later” steps.

Only two reactions are known during the inversion of the stereochemical configuration of (3S, 5S)-clavaminic acid into (3R, 5R)-CA. Clavaminic acid is transformed into N-glycyl-clavaminic acid by the action of N-glycyl-clavaminic acid synthetase (GCAS), *orf17* (Arulanantham et al., 2006), whereas, (3R, 5R)-CA is produced from (3R, 5R)-clavaldehyde by the action of the enzyme NADPH-dependent clavulanic acid dehydrogenase (CAD) (Fulston et al., 2001). However,

the transition from N-glycyl-clavaminic acid to (3R, 5R)-clavaldehyde is not fully understood.

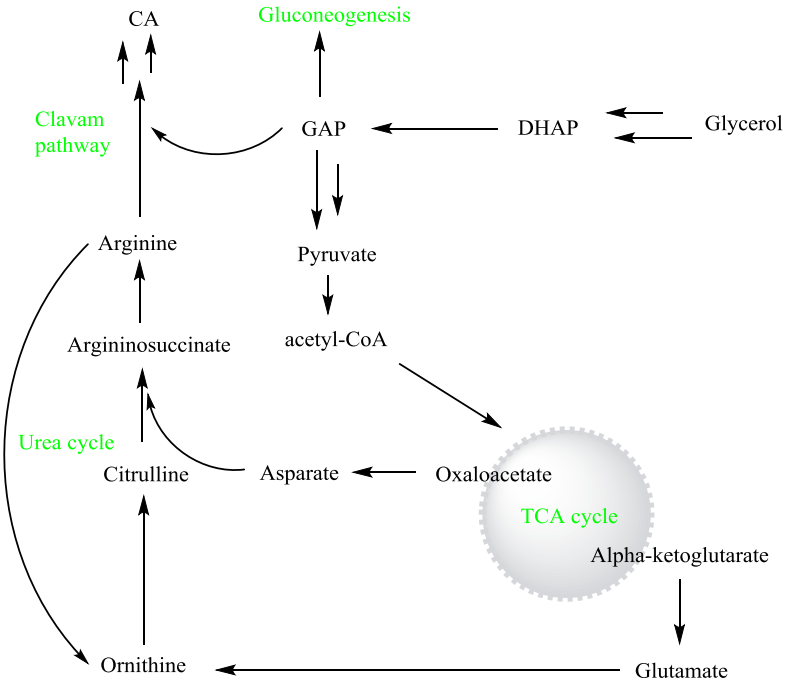

Fig. 1.3. Condensed biosynthetic pathway for CA in *Streptomyces clavuligerus*.

Likewise, within the 5s clavam pathway some steps appear unclear, thus increasing the uncertainty around the whole clavam route. The 5s clavam pathway produces compounds that are structurally similar to CA; however, these compounds - without β-lactamase inhibitory activity - have a 5S stereochemistry instead of 5R, which is a characteristic of CA (Zelyas et al., 2008). Due to the lack of knowledge of certain reactions and the complexity of *Sc* metabolic pathways, a holistic strategy such as flux balance analysis (FBA), rather than a reductionist one, should be used so as to deal with this complex biological endeavor.

1.4. Constraint-based flux balance analysis

FBA is a powerful methodology to study genome-scale metabolic networks and for predicting diverse metabolic phenotypes (Gianchandani et al., 2010). This complex metabolic system can be represented in the form of a stoichiometric matrix $\boldsymbol{S}$. $\boldsymbol{S}$ has a size of (m × n), where m is the number of metabolites, n is the number of reaction

rates (fluxes) and $\boldsymbol{v}$ is the flux vector. Hence, rows represent metabolites, columns symbolize fluxes and entries of the matrix indicate the stoichiometry of metabolites participating in the reactions. Due to the high connectivity of cellular metabolism, a metabolite can participate in more than one reaction i.e. there are more variables (reactions rates) than linear independent equations (metabolites). As a result, an underdetermined system is commonly obtained, which can be solved by optimization with a defined objective function. There exist a wide range of possibilities for objective functions, including maximization of biomass or ATP, maximization of biomass – or ATP - per flux unit, minimization of either nutrient uptake rate or redox potential, among others (Garcia Sanchez et al., 2012; Palsson, 2005; Schuetz et al., 2007).

At steady state conditions, the Linear Programming (LP) problem can be written in matrix form (Stephanopoulos et al., 1998):

$$\text{Max } \boldsymbol{f^T v}$$
$$\text{s.t. } \boldsymbol{S \cdot v} = 0$$
$$\boldsymbol{v_{lb} \leq v \leq v_{ub}}$$

Where $\boldsymbol{f}$ is the objective function vector, whereas, $\boldsymbol{v_{lb}}$ and $\boldsymbol{v_{ub}}$ are the lower and upper bounds for fluxes, respectively.

Further constraints can also be added to the LP problem, which drastically reduces the solution space. Fluxes experimentally measured and thermodynamic constrains are commonly applied to this type of biological problem (Palsson, 2005).

1.5. FBA studies in *Sc*

Various FBA studies have been reported in connection with CA production (Bushell et al., 2006; Kirk et al., 2000; Sánchez et al., 2015). Kirk et al. (2000) studied the metabolic flux distribution in a chemostat culture of *Sc* at a dilution rate of 0.05 h^{-1}. The authors evaluated the effect of carbon, nitrogen and phosphate limitations on CA production, and obtained specific productivities of 0, 0.32 and 3.65 [mg CA/(g*h)], respectively. FBA results indicated that under carbon limitation the anaplerotic metabolism - in this case the carboxylation of PEP to produce

oxaloacetate - was restricted, affecting the TCA cycle intermediates oxaloacetate and alphaketoglutarate, which are in connection with arginine synthesis. Besides, nitrogen limitation affected amino acid biosynthesis, including arginine. Interestingly, under phosphate limitation, CA production achieved its highest specific production rate (compared with both carbon and nitrogen limitation conditions); this metabolic scenario matched the one for the highest flux of the C3 and C5 precursors.

Recently, a small *Sc* metabolic model was reported by Sanchez et al. (2015). The model consisted of 100 reactions and 91 metabolites. The maximization of three metabolic objective functions was studied: specific growth rate, ATP yield and CA production. The effect of carbon, nitrogen, phosphate and oxygen limitation - using the maximization of ATP yield as the best objective function evaluated - on biomass synthesis and CA production rate were also estimated. *In silico* results showed phosphate limitation as the best scenario for CA production. The calculated metabolic flux distribution indicated that metabolic fluxes involved in the urea cycle were highly favored when CA achieved its highest specific production rate.

To date, a single genome-scale metabolic model of *Sc* has been reported (Medema et al., 2010). This model included 1492 reactions (1290/202 internal/exchange fluxes) and 1173 metabolites (971/202 internal/external metabolites); the model has been checked - *in silico* - for biomass synthesis under minimal growth medium conditions (glycerol, ammonia, phosphate and sulfate).

Besides the previous studies, kinetics models have been also reported (Malmberg and Hu, 1991; Roubos et al., 2002). Roubos et al (2002) studied the influence of glycerol, glutamate, phosphate and ammonium on CA degradation on *Sc* fed batch fermentations. High concentration of glycerol and ammonium triggered a major increment in the degradation rate constant. Furthermore, two kinetic models representing CA degradation were developed: a linear model and a fuzzy model. The model considered the CA degradation rate as a function of glycerol and ammonium. Although both models can predict CA-degradation rate to a certain degree, they were not able to represent the degradation of CA caused by metabolic

changes. However, the fuzzy model allowed the prediction of the effect of high glycerol concentration on the degradation rate constant.

Though diverse FBA studies have been published in *Sc* (Bushell et al., 2006; Ives and Bushell, 1997; Sánchez et al., 2015), isotopic labeling and metabolic control analysis studies have not been performed. In this sense, and due to the limitations of the traditional FBA approach (e.g. parallel pathways without any related flux measurements, certain metabolic cycles, bidirectional reactions steps and split pathway when cofactors are not balanced) , the ^{13}C metabolic flux analysis (^{13}C-MFA) technique, an extension of FBA, could be used. ^{13}C-MFA approach relies on ^{13}C-labeling patterns of intermediates and/or end product in ^{13}C substrates labeling experiments; the molecules, with ^{13}C incorporation, are connected with the initial labeled precursor (Krömer et al., 2009). The measurements of isotopic labeling distributions in metabolic products help to estimate metabolic fluxes with a higher accuracy compared to the FBA approach. Currently, methods such as gas chromatographic-mass spectrometry (GC-MS) and nuclear magnetic resonance (NMR) are available for quantification of diverse metabolites with labeled carbon in their structures (Christensen and Nielsen, 1999; Giraudeau et al., 2011; Yuan et al., 2010). Amino acid analysis in biological samples, using GC-MS is a methodology able to determine how many ^{13}C atoms have been incorporated into the amino acids' structures in microbial cultures, using ^{13}C labeling substrates. However, this methodology cannot determine the ^{13}C atoms positions. In contrast, the nuclear magnetic resonance (MNR) strategy is able to determine both how many ^{13}C atoms and its positions on molecules of amino acids. For this, the samples must be pure; it means that all amino acids must be separated from the culture samples. Methods of GC-MS and NMR could provide accurate information of the isotopomer distribution in the metabolic network. These results might be fed into the metabolic model, and the output results compared with the label distribution found experimentally (Wiechert, 2001). Such studies could help to detect bottlenecks in the network, and provide valuable insights about how to solve them. After a detailed ^{13}C-MFA study, a

metabolic control analysis could be performed in order to explore robustness of the network.

In addition, transcriptional analysis, at different stages of the cell cycle, in connection with FBA is an option to explore further correlations even previously undetected in *Sc* metabolism. Besides, the accumulation of metabolic intermediates during CA production has not been previously studied. Thus, studies of TCA cycle intermediates, which are highly demanded during antibiotic biosynthesis (Hodgson, 2000), are an attractive option for gaining knowledge and to unravel *Sc* metabolism.

The lack of knowledge of TCA cycle intermediates accumulation and their connection with CA biosynthesis, led to propose and complete this dissertation.

1.6. Conclusions

In this chapter, a general overview of CA biosynthesis was presented; at first view, enhancing CA productivity entails further studies. Therefore, a multidisciplinary research strategy that combines biology, engineering, biochemistry, molecular biology, analytical chemistry and computational biology would help to unravel the intrinsic metabolic complexity of CA biosynthesis, along with the diverse reaction-steps within the clavam pathway. Though successful bioprocess studies have been presented / performed / reported, novel strategies need to be implemented so as to pave the way to higher CA productivities. For example, single-use systems, process analytical technologies (PAT) and lab automation for a faster and autonomous bioprocess development can be used as strategies for improved productivities of CA in *Sc*. Nonetheless, during diverse FBA studies and well-defined metabolic phenotypes, some unrealistic results - based on *in silico* analysis - of various metabolic scenarios have been obtained; these difficulties are caused probably by a variety of incomplete or poorly-characterized metabolic routes, such as the clavam pathway. To overcome this problem, not only further studies for knowing in detail each reaction step are required, but also suitable analytical methods for the quantification of the metabolites involved.

Published as: **H. Ramirez-Malule**, S. Junne, C. López, J. Zapata, A. Sáez, P. Neubauer, R. Rios-Estepa., An improved HPLC-DAD method for clavulanic acid quantification in fermentation broths of *Streptomyces clavuligerus*, J. Pharm. Biomed. Anal. 120 (2016) 241–247. doi:10.1016/j.jpba.2015.12.035

CHAPTER 2

2. An improved HPLC-DAD method for clavulanic acid quantification in fermentation broths of *Streptomyces clavuligerus* using a C-18 reversed phase column

HIGHLIGHTS

- An improved HPLC-DAD method was developed for CA quantification produced in fermentation broths of *Streptomyces clavuligerus*.
- The HPLC-DAD method was tested using different complex and chemically defined media, and in each case the CA peak was clearly resolved without interferences and/or overlapping peaks.
- The gradient elution configuration avoids overlapping of new peaks, such as β-lactam compounds with *3S, 5S* stereochemistry, with the CA peak, a case commonly found in isocratic elution.
- Experimental evidence of the instability of the clavulanate-imidazole complex at room temperature was also found.

Abstract

Clavulanic acid (CA) is an important secondary metabolite commercially produced by cultivation of *Streptomyces clavuligerus* (*Sc*). It is a potent inhibitor of bacterial β-lactamases. In this work, a specific and improved high performance liquid chromatography (HPLC) method, using a C-18 reversed phase column, diode array detector and gradient elution for CA quantification in fermentation broths of *Sc*, was developed and successfully validated. Samples were imidazole-derivatized for the purpose of creating a stable chromophore (clavulanate-imidazole). The calibration curve was linear over a CA concentration range of 0.2 to 400 mg/L. The detection and

Acknowledgments: H.R.M. thanks the German Academic Exchange Service (DAAD) for financial support

quantification limits were 0.01 and 0.02 mg/L, respectively. The precision of the method was evaluated for CA spiked into production media and a recovery of 103.8%, on average, was obtained. The clavulanate-imidazole complex was not stable when the samples were not cooled during the analysis and the recovery was 39.3% on average. This assay, suitable for complex samples such as fermentation broths, was successfully tested for CA quantification in samples from *Sc* fermentation, both using a chemically defined and a complex medium.

2.1. Introduction

Clavulanic acid (CA) is produced by *Streptomyces clavuligerus (Sc)*. It is an important metabolite that inhibits β-lactamase enzyme activity, secreted by bacteria (Brown et al., 1976; Llarrull et al., 2010; Ozcengiz and Demain, 2013). CA is frequently used in antibacterial formulations, e.g. Augmentin®, for the treatment/eradication of infections caused by β-lactamase-producing bacteria (Elander, 2003; Ozcengiz and Demain, 2013).

Bioassay, spectrophotometry and high performance liquid chromatography (HPLC) methods have been developed and are widely used for CA quantification (Bird et al., 1982; Dubala et al., 2015; Foulstone and Reading, 1982; Liras and Martín, 2005; Meng et al., 2005; Yoon et al., 2004). Early HPLC for the detection of CA applied a precolumn derivatization step, as CA has a low detection wavelength in the UV region and is poorly retained on C-18 reverse phase columns (Foulstone and Reading, 1982; Martín and Méndez, 1988; Shah et al., 1990). Martín and Méndez (1988) and Shah et al. (1990) used 1,2,4-triazole as a derivatizing reagent in the determination of CA and, CA and sulbactam in human serum and urine, respectively, unlike Foulstone and Reading's work where imidazole was used. Later HPLC methods used different sample preparations with/without internal standard instead of a precolumn derivatization step (Foroutan et al., 2007; Hoizey et al., 2002; Tsou et al., 1997). Foroutan et al. (2007) and Hoizey et al. (2002) reported an HPLC-UV method for the simultaneous quantification of CA and amoxicillin in human plasma, with an internal standard and a direct deproteinization of plasma with

methanol, respectively. Recently, the development of methods with high selectivity and sensitivity, such as liquid chromatography-mass spectrometry (LC-MS), has been reported for CA determination in biological samples (Dubala et al., 2015, 2013; Meng et al., 2005; Reyns et al., 2006; Yoon et al., 2004). Dubala et al. (2015) reported an LC-MS method based on solid phase extraction for simultaneous determination of CA and cefixime in human plasma using chloramphenicol (99.9% pure) as internal standard. However, for all the above mentioned methods, that use either isocratic or gradient elution, CA is simultaneously quantified with another antibiotic, such as amoxicillin, in human samples after oral administration (Dubala et al., 2015; Hoizey et al., 2002; Meng et al., 2005; Yoon et al., 2004).

Aside from all these methods, also an early LC-MS and LC-MS/MS method was developed for detection of CA and clavam-2-carboxylate with an imidazole precolumn derivatization step (Eckers et al., 1996). In that work the derivatization step was crucial for the chromatographic separation of both β-lactam compounds. It also improved the detection of the ions in the MS, yet no biological samples were analyzed. Moreover, due to the absence of a specific method for CA quantification in fermentation processes, CA is often quantified by using the Foulstone and Reading's method in isocratic mode (Foulstone and Reading, 1982); however, the appearance of different β-lactam compounds during CA biosynthesis by *Sc,* creates overlapping peaks thus leading to poor efficiency of the method. The gradient elution proposed in this work substantially prevents peak interference thus improving the versatility and efficiency of the method, especially when complex matrix samples, such as fermentation broth, are used.

In this work, we report on a specific and improved gradient based HPLC method for CA quantification with an imidazole precolumn derivatization step, to be applied for the analysis of fermentation broths.

2.2. Experimental

2.2.1. Chemicals and preparation of standard solutions

All reagents and solvents were of analytical and HPLC grade. Potassium clavulanate vetranal, potassium dihydrogen phosphate, sodium dihydrogen phosphate monohydrate (all supplied by Sigma-Aldrich, Seelze, Germany), imidazole (Carl Roth, Karlsruhe, Germany) and methanol HPLC grade (VWR, Darmstadt, Germany) were used throughout this work. 18.2 MΩ ultra-pure water was supplied by a Barnstead EASY pure II water purification system.

A Stock solution of CA was freshly prepared at 800 mg/L in a NaH_2PO_4 buffer (pH 6.8; 100 mM). The solution was stored at 3-4 °C and remained stable for at least three weeks.

2.2.2. Derivatization procedure

CA is poorly retained in C-18 reverse phase columns and does not produce distinctive peaks. Therefore, a derivatization procedure was implemented with the aim of creating a stable chromophore (clavulanate-imidazole) (Fig. 2.1). Therefore 8.25 g of imidazole were dissolved in 24 mL of distilled water; HCl (25% v/v) was used to adjust the pH to 6.8 and distilled water was added up to 40 mL as the final volume. The derivatization was performed as described by Foulstone and Reading (Foulstone and Reading, 1982), wherein 100 µL of imidazole reagent were added to 300 µL of sample and maintained in mixing block at 800 rpm, 30 °C for 30 min.

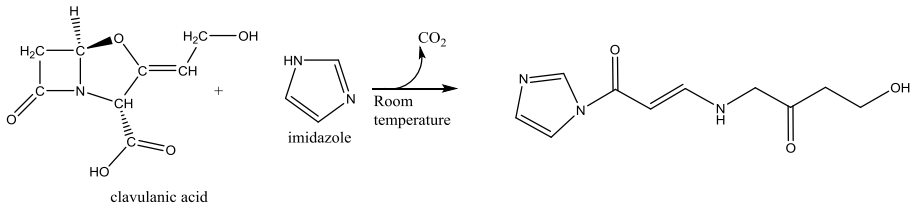

Fig. 2.1. Derivatization scheme for CA with imidazole.

2.2.3. Chromatographic instrumentation and conditions

Samples were derivatized with imidazole as described above and analyzed in an Agilent Technologies 1200 Series HPLC system (Agilent Technologies, Waldbronn, Germany) operated at 30°C with a Zorbax Eclipse XDB-C-18 chromatographic column ($5\ \mu m, 4.6 \times 150\ mm$, Agilent Technologies, Waldbronn, Germany), with a C-18 guard column (Phenomenex®, Aschaffenburg, Germany), with a flow rate of 1mL/min, injection volumes of 25 µL, an auto-sampler at 4 °C and a DAD detector. The mobile phase consisted of a KH_2PO_4 buffer (pH 3.2; 50 mM) as solvent A and HPLC grade methanol as solvent B. The gradient mode was set as follows: linear gradient from 6% to 7.6% solvent B for 8 min, linear gradient to 95% solvent B for 2 min, 95% solvent B for 2 min and linear gradient to 6% solvent B for 2 min. Solvent A was filtered through a 0.45 µL membrane filter. The clavulanate-imidazole complex was detected at a wavelength of 311 nm.

2.2.4. Biological sample preparation

Streptomyces clavuligerus DSM No 41826 was grown at 28 °C in a seed and production medium described by Roubos et al. (2002) (Roubos et al., 2002). The seed medium had the following composition (in g/L): glycerol 15, soy peptone 15, sodium chloride 3, calcium carbonate 1 and an initial pH 6.8. Antifoam 204 was added at a concentration of 1:1000 v/v.

The production medium was slightly modified to have (in g/L): glycerol 9.3, K_2HPO_4 0.8, $(NH_4)_2SO_4$ 1.26, monosodium glutamate 9.8, $FeSO_4 \times 7H_2O$ 0.18, $MgSO_4 \times 7H_2O$ 0.72, MOPS 10.5 and trace element solution 1.44 [mL]. The trace element solution remained (in g/L): H_2SO_4 (96%) 20.4, citrate $\times 1H_2O$ 50, $ZnSO_4 \times 7H_2O$ 16.75, $CuSO_4 \times 5H_2O$ 2.5, $MnCl_2 \times 4H_2O$ 1.5, H_3BO_3 2 and $Na_2MoO_4 \times 2H_2O$ 2. Antifoam 204 was added into the production medium (1:1000 v/v). During fermentation, aliquots (2 mL) were withdrawn at an interval of approx. 12 h. Then, samples were centrifuged at 15,000 rpm and 4 °C for 10 min; supernatants were used for CA quantification either immediately or stored at -20 °C until use.

For the purpose of validating the versatility of the method reported in this work, two additional culture media were evaluated. The first one had the following composition (in g/L): glycerol 15, monosodium glutamate 12, K_2HPO_4 0.8, $MgSO_4 \times 7H_2O$ 0.72 and salt solution 1 [mL]. The composition of salt solution was (in g/L): $MnCl_2 \times 4H_2O$ 0.001, $FeSO_4 \times 7H_2O$ 0.001, $ZnSO_4 \times 7H_2O$ 0.001. The second medium tested was the one described by Rosa et al. (2005) with the following composition (in g/L): glycerol 15, bacto peptone 10, malt extract 10, yeast extract 1, K_2HPO_4 2.5, $MnCl_2 \times 4H_2O$ 0.001, $FeSO_4 \times 7H_2O$ 0.001, $ZnSO_4 \times 7H_2O$ 0.001 and MOPS buffer 21 (100 mM). All culture media were fixed at pH 6.8.

2.2.5. Method validation

The HPLC-DAD method was validated for linearity, limit of detection (LOD), limit of quantification (LOQ), precision and recovery, following the International Conference on Harmonization (ICH) guidelines (ICH, 2005). For linearity validation, six CA concentrations (0.2, 2, 20, 100, 200 and 400 mg/L), were tested and a calibration curve was prepared by plotting peak area versus concentration. The LOD and LOQ were determined using the signal-to-noise (S/N) approach. For LOD the signal-to-noise ratio was 3 (S/N=3:1) while for LOQ a signal-to-noise ratio of 10 was used (S/N=10:1).

The precision of the method was determined by examining the intra-day and inter-day variation. For this, six replicas of CA spiked into production medium (see biological sample preparation) at three concentration levels (400, 200 and 0.2 mg/L) were analyzed, in a single day and on three consecutive days. The recovery of the method was examined by comparison of the areas below the curves of a known amount of CA, spiked to the production medium and its equivalent areas in the standard, determined at three concentration levels (400, 200 and 0.2 mg/L of CA).

2.3. Results and discussion

2.3.1. Chromatography

Representative chromatograms for CA were found at a retention time of 4.65 min for the standard solution (Fig. 2.2). A CA peak was clearly resolved and no interfering peaks were observed in neither a chemically defined medium nor a complex medium (Fig. 2.3). Complex media and chemically defined media are used in microbial cultures for the production of larger CA titers; yet, after certain fermentation time has elapsed, CA is either degraded and/or converted into another unknown compound (Deckwer and Mayer, 1996; Roubos et al., 2002). Also, in our case, possible additional β-lactam compounds are produced presenting *3S, 5S* stereochemistry (Fig. 2.4).

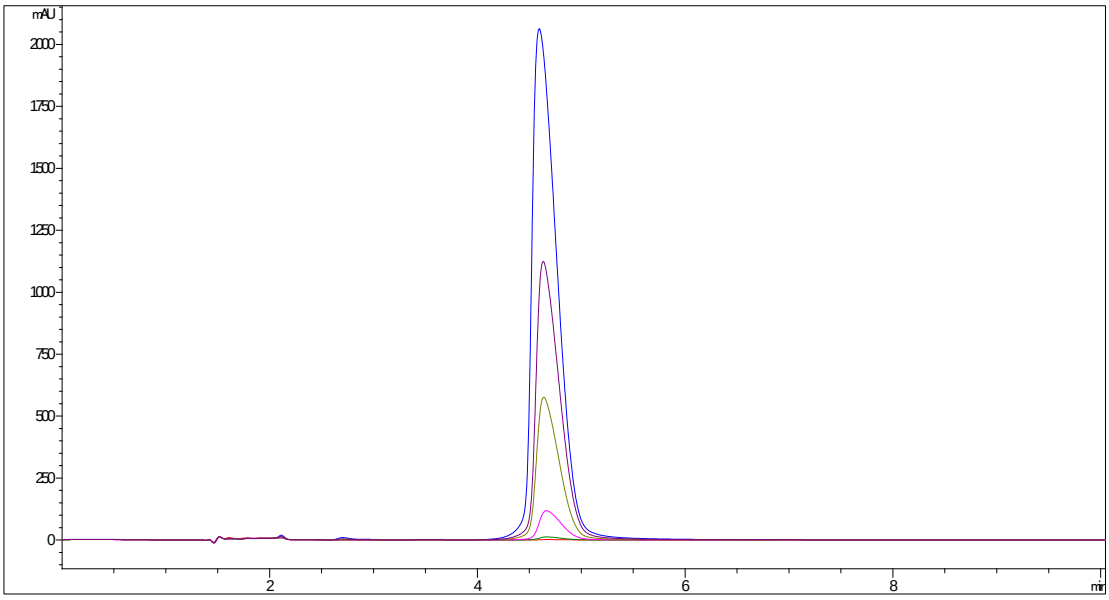

Fig. 2.2. Representative chromatograms of the clavulanate-imidazole complex at 6 different CA concentrations (0.2, 2, 20, 100, 200 and 400 mg/L).

In this work, a CA peak was observed at a retention time of 4.95 min in samples from fermentation broths of *Sc* (Fig. 2.5). Besides, two additional close peaks were found, presumably also β-lactam compounds. These peaks did not overlap with the CA peak, probably due to peak capacity which is higher in gradient than in the isocratic mode (Schellinger and Carr, 2006). As a result, a good

separation of all peaks present in complex samples was obtained compared to the prior isocratic elution method where the peaks interfered with each other. The gradient elution configuration proposed in this paper avoids such an undesirable circumstance, providing versatility to the method. This is especially appropriate for samples coming from complex matrices such as fermentation broths (Fig. 2.5).

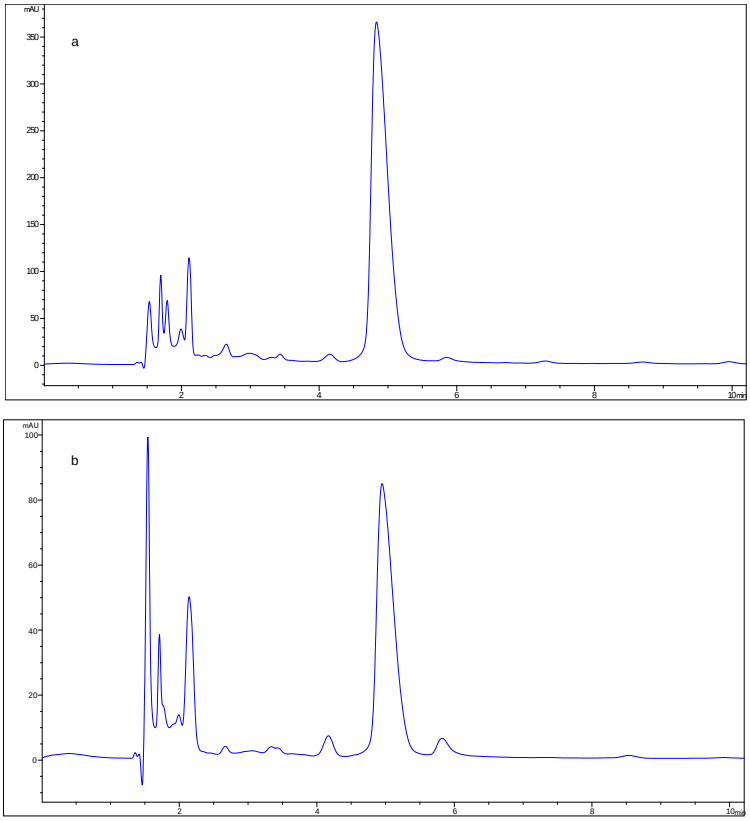

Fig. 2.3. Representative chromatograms of the clavulanate-imidazole complex taken from fermentation samples of *Sc;* a) using a complex medium; b) using a chemically defined medium. Note: The complex medium used was the seed medium described by Rosa et al. (2005).

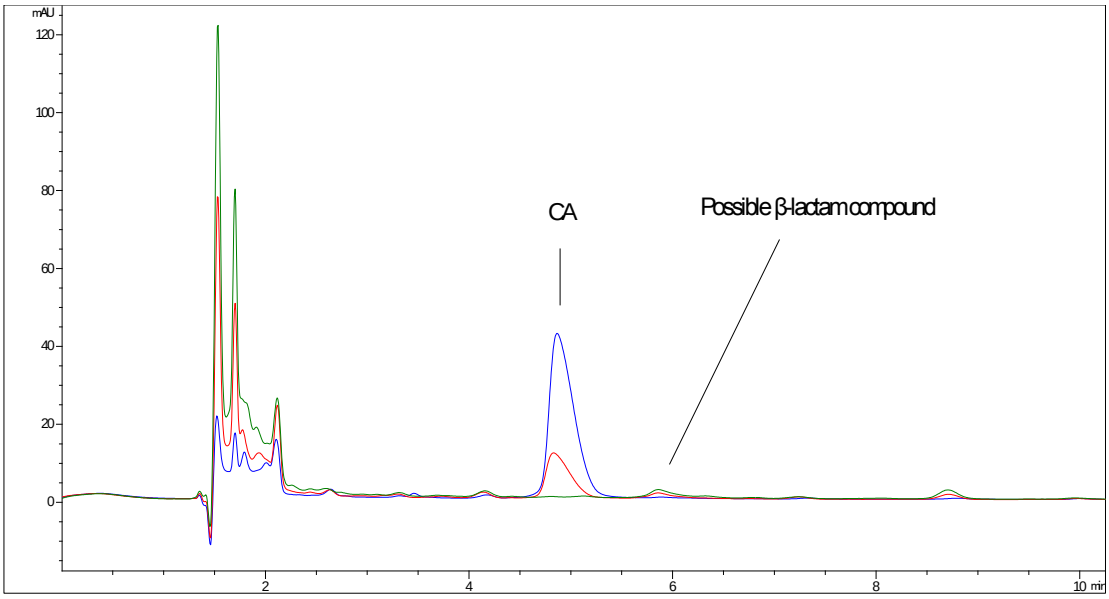

Fig. 2.4. Representative chromatograms of fermentation samples where CA was degraded and/or converted into another unknown compound. The production medium had the following composition (in g/L): glycerol 15, monosodium glutamate 12, K_2HPO_4 0.8, $MgSO_4 \times 7H_2O$ 0.72, salt solution 1 [mL]: $MnCl_2 \times 4H_2O$ 0.001, $FeSO_4 \times 7H_2O$ 0.001, $ZnSO_4 \times 7H_2O$ 0.001. Note: The sequence of samples with respect to fermentation time is: blue, red and green at 0, 29 and 53 h of fermentation time, respectively. Here, CA was produced in a complex medium; then, this broth was used as inoculum in the above-mentioned medium. At this stage CA showed a clear degradation.

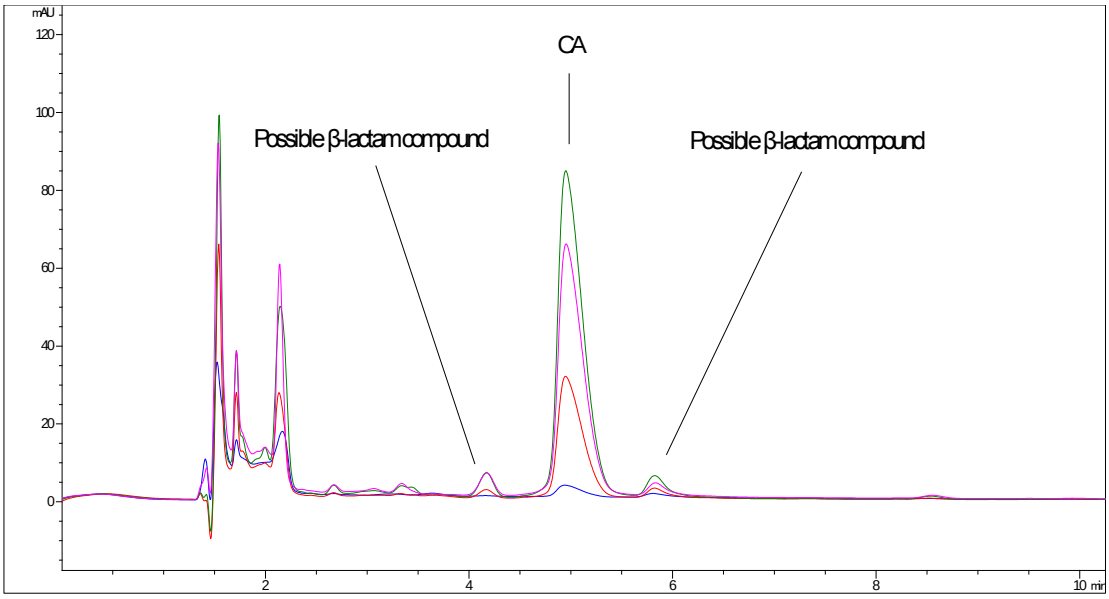

Fig. 2.5. Chromatographic profiles for CA during fermentation process of *Sc.* Note: The sequence of the samples with respect to fermentation time is: blue, red, green and pink at 0, 24.4, 36 and 57 h of fermentation time, respectively.

2.3.2. Method validation

2.3.2.1. Linearity, limit of detection and limit of quantification

In order to determine the linearity of the method, six points (0.2, 2, 20, 100, 200 and 400 mg/L for CA) were processed separately and analyzed in triplicate. The regression analysis was performed using the least squares method and the regression estimates were evaluated in a confidence interval of 95%. For CA quantification, the calibration curve was linear over a CA concentration range of 0.2 to 400 mg/L and a good linear relationship was found, as described by the following linear equation:$y = 86.73(\pm 0.39)x + 155.86(\pm 73.61)$ $(r^2 = 0.9997)$, where y is the peak area of CA and x is the CA concentration in mg/L. The relative standard deviation (RSD) of $\left(\frac{y}{x}\right)$ was $\leq 4.3\%$ for the analysis $(n = 18)$ in 6 levels of standard solution of CA.

The LOD and LOQ were 0.01 and 0.02 mg/L, respectively. The summary of quality parameters are presented in Table 2.1.

Table 2.1. Quality parameters for low, medium and high CA concentrations in a fermentative medium.

Linearity				CA concentration added into the production medium (mg/L)	Precision RSD(%)		Recovery	
Equation	Range mg/L	LOD (mg/L)	LOQ (mg/L)		Intraday (n=6)	Interday (n=18)	Mean (%)	RSD(%)
y=86.73x + 155.86	0.2-400	0.01	0.02	0.2	4.7	5.2	94.7	4.5
				200	1.9	8.5	100.2	9.5
				400	2.3	7.8	116.6	7.9

2.3.2.2. Precision and Recovery

The intraday precision at the different levels of CA concentration showed a %RSD between 1.9% and 4.7% while the interday precision had a %RSD between 5.2% and 8.5%. These results are within the ICH criteria, where the %RSD should be lower than 20% and 15% for the low and high concentrations, respectively (ICH, 2005). The mean recovery of the CA spiked into the production medium was between 94.7% and 116.6%. Besides, the recovery percentages had a %RSD in a range of 4.5% and 9.5%. Bearing in mind all the above-mentioned results one can conclude that the method is reliable, including precision and accuracy.

2.3.2.3. Clavulanate-imidazole complex stability

Owing to an experimentally observed CA degradation during fermentation processes (Roubos et al., 2002), we wanted to further explore the clavulanate-imidazole complex stability, during the quantification step. For this, the same levels and equal number of replicas as in section 3.2.2 were evaluated. A fresh 800 mg/L CA stock solution was prepared at in NaH_2PO_4 buffer (pH 6.8; 100 mM) and kept at room temperature for a day. Next, the solution was stored at 3-4 °C for a week. Afterwards, aliquots of this solution were subjected to sample preparation procedures as in section 2.2. The clavulanate-imidazole complex was quantified by HPLC-DAD as described in section 2.3, during three consecutive days, using an uncooled auto-sampler carousel.

The clavulanate-imidazole complex was shown to be unstable; a clear reduction of the peak area was observed (Fig. 2.6). The intraday stability had a %RSD, between 4.6% and 7.9%, while the interday stability showed a %RSD between 4.4% and 61%. The recovery of the CA spiked into the production medium was between 88.6% and 13.6%. Likewise, the CA stock solution was unstable at room temperature, since the peak areas at medium and high CA concentration levels were considerably lower than those compared with their equivalent areas, when the solution was freshly prepared. A decline in the CA concentration of 46.9% every 20.77 h, on average, was observed at 200 and 400 mg/L of CA (Fig. 2.6). The half-life times, $t_{1/2}$ at low and high CA concentrations were 17.29 h and 19.58 h at 200 and 400 mg/L of CA, respectively; thus, the rate of clavulanate-imidazole complex degradation appeared rather constant.

These results indicate that for an accurate quantification of CA, the clavulanate-imidazole complex samples must remain cooled at all time, during its quantification process.

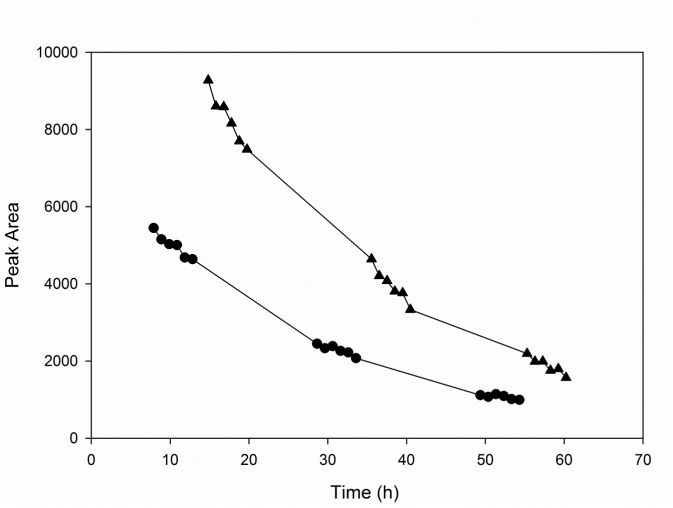

Fig. 2.6. Peak area profiles of clavulanate-imidazole complex at 200 (-●-) and 400 (-▲-) mg/L of CA in three consecutive days.

2.3.2.4. Features of the improved method

Table 2.2, summarizes and compares five different HPLC methods, taking into account LOD and interference. In addition to having a lower LOD, our method

provides versatility in using either chemically defined media or complex media, during a fermentation process. Furthermore, our method avoids overlapping peaks when β-lactam compounds are produced, as it is observed during CA production by *Sc.*

Table 2.2. Comparison between the HPLC-DAD method and other quantitative methods reported in literature.

Method	**LOD (mg/L)**	**Applicability**	**Interference**
Spectrophotometric Assay (Bird et al., 1982)	2	CA quantification in biological samples.	CA and other β-lactams compounds give strongly absorbing products under the assay condition.
HPLC-UV (isocratic) (Foulstone and Reading, 1982)	0.1	Applied for Augmentin quantification in body fluids. Currently, the method is also used for CA quantification in biological samples.	The appearance of additional β-lactams compounds during CA production by *Sc,* creates overlapping peaks causing poor/low efficiency.
HPLC-UV (gradient) (Hoizey et al., 2002)	0.08	Applied to a pilot pharmacokinetic study in healthy volunteers after a single-oral administration of amoxicillin/CA combination (500/125 mg).	CA stability is reduced in methanol.
LC-MS (Yoon et al., 2004)	0.02	Applied to analysis of amoxicillin and CA in human plasma. The method was tested in clinical studies.	The internal standard used is not structurally related to CA
LC-MS (Dubala et al., 2015)	0.1 of LOQ	Applied for analysis of plasma obtained after oral administration of cefixime/CA combination (200/125 mg).	The internal standard used is not structurally related to CA
This method, HPLC-DAD (gradient)	0.01	CA quantification in samples from *Sc* fermentation broths.	None

2.4. Conclusions

HPLC methods for simultaneous quantification of CA and other antibiotics, using either isocratic or gradient elution, have been widely used. To the best of our knowledge, gradient elution methods for CA quantification in samples from *Sc* fermentation, using both a chemically defined medium and a complex medium with a C-18 reversed phase column and DAD, have not been reported. This work demonstrates its applicability to resolve clavam overlapping peaks. The gradient

elution configuration proposed in this work avoids overlapping of new peaks (possibly β-lactam compounds with *3S, 5S* stereochemistry) with the CA peak, a case commonly found in isocratic elution. This method proved to be precise and accurate within the concentration range studied. The method was also tested using different complex and chemically defined media, and in each case, the CA peak was clearly resolved without interferences and/or overlapping peaks. Additionally, we demonstrate that due to its instability, the clavulanate-imidazole complex samples must remain cooled at all times during its quantification to obtain reliable data.

CHAPTER 3

3. Sensitivity analysis of clavulanic acid biosynthesis in *Streptomyces clavuligerus*: TCA cycle intermediates as a case study

HIGHLIGHTS

- A sensitivity analysis showed a trade-off between succinate, acetate and oxaloacetate secretion, and CA production and biomass synthesis.
- A ratio lower than 2 between arginine synthesis and the net flux of glyceraldehyde-3-phosphate is a necessary condition for CA biosynthesis.
- The urea cycle, wherein arginine is synthesized, is highly favored by succinate secretion.

Abstract

Streptomyces clavuligerus (*Sc*) has been widely studied due to its ability to produce clavulanic acid (CA), a potent inhibitor of β-lactamase enzymes. Despite the abundance of CA production studies in connection with metabolic flux distribution, analysis of metabolic patterns that embrace a sensitivity analysis are still scarce. In this work I performed a sensitivity analysis together with a Flux Balance Analysis (FBA) so as for studying the role of acetate and TCA cycle intermediates in the biosynthesis of CA.

The effect of succinate, acetate and oxaloacetate secretion on biomass synthesis and CA production, was evaluated *in silico*. A sensitivity analysis showed a trade-off between secretion of these metabolites, CA production and biomass synthesis. The urea cycle, wherein arginine (CA's precursor) is synthesized, was highly favored by succinate secretion. Moreover, for all cases, a ratio lower than 2 between arginine synthesis (from the urea cycle) to the net flux of glyceraldehyde-3-phosphate (from both glycolysis and pentose phosphate pathway) was identified as a necessary condition for

CA biosynthesis. In brief, evaluating the effect of secretion of the above-mentioned metabolites allowed for identifying pathway participation during CA biosynthesis.

3.1. Introduction

Streptomyces clavuligerus (Sc) has been widely studied due to its ability to produce clavulanic acid (CA); this low activity antibiotic is a potent inhibitor of β-lactamase enzymes, with pharmaceutical interest (Brown et al., 1976; Elander, 2003; Llarrull et al., 2010). Though many important achievements have been made, fermentative processes still render low CA titers, thus encouraging novel studies to address a deeper understanding of *Sc* metabolism (Hamed et al., 2013; Saudagar et al., 2008).

Genome scale metabolic models have been widely used for improving the understanding of microbial metabolism (Gianchandani et al., 2010). A genome scale metabolic network of enzyme-catalyzed reactions occurring within the cell is reconstructed based on genome annotation and related scientific literature; this information can be integrated into a stoichiometric model of metabolism which can be used for a detailed analysis of its metabolic capabilities. Flux Balance Analysis (FBA) uses stoichiometric models for predicting the flux distribution through biochemical networks, by solving a Linear Programming (LP) problem, for a selected objective function (Gianchandani et al., 2010; Stephanopoulos et al., 1998; Villadsen et al., 2011). Furthermore, by solving the associated dual problem, it is possible to perform sensitivity analysis, through the calculation of shadow prices. Such analyses are used for predicting and explaining the different phenotypes resulting from diverse environmental conditions. Besides, Phenotypic Phase Planes is a methodology for evaluating how biomass growth rates are affected by changes in culture conditions e.g., rates of substrate uptake (Bell and Palsson, 2005; Edwards et al., 2002). Currently, there exist various reports that have used the concept of shadow price for explaining experimental findings and gaining knowledge about the physiological behavior of a system (Grafahrend-Belau et al., 2009; Reznik et al., 2013). Reznik et al. (2013) explored the

meaning of shadow price, from a biological point of view, by integrating gene expression data with a stoichiometric model (Reznik et al., 2013). In that work, the shadow price value was correlated with the prediction of metabolite abundance (either rising or dropping concentrations) taking into consideration gene expression data. Grafahrend-Belau et al. (2009) performed a phenotypic phase plane analysis in order to evaluate the effect of oxygen and sucrose supply for storage patterning in developing barley seeds. The authors conducted simulations under anoxic, hypoxic and aerobic environmental conditions, which showed to be in good agreement with previously published experimental results (Grafahrend-Belau et al., 2009).

Although there are plenty of reports connecting CA production to metabolic flux distribution (Bushell et al., 2006; Kirk et al., 2000), analysis of metabolic patterns in association with sensitivity analysis, based on the interpretation of shadow prices, are still scarce.

In this work, a sensitivity analysis, in the form of a robustness and phenotypic phase plane analysis, was carried out so as to identify the role of TCA intermediates in the biosynthesis of CA in *Sc.*

3.2. Materials and Methods

3.2.1. Genome scale metabolic modeling of *Sc*.

3.2.1.1. Base genome scale model of *Sc*

The genome scale metabolic model of *Sc* reported by Medema et al. (2010), comprised 1492 reactions (1290/202 internal/exchange fluxes) and 1173 metabolites (971/202 internal/external metabolites); it was used as a reference to build the model used in this work. Medema's model includes the major metabolic pathways i.e., glycolysis, gluconeogenesis, pentose phosphate (PP), tricarboxylic acid cycle (TCA cycle), urea cycle, glyoxylate cycle, anaplerotic reactions, clavam pathway, cephalosporin C biosynthesis,

cephamycin C biosynthesis, as well as the biosynthesis of macromolecular components of biomass, such as RNA and DNA. After a computational analysis for dead end metabolite detection and gap filling, the model was tested, for biomass formation, by *in silico* simulations (Medema et al., 2010).

3.2.1.2. Our improved genome scale model of *Sc*

The base model of *Sc* was manually curated using information from different data sources, including KEGG pathways (http://www.genome.jp/kegg/), gene-reaction associations (http://www.enzyme-database.org/), and extensive open scientific literature (Bushell et al., 2006; Medema et al., 2010; Roubos, 2002). The Model and Constraint Consistency Checker (MC^3) algorithm was used to identify further dead-end metabolites, single-connected metabolites, and zero-flux reactions (Yousofshahi et al., 2013). In consequence, gaps were found and as much as possible reactions were added. The biomass reaction was modified to account for 47 molecules of adenosine diphosphate (ADP) and 47 molecules of phosphate (pi), which are commonly used in genome scale models of *Streptomyces coelicolor* and *Mycobacterium tuberculosis* (Alam et al., 2010; Borodina et al., 2005; Jamshidi and Palsson, 2007). The clavam biosynthesis pathway was expanded to consider the 5s clavam route, as a results of which 10 reactions were inserted. Furthermore, in the transition of clavaminic acid to CA one reaction was removed and three reactions were added, to account for the metabolites N-glycyl-clavaminic acid and N-acetyl-glycyl-clavaminic acid (Arulanantham et al., 2006). Similarly, a metabolite named “clavam5s” was added at the end of the 5s clavam route, as this pathway is still under construction (Ozcengiz and Demain, 2013; Zelyas et al., 2008). Additionally, exchange and transport reactions for oxaloacetate, clavam-2-carboxylate and alanyl-clavam were inserted; in summary, a total of 18 reactions were added to the base model, resulting ultimately in a model *i*HR1510 comprising 1510 reactions (1305/205 internal/exchange fluxes) and 1187 metabolites (982/205 internal/external metabolites). The SBML version of the full model is available upon request.

3.2.2. Shadow price as a tool for flux and sensitivity analysis

FBA has been traditionally used to predict the metabolic flux distribution of an entire metabolic network (Stephanopoulos et al., 1998; Villadsen et al., 2011). This approach involves the mass conservation law, where a pseudo-steady-state mass balance for all metabolites is applied, and changes in pooled metabolites are neglected, thus leaving a set of linear algebraic equations. In biological systems, a single metabolite can participate in more than one reaction; therefore, more variables than linearly independent equations are obtained, thus generating an underdetermined system, which is solved by the optimization of a defined objective function (Stephanopoulos et al., 1998; Villadsen et al., 2011). Under the assumption of steady state, the net flux of production and consumption of a metabolite equals zero. Therefore, a system of linear equations arises, which, in matrix form, is written as:

$$\boldsymbol{S} \cdot \boldsymbol{v} = 0$$

Where $\boldsymbol{S}$ is the (m × n) matrix of stiochiometric coefficients, m is the number of metabolites, n is the number of reaction rates (fluxes) and $\boldsymbol{v}$ is the flux vector.

The LP problem for solving the system is written as:

$$\begin{aligned} &\text{Max } \boldsymbol{f^T v} \\ &\text{s.t. } \boldsymbol{S} \cdot \boldsymbol{v} = 0 \\ &\boldsymbol{v_{lb}} \leq \boldsymbol{v} \leq \boldsymbol{v_{ub}} \end{aligned}$$

Where $\boldsymbol{f}$ is the objective function vector, whereas, $\boldsymbol{v_{lb}}$ and $\boldsymbol{v_{ub}}$ are the lower and upper bounds for fluxes, respectively.

Formulation of the dual problem associated to the original primal LP problem is very important in systems biology, due to the valuable information that can be extracted from its solution, in terms of shadow price interpretation.

The biological interpretation of shadow price and its calculations, used in this work, can be found elsewhere (Grafahrend-Belau et al., 2009; Palsson, 2005; Reznik et al., 2013). Following is a quantitative description of their meaning.

- Metabolites which are limiting (positive effect) for the selected objective function have a negative value of shadow price.

- Metabolites which are not limiting (no effect) for the selected objective function have a zero value of shadow price.
- Metabolites available in excess have a positive value of shadow price.

3.2.3. Flux Balance Analysis

There is no universal objective function for FBA studies, which perhaps is the main limitation of this approach (Gianchandani et al., 2010; Schuetz et al., 2007). Indeed, different objective functions are commonly tested, and the one that best matches experimental data is selected. Different methodologies have been developed for the prediction of *in vivo* cellular behavior and/or chemical production (Burgard et al., 2003; Gianchandani et al., 2010; Schuetz et al., 2007). One of the objective functions (which always has a biological meaning) is the maximization of growth per flux unit, which is the maximization of growth followed by the minimization of the overall flux (Grafahrend-Belau et al., 2009). The minimization of the overall flux (the squared sum of all fluxes) basically entails a maximal enzymatic efficiency, leading to an efficient metabolic flux distribution (Grafahrend-Belau et al., 2009; Holzhütter, 2004). The flux of biomass obtained in the maximization of growth is typically used as an extra constraint in the minimization of the overall flux. For the case of chemostat cultures of *Sc*, the product CA is synthesized while the cell grows at a constant rate and phosphate deficiency. In order to deal with this metabolic regime, and under the premise of a maximal enzymatic efficiency for cellular growth, a two-stage optimization procedure (Schuetz et al., 2007) was employed. First, a LP problem was solved using the maximization of a composite objective function (biomass synthesis and CA production). Second, a Non Linear Programming (NLP) problem using the minimization of the overall intracellular flux as the objective function, was solved. The NLP problem formulation included two additional constraints obtained from solving the problem at stage one: the biomass flux and exchange flux of CA were used for both robustness and phenotypic phase plane analysis. The additional constraints used at the second

stage reduced the solution space for the optimization problem, which led to obtain reliable *in silico* metabolic phenotypes.

For the purpose of model validation, a set of simulations using the COBRA Toolbox v.2.0 (Schellenberger et al., 2011) was conducted, using a composite objective function, as described below.

The mathematical representation of the optimization problem is as follows:

Stage one

$$Max\ w_{biomass} * v_{biomass} + w_{CA} * v_{CA\ intracellular}$$

$$\text{s.t.}\quad \boldsymbol{S} * \boldsymbol{v} = 0$$

$$v = v_j$$

$$\boldsymbol{v_{lb}} \leq \boldsymbol{v} \leq \boldsymbol{v_{ub}}$$

Stage two:

$$Min \sum \boldsymbol{v_i^2},$$

$$\text{s.t.}\quad \boldsymbol{S} * \boldsymbol{v} = 0$$

$$v = v_{secretion\ or\ uptake\ rate}$$

$$v_{biomass} = v_{optbiomass}$$

$$v_{CA\ extracellular} = v_{otpCA\ extracellular}$$

$$\boldsymbol{v_{lb}} \leq \boldsymbol{v} \leq \boldsymbol{v_{up}}$$

Where $w_{biomass}$ and w_{CA} are the weight factors for biomass and intracellular CA fluxes. $v_{biomass}$, $v_{CA\ intracellular}$ and v_j are the biomass flux, intracellular flux of CA and either secretion or uptake rate of a selected metabolite, respectively. $v_{optbiomass}$ and $v_{optCA\ extracellular}$ are the optimal values for biomass and extracellular CA that resulted from solving the problem stated at stage one.

3.2.3.1. Robustness analysis

A robustness analysis was addressed to evaluate the variation in the composite objective function, when the optimal flux (allowable) of succinate, acetate, oxaloacetate or oxygen was changed. To achieve this, the secretion

flux of each metabolite was varied in a stepwise fashion for a range of interest, while the objective function was maximized. The above-mentioned metabolites were selected based on experimental evidence that will be presented in chapter 4.

3.2.3.2. Phenotypic phase plane analysis

Phenotypic phase plane (PhPP) analysis was performed to explore the steady-state solution space of two important independent-variables, glycerol and oxygen uptake rates (Bell and Palsson, 2005; Edwards et al., 2002), and its effect on biomass growth and product biosynthesis. Glycerol and oxygen were varied simultaneously, from 0 to 1.6 mmol/(g_{CDW}*h), while the objective function was maximized.

3.2.3.3. *In silico* single-gene knockout

In silico single-gene knockout of *gap1 and gap2* that encoded for different types of glyceraldehyde-3-phosphate dehydrogenases (GAPDHs) was carried out. For this purpose, the flux through the reaction mediated by GAPDH/*gap1* was set to zero.

3.3. Results and discussion

3.3.1. Robustness analysis: Effect of varying a single parameter

Sensitivity analysis with respect to one parameter was performed in order to evaluate the different metabolic phenotypes of *Sc* when the optimal stage (maximization of the composite objective function described in section 3.2.3) was achieved.

3.3.1.1. Effect of varying oxygen uptake rate

The effects of varying the oxygen uptake rate (from zero to a reasonable oxygen uptake rate i.e., required for fully glycerol oxidation) on the ability of *Sc* to growth can be seen in Fig. 3.1 A. There are three linear segments indicating equal values for shadow prices of oxygen and the corresponding metabolic phenotypes. Profiles for shadow price values of oxygen and CA

were more positive (negative values were approaching to zero) as oxygen uptake rate increased, thus indicating a diminished effect on growth and CA biosynthesis (Fig. 3.1 B). The biomass synthesis was negatively affected at high oxygen uptake rates; however, this effect has not been reported in *Sc*. This could be interesting for experimental validations.

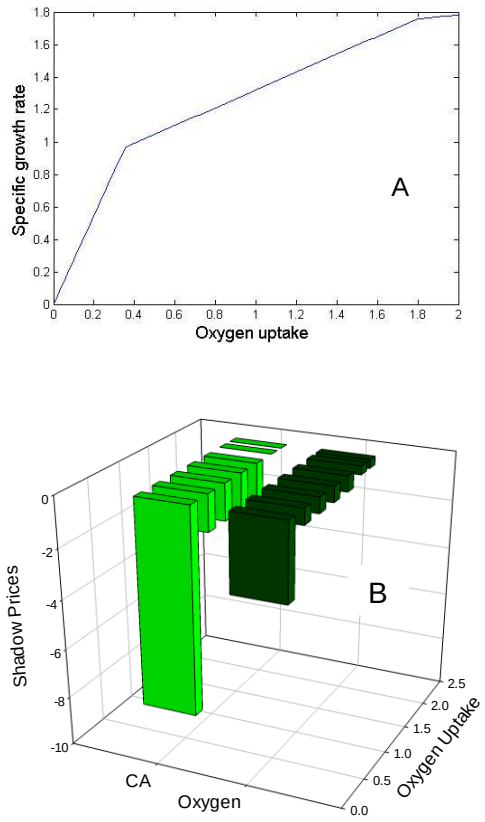

Fig. 3.1. Robustness analysis of biomass growth while varying oxygen uptake rate. A) Effect of varying oxygen uptake rate [mmol/(g_{CDW}*h)] on the specific growth rate (h^{-1}). B) Profile of shadow prices for oxygen and CA at different oxygen uptake rates.

Additional metabolites were analyzed, for which a different trend was observed (Fig. 3.2 B). Here, it can be seen that when oxygen uptake rate increased, oxaloacetate, acetate and malate were not secreted - even when CA was synthesized and secreted - and their shadow prices were either zero or negative (Fig. 3.3). The declared metabolites, and alpha-ketoglutarate, glyceraldehyde-3-phosphate (GAP) and glucose-6-phosphate had negative

shadow prices under the investigated oxygen uptake rate. Consequently, all these compounds might be catalogued as limiting for biomass synthesis and CA production. In contrast, succinate was secreted and had a positive shadow price. However, CA was secreted without secretion of succinate (Table 3.1). Under this circumstance one can argue that there exists a trade-off between the CA and succinate pools; the clavam pathway, where CA is synthesized, supports this relationship. Apparently, while the former compound (CA) is being synthesized, the latter (succinate) is released as byproduct at three intermediate clavam reactions (Ozcengiz and Demain, 2013; Townsend, 2002; Zhang et al., 2002). Chapter 4 of this thesis demonstrates how succinate, acetate and oxaloacetate were secreted while CA was produced, an observation that contrast the *in silico* results.

CA secretion at moderate oxygen uptake rates (Table 3.1) could be elucidated with the aid of the experimental observations of Rosa et al. (2005). Although there is not a direct association between shear rate and oxygen uptake rate, higher shear rates might improve glycerol uptake rate, thus leading to increase oxygen consumption and also to release CA towards the medium (Rosa et al., 2005). Furthermore, the enhancement of glycerol uptake rate would lead to a greater demand and consumption of oxygen. Moreover, CA production is highly favored at low dilution rates (Bushell et al., 2006). Bushell and co-workers (2006) found that the maximum flux to CA was obtained at the lowest dilution rate. Likewise, the same authors reported that CA production ceased when the dilution rate was increased. To the light of these results, we expected a negative effect of high oxygen uptake rates on CA production. Figure 3.2 A shows how CA production decreases at an unrealistic oxygen uptake rate. Despite the improbable value of oxygen uptake rate obtained to represent its negative effect on CA production, the tendency of the *in silico* results is in agreement with experimental evidence reported in scientific literature (Bushell et al., 2006; Rosa et al., 2005).

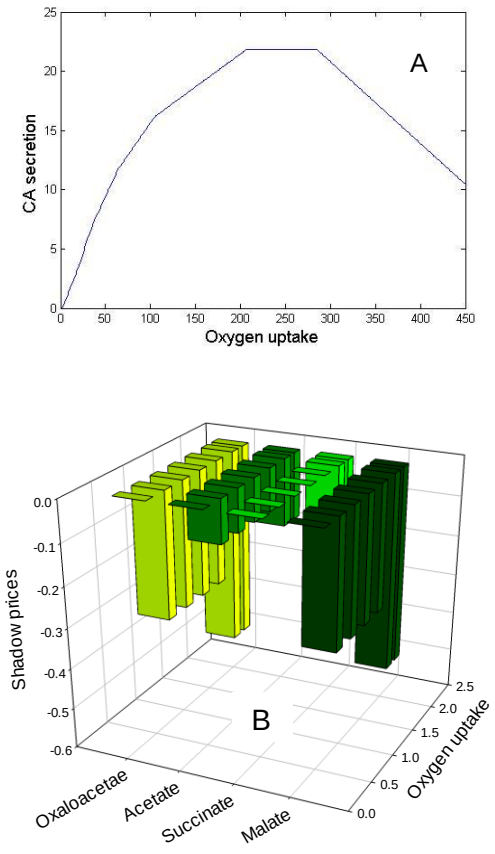

Fig. 3.2. Robustness analysis of CA production while varying oxygen uptake rate. A) Effect of varying oxygen uptake rate on the CA production. B) Profile of the shadow prices of oxaloacetate, acetate, succinate and malate varying oxygen uptake rate. Flux units [mmol/(g_{CDW}*h)]

Table 3.1. Exchange flux and shadow prices of succinate while varying oxygen uptake rate. The given numbers are exchange fluxes [mmol/(g_{CDW}*h)], followed by shadow prices in parenthesis.

Oxygen uptake	**Exchange flux of CA**	**Exchange flux of succinate**
0.3	0 (-8.2132)	1.0738 (0)
1.2	0 (-1.4399)	0.5222 (0)
2.0	0.0397 (0)	0 (-0.3165)

Following with the analysis, glucose-6-phosphate is a glycolytic intermediate and also a metabolic node for glycolysis and pentose phosphate pathway; some precursors of biomass are produced in the pentose phosphate pathway. Therefore, one would consider glucose-6-phosphate as limiting for growth. This effect was predicted by the negative shadow prices obtained for this metabolite (data not shown). Instead, we analyzed and report the behavior of intracellular fluxes through key reactions; results are shown in Fig. 3.3. Due to the relationship between GAP and arginine, which are the main precursors of CA biosynthesis, we focused on glycerol assimilation, urea cycle and two enzymatic reactions between TCA cycle and urea cycle. The intracellular flux of each selected reaction increased when the oxygen uptake rate increased. So, at moderate oxygen uptake rate, the pool of GAP and arginine were highly increased and further available for condensation and CA formation (Bascarán et al., 1989; Bushell et al., 2006; Khaleeli et al., 1999; Li and Townsend, 2006; Valentine et al., 1993). All these facts show the remarkable role of oxygen on *Sc* metabolism and CA biosynthesis.

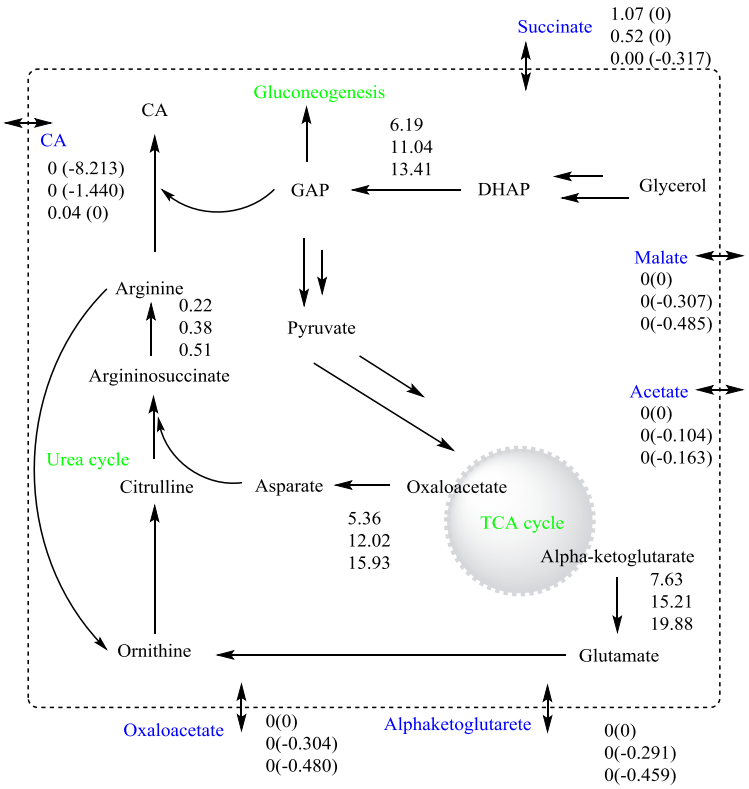

Fig. 3.3. A summary of exchange fluxes of key metabolites, intracellular fluxes and shadow price values in the *Sc* metabolic network when increasing the oxygen uptake rate. The numbers given are the rates in mmol/(g_{CDW}*h) for three different values of oxygen uptake rate (0.3, 1.2 and 2, up to down respectively), followed by shadow prices in parenthesis.

3.3.1.2. Effect of varying the succinate secretion rate

Succinate is a TCA cycle intermediate; it is also produced as byproduct at the clavam pathway (Ozcengiz and Demain, 2013; Zhang et al., 2002). Therefore, when CA is synthesized, an increment of succinate pool is expected. In order to evaluate the role of succinate upon the specific growth rate and CA production, a robustness analysis varying the succinate secretion was performed (Fig. 3.4). The secretion of succinate - prior to 0.7 mmol/(g_{CDW}*h) - had clearly a positive effect on biomass synthesis with no CA production. Afterward, biomass synthesis ceased while a significant increase on CA production was observed. The activation of the secondary metabolism led to an increment of carbon flux through the clavam pathway and a re-

distribution of the carbon flux through the network, including pathways where biomass precursors are involved.

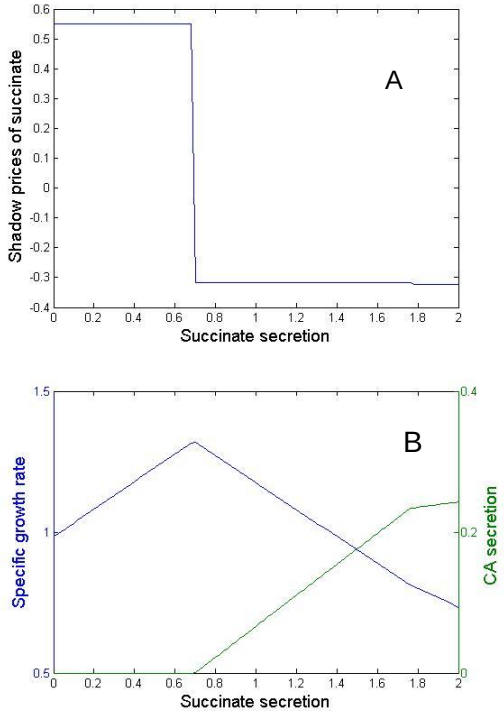

Fig. 3.4. Robustness analysis of biomass growth and CA production while varying succinate secretion. A) Shadow prices of succinate as a function of succinate secretion rate. B) Effect of varying succinate secretion on the specific growth rate (h^{-1}) and CA production. Flux units [mmol/(g_{CDW}*h)]

The change in the shadow price of succinate is an indication of the appearance of another metabolic phenotype (Fig. 3.4). Interestingly, CA biosynthesis appears to be favored when a negative effect on biomass synthesis occurs. In order to evaluate the different metabolic patterns, one value of succinate secretion rate for each shadow price value of succinate was selected; i.e. 0, 0.7 and 1.78 mmol/(g_{CDW}*h) (Fig. 3.5).

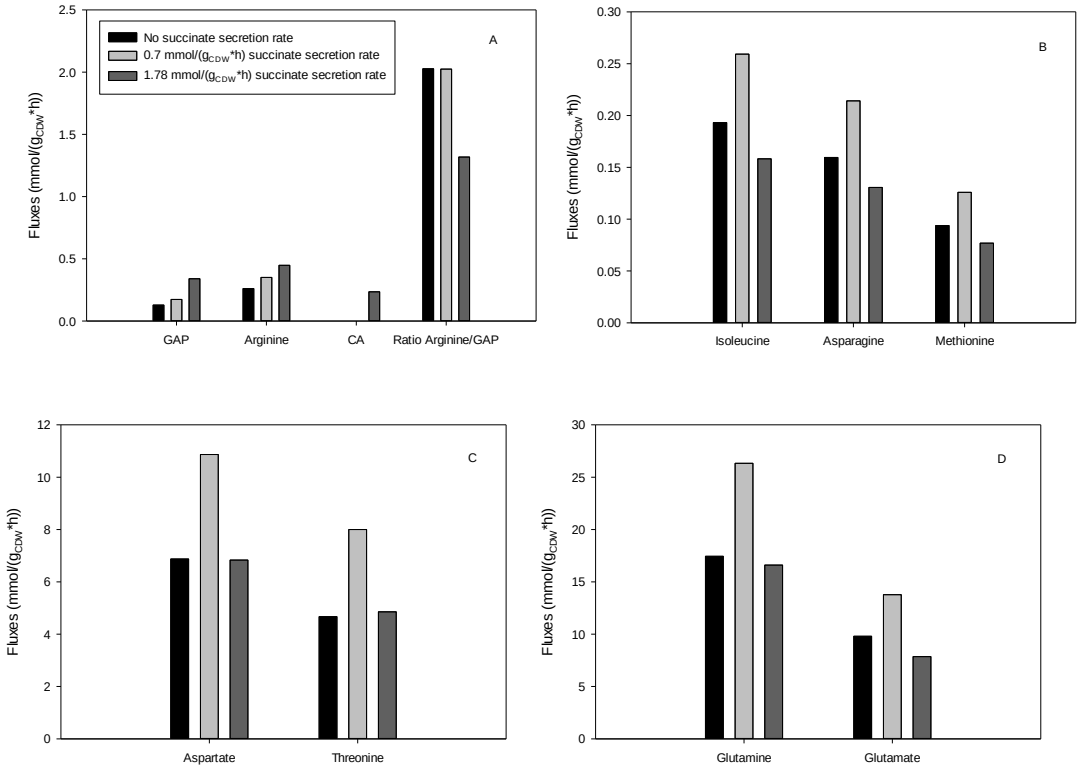

Fig. 3.5. Flux changes for a selected group of metabolites involved in CA biosynthesis at different metabolic patterns. A) CA secretion, intracellular fluxes for GAP and arginine, and a ratio between the latter two compounds. B) and C) Intracellular fluxes for the Oxaloacetate-family of amino acids. D) Intracellular fluxes for the alpha-ketoglutarate-family of amino acids.

The main metabolic precursors of CA, GAP and arginine, increased their flux values when succinate secretion increased (See Fig. 3.5 A) which indicates that succinate release into the medium might have a positive effect on CA production, unlike biomass synthesis, where a negative effect was observed. A decrease in both the main catabolic pathways and the synthesis of amino acids (Fig. 3.5 B and D), when biomass synthesis ceased, was expected. In this case, isoleucine, asparagine and methionine showed a diminution of 18.1% on average on their flux values (from 0 to 1.78 mmol/(g_{CDW}*h) of succinate secretion), whereas for glutamine and glutamate, these percentages were 4.8% and 19.8%, respectively. In contrast, the fluxes of

GAP and arginine increased at the selected rates of succinate secretion. Hence, we focused our analysis on the routes where GAP and arginine are synthesized. The urea cycle, where arginine is produced, has two main sources (Haines et al., 2011): the carbon flux from alpha-ketoglutarate and oxaloacetate via glutamate and aspartate, respectively. Although the reaction catalyzed by glutamate dehydrogenase decreased its flux in a 19.8% (Fig. 3.5 D) during the three evaluated environmental conditions, the reaction driven by aspartate aminotransferase only reduced its flux in a 0.6% (Fig. 3.5 C). Further, the carbon flux from aspartate towards asparagine and methionine decreased (18.1%). In contrast, the flux in the direction of threonine had a slight increase (3.9%) (Fig. 3.5 C). Therefore, aspartate was further available to condense with citrulline, a reaction catalyzed by argininosuccinate synthetase (Haines et al., 2011). On one hand, the net flux of GAP from both glycolysis and pentose phosphate pathway increased, while succinate secretion increased, even when biomass synthesis ceased. So, as succinate is liberated into the spent medium, a further pool of arginine and GAP was available for its condensation, thus promoting CA biosynthesis. On the other hand, we found that a ratio lower than 2 between arginine synthesis, (from the urea cycle) to the net flux of GAP (from both glycolysis and pentose phosphate pathway) was a necessary condition for CA biosynthesis (Fig 3.5. A); i.e. when biomass synthesis was decreased, CA production was induced. This circumstance is consistent with reported results by Bushell et al. (2006), where the maximum CA production was obtained at the lowest dilution rate evaluated.

3.3.1.3. Effect of varying acetate secretion rate

Due to the fact that N-acetylated clavaminic acid intermediates have been detected in mutants of *Sc* (Arulanantham et al., 2006; Elson et al., 1988; Jensen et al., 2004), there is a growing scientific interest to further explore the role of acetate in CA biosynthesis (Iqbal et al., 2010; Paradkar, 2013). In this regard, I carried out an *in silico* analysis for improving the understanding of how acetate secretion rate is connected with CA production (Fig. 3.6).

Biomass synthesis was negatively affected with acetate release into the spent medium; however, CA was produced only in an interval of 3.70-4.15 mmol/(g_{CDW}*h) of acetate secretion (Fig. 3.6 B).

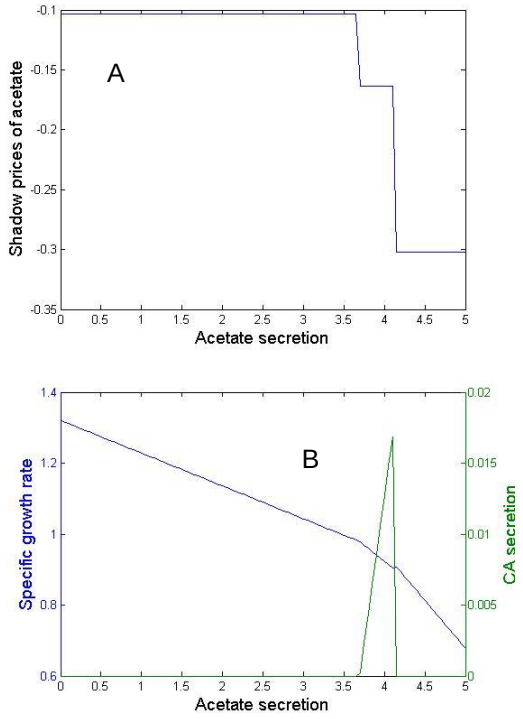

Fig. 3.6. Robustness analysis of biomass growth and CA production while varying acetate secretion. a) Shadow prices for acetate as a function of acetate secretion rate. b) Effect of varying acetate secretion rate on the specific growth rate (h^{-1}) and CA production. Flux units [mmol/(g_{CDW}*h)]

Although N-acetyl-glycyl-clavaminic acid and N-acetyl-clavaminic acid have been reported to be intermediates in the clavam pathway (Elson et al., 1988; Jensen et al., 2004), a reaction mechanism for the acetylation is still unknown (Arulanantham et al., 2006). In this sense, the process could involve the formation of N-acetylated clavaminic acid intermediates (Paradkar, 2013), and the availability of acetate (either supplemented in a culture medium or secreted by cells) would favor the biosynthesis of CA and the above mentioned compounds. Nonetheless, continuous secretion of acetate could also act as an inhibitor of some steps involved in CA biosynthesis, thus generating another metabolic phenotype not involving CA production

(according to *in silico* results shown in Fig. 3.6 B, for fluxes above 4.15 mmol/(g_{CDW}*h) of acetate secretion). However, we demonstrated (experimentally) a strong association between accumulation of acetate and CA production by *Sc* (See chapter 4), indicating a good prediction by the model.

Acetylation might be mediated by o*rf14* due to a demonstrated similarity with GCN5-acetyltransferases (Iqbal et al., 2010). The authors found that *orf14* is a member of a tandem GCN5-related acetyltransferase (GNAT) protein, where the *C*-terminal domain of acetyl transferase probably possesses acyl transfer activity and the *N*-terminal GNAT domain can bind to a single acetyl-CoA molecule.

Despite the decrement in arginine biosynthesis (31%, on average), the above-mentioned ratio between arginine and GAP - lower than 2 - was again needed for CA synthesis (Fig. 3.7). As for succinate, this instance indicates that the ratio arginine/GAP decreased while the dilution rate was decreased.

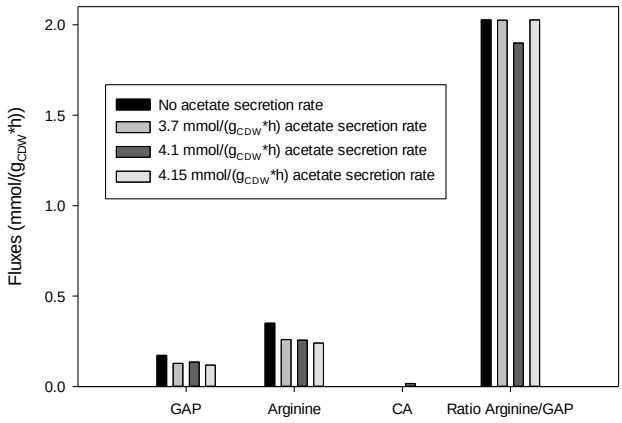

Fig. 3.7. Profile of CA secretion, intracellular fluxes for GAP and arginine, and arginine/GAP ratio while acetate is secreted.

3.3.1.4. Effect of varying oxaloacetate secretion rate

Following the same methodology that was implemented in the robustness analysis for succinate and acetate, here we explore the role of oxaloacetate secretion rate upon biomass synthesis and CA production. In fact, a beneficial

effect over CA production was evidenced when oxaloacetate was secreted (Fig. 3.8). Interestingly, the ratio arginine/GAP lower than 2 remained invariable as a condition for CA production (Fig. 3.9).

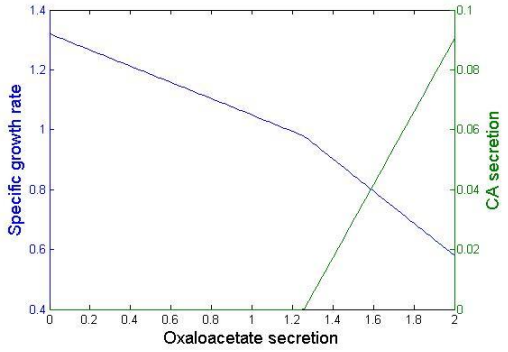

Fig. 3.8. Robustness analysis of biomass growth and CA production while varying oxaloacetate secretion rate. Specific growth rate (h^{-1}), flux units [mmol/(g_{CDW}*h)].

While arginine production decreased an average of 30%, the net flux of GAP (coming from both glycolysis and pentose phosphate pathway) only diminished 4%. Thus, oxaloacetate secretion led to an increased availability of C3 precursors (in this case GAP) in relation with arginine, a critical step for the clavam pathway, where finally the production of CA occurs (Ives and Bushell, 1997; Ozcengiz and Demain, 2013). Bushell and co-workers (2006) reported that feeding amino acids from the oxaloacetate-family improved the CA yield more than 10-fold compared to non-supplemented chemostat cultivations.

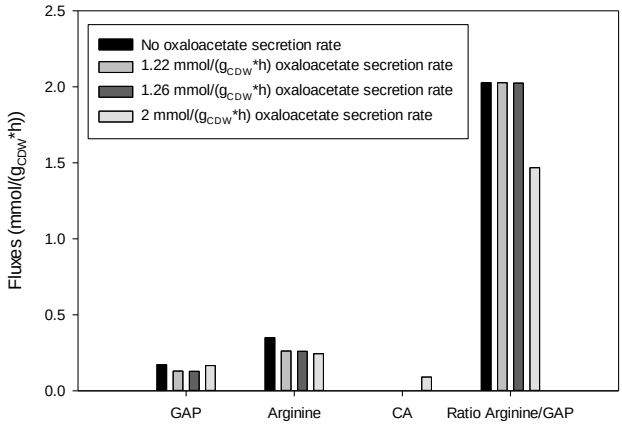

Fig. 3.9. Profile of CA secretion, intracellular fluxes for GAP and arginine, and arginine/GAP ratio when oxaloacetate was secreted.

It can be concluded that there is a positive association between secretion of succinate, acetate and oxaloacetate and CA production, thus suggesting that the accumulation of TCA cycle intermediates is related to CA biosynthesis.

3.3.2. Phenotype phase plane (PhPP) analysis

3.3.2.1. Composite objective function as a dependent variable of glycerol and oxygen uptake rate

In order to explore the effect of two metabolites as independent variables, *in silico* simulations were performed, where the composite objective function (biomass synthesis and CA production) was optimized while the oxygen and glycerol uptake fluxes were varied. The growth dependence on glycerol and oxygen uptake can be seen in the phase plane diagram depicted in Fig. 3.10 A. The regions having the same color correspond to metabolic phenotypes where the objective function had the same value. These different regions are divided by isoclines. For clarity, α (taken as a ratio of the relative shadow prices between glycerol and oxygen, corresponds to the slope of the isocline) was used and three types of values were found.

Infinite value of α is seen as a vertical isocline, with zero shadow prices of oxygen. This metabolic region is observed at conditions of glycerol limitation and high oxygen availability, resulting in no cell growth (blue zone in y-axis). The same behavior, no growth of cells, was observed with oxygen limitation and high glycerol uptake, leading to α = 0; this can be seen as a horizontal isocline and zero shadow price of glycerol (blue zone in x-axis). Both phases are observed under a single substrate limitation, oxygen and glycerol, respectively. The rest of the graph had an α with negative value and an absolute value less than unity, thus indicating a dual limitation of glycerol and oxygen, and also that oxygen had a greater effect than glycerol upon the growth and CA production.

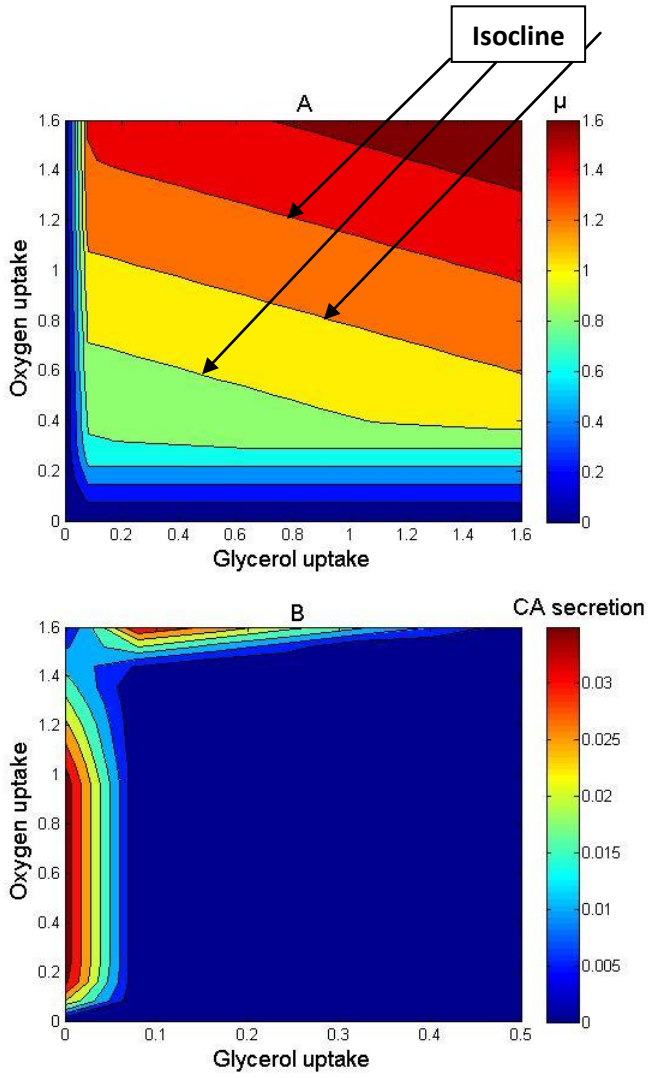

Fig. 3.10. Phase plane diagram of oxygen and glycerol uptake rates while optimizing for a composite objective function. A) Growth rate, the color bar is for specific growth rate μ (h^{-1}). B) CA secretion, the color bar is for CA flux in mmol/(g_{CDW}*h).

The above results indicate that while there is no oxygen consumption by *Sc*, the strain is unable to grow in spite of the availability of glycerol in the medium; the opposite case is also observed. These findings are in agreement with *Sc* being an obligate aerobe: *Sc* cannot grow without oxygen. Besides, in the absence of glycerol there is no carbon source for growth. The specific growth rate increases as both oxygen and glycerol uptake increase, reaching a maximum value of 1.76 h^{-1}, when the fluxes of both, oxygen and glycerol were 1.6 mmol/(g_{CDW}*h). However, the specific growth rate reached an

unrealistic value, but its trend agrees with previously reported results by Bushell et al. (2006).

Results showing CA production as a function of oxygen and glycerol uptake can be seen in the phase plane diagram represented in Fig. 3.10 B. Although the *in silico* simulations showed that the maximum CA flux is achieved at glycerol limiting conditions, this is unlikely because, under these environmental conditions, *Sc* activates the glyoxylate shunt (Soh et al., 2001) ceasing the flux towards the urea cycle. However, CA flux reached reasonable physiological values with the increase of glycerol uptake (See the top in Fig. 3.10 B). These results are in agreement with previously reported results by Rosa et al. (2005), who suggested that improving the rate of transfer of glycerol into the cells, results in an improved CA concentration.

Since the maximum CA production was achieved at high oxygen uptake rate and moderate glycerol uptake rate, an analysis of carbon flux distribution of reactions involved in CA production was carried out (Fig. 3.11). Here, the net flux of GAP, from glycolysis and pentose phosphate pathway, had a slight decrement (3.1%, on average) when the glycerol uptake increased at 200%. Furthermore, arginine was rather constant, only an increment of 0.6% was observed. Despite the minor change in the availability of arginine and GAP, the trend of arginine/GAP ratio had a small increase - always lower than 2 - with CA production.

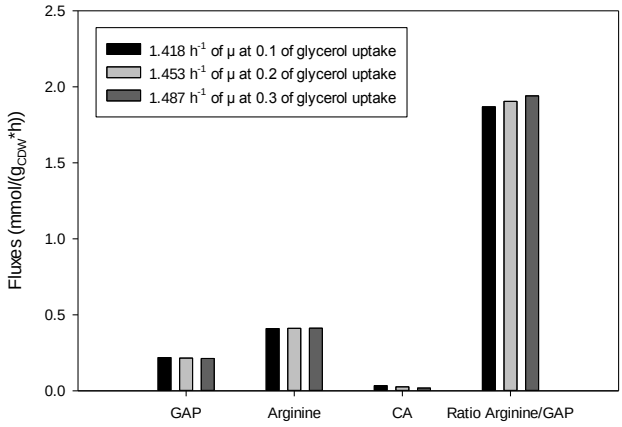

Fig. 3.11. Transitions of intracellular flux for reactions involved in CA production with varying glycerol uptake rate, and keeping constant oxygen uptake rate at 1.6 mmol/(g_{CDW}*h).

3.3.2.2. *In silico* single-gene knockout mutant in *Sc*: GAPDH/gap1

In the work by Li and Townsend (2006), two genes (*gap1 and gap2)* that encode for different types of glyceraldehyde-3-phosphate dehydrogenases (GAPDHs) were inactivated in *Sc* by a targeted gene disruption technique. The authors found that CA production was duplicated when *gap1* was disrupted (Li and Townsend, 2006). In order to mimic the above-mentioned genetic modification and determine which pathways were favored resulting in an appreciable increase on CA production, we performed a single-gene knockout for GAPDH/*gap1* - a reaction where 1,3-bisphosphoglycerate is formed from GAP - by setting to zero the corresponding flux. The phase plane diagram can be seen in Fig. 3.12 A.

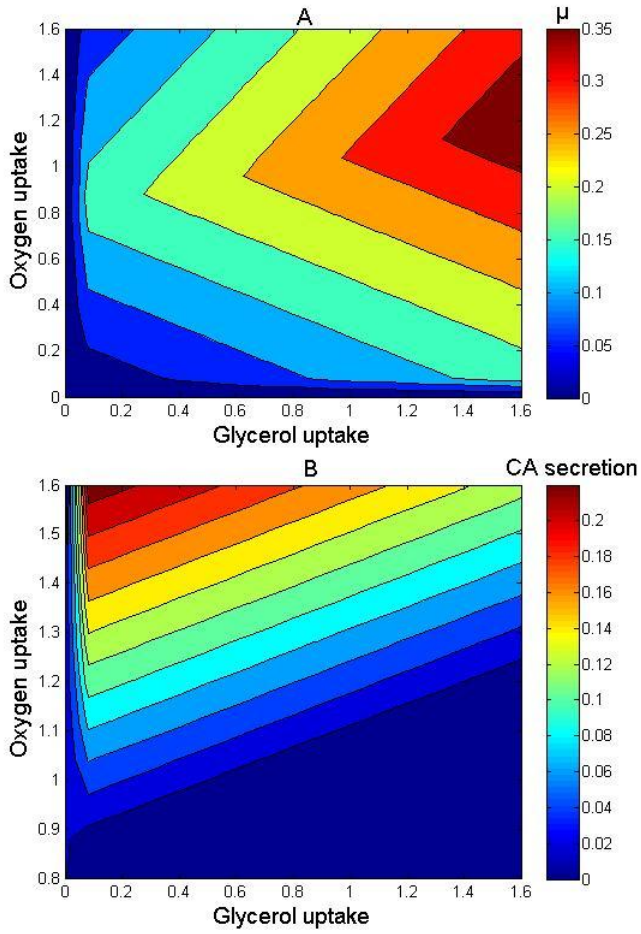

Fig. 3.12. Phase plane diagram of oxygen and glycerol uptake rates while optimizing for a composite objective function with a single-gene knockout (GAPDH/*gap1*). A) Growth rate, the color bar is for specific growth rate μ (h^{-1}). B) CA secretion, the color bar is for CA flux in mmol/(g_{CDW}*h).

The single-gene knockout *Sc* mutant, GAPDH/*gap1*, blocked the glycolytic pathway. Although glycerol is commonly metabolized to form GAP, an alternative pathway can be used for glycerol assimilation. Here, glycerol was metabolized through glycerol hydrogenase, aldehyde dehydrogenase and glycerate kinase to produce 2-phosphoglycerate (a glycolytic intermediate), and finally the carbon flux was directed towards the TCA cycle, (Fig. 3.13) (Li and Townsend, 2006). The alternative pathway present in *Sc* can be active either in the wild-type or in the mutant. This behavior was predicted by the model since the declared pathway had fluxes different from zero (See table

3.2). Here, it was clear that the alternative pathway was inactive at the first two scenarios of glycerol uptake rate, whereas, in the mutant's case the pathway was always active (See glycerol hydrogenase in table 3.2). In addition, for the wild-type, the carbon flux through the reaction mediated by glycerol kinase was active, at all times. Furthermore, for the wild-type case, the specific growth rate was higher than that for the mutant, indicating a diminished carbon flux towards biomass precursors in the mutant's case. In contrast, (for the mutant case), carbon flux towards the clavam pathway was escalating (data not shown), thus leading to the highest CA titer.

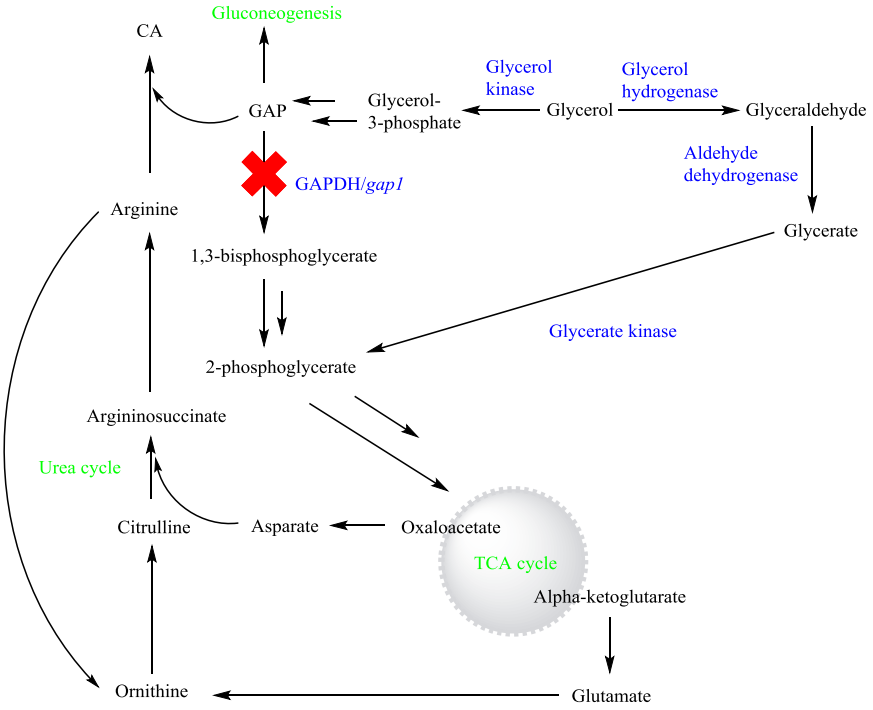

Fig. 3.13. CA biosynthetic scheme for targeted gene disruption of *gap1*. Adapted from Li and Townsend (2006).

Table 3.2. Intracellular fluxes for key reactions of alternative glycerol assimilation in *Sc* with varying glycerol uptake rate, while keeping constant oxygen uptake rate at 1.6 mmol/(g_{CDW}*h).

Glycerol uptake	μ (h^{-1})		Glycerol kinase		Glycerol hydrogenase	
	Wild-type	Mutant	Wild-type	Mutant	Wild-type	Mutant
0.4	1.52	0.13	0.33	0	0	0.39
0.8	1.61	0.20	0.72	0	0	0.79
1.2	1.68	0.27	0.81	0	0.31	1.19

The maximum exchange flux of CA by the mutant (Fig. 3.12 B) was 6.1-fold highest than those for the wild-type strain (Fig. 3.10 B). Although the increment in CA production was 6.1-fold instead of 2-fold, which was experimentally reported by Li and Townsend (2006), this model still represents a similar metabolic phenotype of CA biosynthesis when GAPDH/*gap1* is blocked. This difference might be caused by the lack of experimental data as constraints for the different simulations. Besides, in both cases, wild type and single-gene knockout mutant, the highest CA production was achieved at high oxygen uptake rate and moderate glycerol uptake rate; nonetheless, CA production for the mutant was considerably enhanced.

3.4. Conclusions

Sensitivity analysis using the concept of shadow prices has been successfully used for explaining and predicting the effect of various metabolites as independent variables on a specific metabolic objective function. Here, an *in silico* analysis using FBA and a sensitivity analysis showed a trade-off between succinate, acetate and oxaloacetate secretion, and CA production and biomass synthesis. In the case of succinate, the urea cycle, wherein arginine is synthesized, was highly favored. Moreover, it was found that for all the analyzed scenarios, a ratio lower than 2 between arginine synthesis (from the urea cycle) to the net flux of GAP (from both glycolysis and pentose phosphate pathway) was a necessary condition for CA biosynthesis. PhPP analysis showed a positive

effect of oxygen greater than that of glycerol on biomass synthesis and CA production. Further studies on oxygen uptake in *Sc*, e.g., oscillatory oxygen availability, might improve carbon flux through the CA pathway, thus rendering higher titers. The developed model was able to represent different metabolic phenotypes, by means of an FBA and the interpretation of shadow prices.

Acknowledgments

H.R.M thanks Prof. Dr. Rainer Breitling (Unviversity of Manchester, England) for providing the genome scale model of *Sc,* reported by Medema et al. (2010).

Howard Ramirez-Malule, Stefan Junne, Peter Neubauer, Rigoberto Rios-Estepa. A combined FBA and A-stat approach identifies a strong association between the TCA cycle intermediate accumulation and clavulanic acid biosynthesis in *Streptomyces clavuligerus***.** Submitted to *Applied Microbiology and Biotechnology*.

CHAPTER 4

4. A combined FBA and A-stat approach identifies a strong association between the TCA cycle intermediate accumulation and clavulanic acid biosynthesis in *Streptomyces clavuligerus*

HIGHLIGHTS

- A combined FBA and A-stat approach showed a strong association of acetate and TCA cycle intermediate accumulation, with CA production by *Streptomyces clavuligerus*.
- The activation of the glyoxylate pathway was observed under glycerol and phosphate limitation.
- *In silico* identification of the carboxylation of phosphoenolpyruvate (PEP) by PEP carboxylase was consistent with oxaloacetate accumulation and the highest CA production.

Abstract

Clavulanic acid (CA) is produced by *Streptomyces clavuligerus (Sc)* as a secondary metabolite; it exhibits pharmaceutical interest due to its potential to inhibit β-lactamase enzymes, secreted by bacteria as a defense mechanism against β-lactam antibiotics. Due to metabolic limitations, CA titers are low which urges further studies; thus, knowledge about the fate of carbon along the various *Sc* pathways would certainly provide insights about how to optimize productivity. In order to evaluate metabolic patterns and the possible accumulation of TCA cycle intermediates during CA biosynthesis, the accelerostat technique (A-stat) was implemented; an *in silico* approach for explaining carbon flux distribution and how it is related with intermediate accumulation was also used. While achieving steady state conditions, accumulation of succinate, oxaloacetate and

acetate was observed and associated with CA production. Malate accumulated prior to starting the decline of the dilution rate and within the whole A-stat stage. To the best of our knowledge, this is the first work showing a strong association of succinate, oxaloacetate, malate and acetate accumulation, with CA production by *Sc*.

When the strain was exposed to glycerol and phosphate limitation, the activation of the glyoxylate pathway was also observed. Furthermore, the *in silico* identification of the carboxylation of phosphoenolpyruvate (PEP) by PEP carboxylase was consistent with oxaloacetate accumulation and the highest CA production. Based on the *in silico* results, the reaction driven by glutamate dehydrogenase and aspartate aminotransferase became potential candidates for a potential genetic modification so as to obtain a desirable CA-overproducer strain. Finally, Flux balance Analysis (FBA) was used as a tool for explaining the experimental observations. In this regard, a set of simulations was performed by using a genome scale model of *Sc*, constrained by data from the A-stat cultivation; the set up comprised a batch stage and three selected dilution rates within the A-stat stage. The genome scale model showed a good agreement, 10% deviation, on average, between the observed dilution rates and simulated specific growth rates, thus indicating the general validity of this model.

4.1. Introduction

Clavulanic acid (CA) is produced by *Streptomyces clavuligerus (Sc);* it is a secondary metabolite with pharmaceutical interest due to its potential to inhibit β-lactamase enzymes secreted by bacteria, as a defense mechanism against β-lactam antibiotics (Brown et al., 1976; Llarrull et al., 2010). Though CA is produced in submerged cultures under different modes of operation, the higher productivity is achieved in continuous fermentation (Neto et al., 2005). Nevertheless, reaching steady state conditions is time consuming - at least 5 residence times are required - and would eventually lead to genetic modifications as the strain is largely exposed to the same environmental conditions as well as a high risk of contamination. However, an advanced continuous cultivation method such as the accelerostat (A-stat) can

overcome some of the chemostat limitations. The A-stat technique, in which - after reaching steady state conditions - a smooth change in the dilution rate D at a constant acceleration, allows the microorganism to adapt to new environmental conditions (quasi-stationarity), thus rendering information about metabolic patterns at different feeding conditions, in a single test (Albergaria et al., 2000; Kasemets et al., 2003; Paalme et al., 1997; Paalme et al., 1995; van der Sluis et al., 2001).

In most cases, the large scale production of antibiotics is performed at growth-limiting concentrations of inorganic phosphate (Hwang et al., 2014; Ozcengiz and Demain, 2013). Phosphate deficiency plays a remarkable role on glyceraldehyde-3-phosphate (GAP) availability and, indirectly, upon CA synthesis since it is strongly dependent on GAP (Bushell et al., 2006; Ives and Bushell, 1997; Kirk et al., 2000).

There are two main steps involved in CA biosynthesis: the so called early and later steps; the early steps account for the condensation of GAP and arginine to produce *L*-N^2-(2-carboxy-ethyl) arginine by the action of the enzyme N^2-(2-carboxy-ethyl) arginine synthase (CEAS1/CEAS2) (Chen et al., 2003; Khaleeli et al., 1999; Ozcengiz and Demain, 2013). Next, the (3S, 5S)-clavaminic acid intermediate is synthesized in five - well known - continuous reactions (Bachmann et al. 1998; Wu et al. 1995; Zhang et al. 2002). Afterwards, in the later steps, also called the clavam pathway, a partially known series of reactions lead to the accumulation of CA (Ozcengiz and Demain, 2013).

Though academic reports concerning central carbon metabolism and CA biosynthesis are abundant (Bushell et al., 2006; Chen et al., 2003; Ives and Bushell, 1997; Roubos, 2002; Saudagar and Singhal, 2007), experimental reports considering extracellular metabolite and/or a quantitative description of intermediate metabolite accumulation in *Sc* metabolism are rather scarce (Arulanantham et al., 2006; Khaleeli et al., 1999). In Streptomycetes, TCA cycle intermediates are highly demanded when antibiotics are synthesized (Dekleva and Strohl, 1988; Hodgson, 2000). Nevertheless, there are no quantitative descriptions about levels of accumulation and how this is related to clavam metabolism. Attempting to decipher such a puzzle would require not only data for CA and intermediate carbon flux distribution and accumulation, but also a holistic view of its metabolic connectivity,

for which a technique such as Flux Balance Analysis (FBA) would aid. FBA has been traditionally used to predict the metabolic flux distribution of an entire metabolic network; further understanding of cellular metabolism would require experimental data as constraints for FBA calculations and analysis (Stephanopoulos et al., 1998; Villadsen et al., 2011).

In this work, an A-stat cultivation was performed with *Streptomyces clavuligerus* DSM No 41826 for the purpose of explaining levels of accumulation of TCA cycle intermediates and their role on CA production; the experimental set up included *Sc* cultivations at bioreactor scale, using a chemical defined medium, at different dilution rates. FBA, with biomass synthesis and CA production as a composite objective function, was used for explaining experimental observations related to intermediate metabolite consumption and/or accumulation.

4.2. Materials and methods

4.2.1. Microorganism

Streptomyces clavuligerus DSM No 41826 was used throughout this work. Stock cultures were stored at -80°C in a glycerol solution (16.7% v/v).

4.2.2. Culture media and A-stat experimental conditions

In this work, the seed and production medium, described by Roubos et al. (2002) was used. The seed medium had the following composition (in g/L): glycerol 15, soy peptone 15, sodium chloride 3, and calcium carbonate 1, at an initial pH of 6.8. Antifoam 204 (Sigma Inc., St. Louis, MO) was added at a concentration of 1:1000 v/v.

The production medium was slightly modified as follows (in g/L): glycerol 9.3, K_2HPO_4 0.8, $(NH_4)_2SO_4$ 1.26, monosodium glutamate 9.8, $FeSO_4 \times 7H_2O$ 0.18, $MgSO_4 \times 7H_2O$ 0.72, MOPS 10.5 and trace element solution 1.44 [mL]. The composition of the trace element solution was (in g/L): H_2SO_4 (96%) 20.4, citrate $\times 1H_2O$ 50, $ZnSO_4 \times 7H_2O$ 16.75, $CuSO_4 \times 5H_2O$ 2.5, $MnCl_2 \times 4H_2O$ 1.5, H_3BO_3 2 and $Na_2MoO_4 \times 2H_2O$ 2. Antifoam 204 was added at a concentration of 1:1000

v/v. The feeding medium had the same composition as the production medium, except for K_2HPO_4 which was added at a concentration of 0.58 g/L, without MOPS.

Cryotube cell suspensions (1.2 mL) were inoculated into 50 mL of seed medium in a 250 mL UltraYield© shake flask (Thomson Instrument Company, Oceanside, CA). Cells were grown in a rotary shaker incubator for 26 h at 200 rpm and 28 °C. 250 mL UltraYield© shake flasks were filled with 45 mL of production medium and inoculated with 5 mL of cultivated seed broth. Cells were grown for 20 h. The preculture was inoculated at 10% v/v into the reactor medium.

Culture samples (2 mL) were withdrawn at an interval of approx. 12 h. Samples were centrifuged at 15,000 rpm and 4 °C for 10 min; supernatants were used for CA, intermediate metabolites and glycerol quantification, via HPLC-DAD and HPLC-RID. Wet biomass was washed with 0.9% NaCl and centrifuged. Lastly, test tubes were dried over night at 75 °C for dry cell weight determination.

A-stat cultivation was conducted in a 0.5 L bioreactor, using a working volume of 0.3 L, equipped with pH and DO sensors, a cooling bath for temperature control and an exhaust gas device. The strain was grown at 28 °C, with a magnetic stirring, 2 vvm of aeration rate and a constant pH of 6.8, automatically controlled by addition of HCl (1 M). Air supply was started after 5 h of fermentation in order to maintain CO_2 availability as a co-substrate, and to induce the anaplerotic reaction (carboxylation of phosphoenolpyruvate to produce oxaloacetate).

After 36 h of fermentation, the batch mode was switched to continuous and the feeding of fresh medium to the reactor was started. The dilution rate (D) was set to 0.050 h^{-1} based on pre-experimental work. Later on - after 155 h of fermentation - a smooth change (decrease) in the dilution rate was performed with a constant acceleration rate (a) of -0.00039 h^{-2}. The dilution rate profile was represented by the following equation (Paalme et al., 1995):

$$D = D_0 + a * t \quad (1)$$

Where D is the current dilution rate, D_0 is the initial dilution rate, a is the acceleration rate and t is time.

The specific growth rate, μ, the product formation I_P, and substrate consumption I_S, in continuous culture, were determined based on the biomass, product and substrate balance equations, respectively (Paalme et al., 1995):

$$\mu = \frac{1}{X_m}\frac{\Delta X}{\Delta \mathrm{t}} + \frac{1}{V_m}\frac{\Delta V}{\Delta \mathrm{t}} + D_m \quad (2)$$

$$I_p = V_m\frac{\Delta \mathrm{P}}{\Delta \mathrm{t}} + P_m\frac{\Delta V}{\Delta \mathrm{t}} + D_m P_m V_m \quad (3)$$

$$I_s = V_m\frac{\Delta \mathrm{S}}{\Delta \mathrm{t}} + S_m\frac{\Delta V}{\Delta \mathrm{t}} + D_m V_m(S_0 - S_m) \quad (4)$$

Where X_m, V_m, D_m, P_m and S_m are the mean value of biomass concentration, volume, dilution rate, product and substrate, between two consecutive data points, respectively; ΔX, $\Delta \mathrm{t}$, ΔV, $\Delta \mathrm{P}$ and ΔS are the difference of biomass concentration, time, volume, product and substrate, between two consecutive data points, respectively.

For the batch stage, μ and I_P were quantified by applying the following equations (Lee et al., 2009).

$$\mu = \frac{1}{X_m}\frac{\Delta X}{\Delta \mathrm{t}} \quad (5)$$

$$I_p = \frac{1}{X_m}\frac{\Delta \mathrm{P}}{\Delta \mathrm{t}} \quad (6)$$

4.2.3. Analytical Methods

CA was determined by high performance liquid chromatography (HPLC), using a method based on the work of Foulstone and Reading (1982) and Ramirez-Malule *et al*. (Foulstone and Reading, 1982; Ramirez-Malule et al., 2016). Potassium clavulanate vetranal (Sigma-Aldrich) was used for calibration. Samples were derivatized with imidazole and analyzed with an Agilent 1200 system (Agilent Technologies, Waldbronn, Germany) operated at 30 °C with a Zorbax Eclipse XDB-C-18 reverse phase column $(5\ \mu m, 4.6 \times 150\ mm)$, using a C-18 guard column (Phenomenex®), with a flow rate of 1mL/min and diode array detector (DAD). The mobile phase consisted of solvent A (KH_2PO_4 50 mM, pH 3.2) and solvent B (methanol grade HPLC) used in a gradient mode as

follows: linear gradient from 6% to 10% solvent B for 20 min, linear gradient to 76% solvent B for 22 min, 76% solvent B for 10 min and linear gradient to 6% solvent B for 1 min. The clavulanate-imidazole complex was detected at 311 nm. Glycerol was quantified with an Agilent 1200 series HPLC system operated at 15 °C with a HyperREZ^{TM} XP carbohydrate H^+ column (thermo scientific) $(300 \times 7.7\ mm, 8\ \mu m)$, 0.5ml/min flow rate and refractive index detector (RID). The isocratic mode was used with sulfuric acid (5mM) as the mobile phase. This method was also used to quantify metabolite concentrations from central carbon metabolism, such as glucose, oxaloacetate, malate, succinate, acetate, lactate, pyruvate, alpha-ketoglutarate and formate (Junne et al., 2011).

4.2.4. Genome Scale Metabolic Modeling of *Sc*

The metabolic model reported by Medema et al. (2010) was manually curated and used for FBA simulations. The model consisted of the major metabolic pathways i.e., glycolysis, gluconeogenesis, pentose phosphate (PP), tricarboxylic acid cycle (TCA cycle), urea cycle, glyoxylate cycle, anaplerotic reactions, clavam pathway, cephalosporin C biosynthesis, cephamycin C biosynthesis, as well as, the biosynthesis of macromolecular components of biomass such RNA and DNA. The published model has 1492 reactions (1290/202 internal/exchange fluxes) and 1173 metabolites (971/202 internal/external metabolites).

For curation purposes the model was tested and modified according to open scientific literature (Arulanantham et al., 2006; Bushell et al., 2006; Ozcengiz and Demain, 2013; Roubos, 2002) and public databases (KEGG pathways (http://www.genome.jp/kegg/), gene-reaction associations (http://www.enzyme-database.org/)). The Model and Constraint Consistency Checker (MC^3) algorithm was used to identify dead-end metabolites, single-connected metabolites, and zero-flux reactions (Yousofshahi et al. 2013). As a result, gaps were identified and as much reactions as possible were added. The biomass reaction was modified to consider 47 molecules of adenosine diphosphate (ADP) and 47 molecules of inorganic phosphate (pi), which are commonly used

in genome scale models of *Streptomyces coelicolor* and *Mycobacterium tuberculosis* (Alam et al., 2010; Borodina et al., 2005; Jamshidi and Palsson, 2007). The clavam pathway was extended to consider the route of 5s clavams (10 reactions were added); besides, in the transition of clavaminic acid to CA, further reactions were added taking into consideration the metabolites N-glycyl-clavaminic acid and N-acetyl-glycyl-clavaminic acid (one reaction was removed and three reactions were added) (Arulanantham et al., 2006). Likewise, a metabolite named "clavam5s" was added at the end of the 5s clavam route, as this pathway is still under construction (Ozcengiz and Demain, 2013; Zelyas et al., 2008). The exchange and transport reactions for oxaloacetate, clavam-2-carboxylate and alanylclavam were inserted. In summary, a total of 18 reactions were added to Medema´s model. The new model consisted of 1510 reactions (1305/205 internal/exchange fluxes) and 1187 metabolites (982/205 internal/external metabolites); it was validated following standard protocols reported by Palsson (2005) and Lee et al. (2009). The SBML version of the full model is available upon request.

4.2.5. Design of *in silico* experiments

The software COBRA Toolbox v2.0 running in a Matlab® environment, using the Gurobi optimization software, was used to solve all optimization problems (Schellenberger et al., 2011). The genome scale model was constrained with data from a medium mimicking the composition of the medium experimentally used (Supplementary material 1). As for identifying the set of metabolic pathways that were favored and disfavored (pathways which increase or decrease its overall metabolic flux) under A-stat cultivation, and their association with TCA intermediate accumulation and CA production, an *in silico* FBA study was performed. For the purpose of performing comparative analysis among metabolic flux distributions, four points of an A-stat cultivation were selected: one at the batch stage and three dilution rates within the A-stat stage, (0.05, 0.045 and 0.035 h^{-1}). The model was constrained with experimentally determined fluxes of succinate, oxaloacetate, malate, acetate, oxygen, glycerol,

carbon dioxide and/or CA. Additionally, in order to deal with the conflict of metabolic objectives in the cell - which occurs when the CA is synthesized while *Sc* keeps growing at a constant rate - with a maximal enzymatic efficiency for cellular growth, a two-stage optimization procedure was used. First, a Linear Programming (LP) Problem was solved using the maximization of a composite objective function (biomass synthesis and CA production). Second, a NonLinear Programming (NLP) problem, using the minimization of the overall intracellular flux as the objective function, was solved. The NLP problem formulation included two additional constraints obtained from solving the problem at stage one: the biomass flux and the intracellular flux of the reaction catalyzed by phosphoenolpyruvate (PEP) carboxylase were used for the batch stage, whereas, the biomass flux and the intracellular flux of the reaction driven by isocitrate lyase (ICL) were used for the A-stat stage. The above-mentioned additional constraints, used at the second-stage, were based on experimental evidence, found in this work. The use of experimental constraints drastically reduced the solution space for the optimization problem, thus leading to more consistent metabolic phenotypes. This computing environment allowed for calculating the metabolic flux vector for each point - four metabolic scenarios - previously selected in the A-stat cultivation. Differences among flux vectors were used to explain experimental observations. All simulations were carried out in a notebook equipped with a 64-bit, AMD Dual-core A6-4455M running at 2.10 GHz and 4.0 GB RAM memory.

4.3. Results and discussion

4.3.1. A-stat cultivation of *Sc*

Pre-experimental work was performed at different acceleration rates so as to gain knowledge about the best dilution rate to use, so the system would still remain at pseudo steady state (See a scheme of A-stat cultivation of *Sc* in the supplementary material 2). The dilution rate was varied from 0.050 h^{-1} to 0.025 h^{-1} with an acceleration rate constant of -0.00039 h^{-2}. After the first 36 h of

fermentation (batch mode), the culture was kept at a dilution rate of 0.050 h^{-1} for over 4 residence times (τ) and next, gradually decreased to 0.025 h^{-1} in the subsequent 50 hours. Figure 4.1 shows a narrow difference, 10% on average, between the observed dilution rate and specific growth rate, thus indicating the adequacy of the A-stat approach, under the investigated dilution-rate interval.

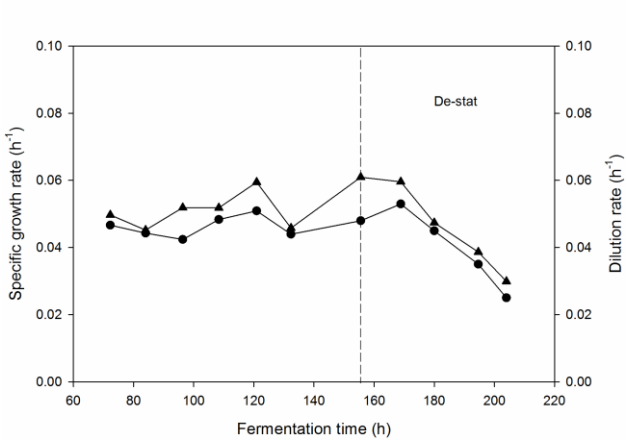

Fig. 4.1. A-stat cultivation of *Sc* exposed to D-gradual variation from D=0.050 h^{-1} to D=0.025 h^{-1}. Notation: Specific growth rate (-▲-) and observed dilution rate (-●-).

Biomass concentration was nearly constant (from 57 h to 155.58 h of fermentation) at a dilution rate of 0.050 h^{-1}; a small biomass reduction (~ 2 g/L) was observed when the dilution rate was changed from 0.050 h^{-1} to 0.025 h^{-1}. Once the culture is exposed to a reduction in the dilution rate, the residence time increases accordingly, and the availability of glycerol gradually decreases (from 0.092 to 0.020 g/L of glycerol between 155.58 and 204 h of fermentation). Consequently, carbon flux through the entire metabolic network gradually diminishes, thus leading to a reduction of intermediate metabolite pools, e.g., TCA cycle intermediates and biomass precursors. The highest CA production was reached at 36 h of fermentation (Fig. 4.2). After that, a clear decrease of CA concentration was observed from 36 to 156 h of cultivation time. At first sight, decreasing of CA concentration is caused by a lower synthesis of CA in the continuous mode. However, CA has been reported to be unstable in synthetic buffer solutions (Ramirez-Malule et al., 2016) and fed batch cultivations (Roubos et al., 2002). Therefore, CA degradation should be considered in the analysis,

and as result, decreasing concentration of CA was probably due to a combined effect of lower synthesis and degradation of CA (See supplementary material 3).

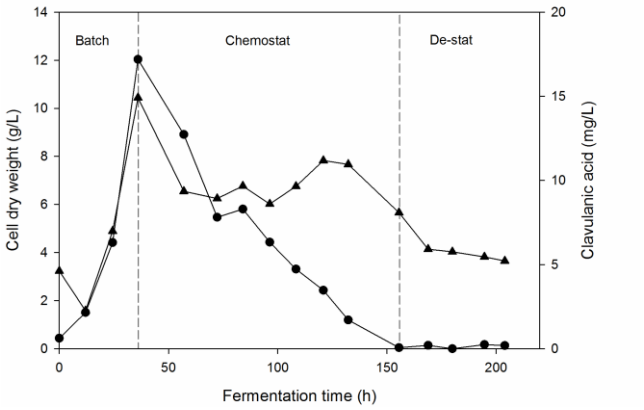

Fig. 4.2. A-stat cultivation of *Sc* indicating cell dry weight (-▲-) and CA (-●-) as a function of fermentation time.

The effect of phosphate concentration on CA production by *Sc* has been well studied (Bushell et al., 2006; Ives and Bushell, 1997; Kirk et al., 2000). However, the accumulation of intermediate metabolites in *Sc* cultures under phosphate limitation is not well documented. Figure 4.3 A shows an accumulation of oxaloacetate at 36 h of fermentation; at this point, there are two potential sources of oxaloacetate: the TCA cycle and the carboxylation of PEP mediated by PEP carboxylase. Oxaloacetate, as aspartate precursor, could eventually direct carbon flux into the urea cycle, thereby promoting the production of the second CA precursor, arginine (Haines et al., 2011). The highest accumulation of oxaloacetate and malate was acquired in the A-stat stage, with glycerol depletion; this accumulation progressively decreased when the dilution rate was varied from 0.050 h^{-1} to 0.025 h^{-1} (see Fig. 4.3 B). Bushell et al. (2006) reported that the CA yield was highly favored when amino acids were fed in chemostat cultivations of *Sc*. The authors found that the feeding of oxaloacetate-family amino acids incremented CA yield by 10-fold, compared with not supplemented chemostat cultivations.

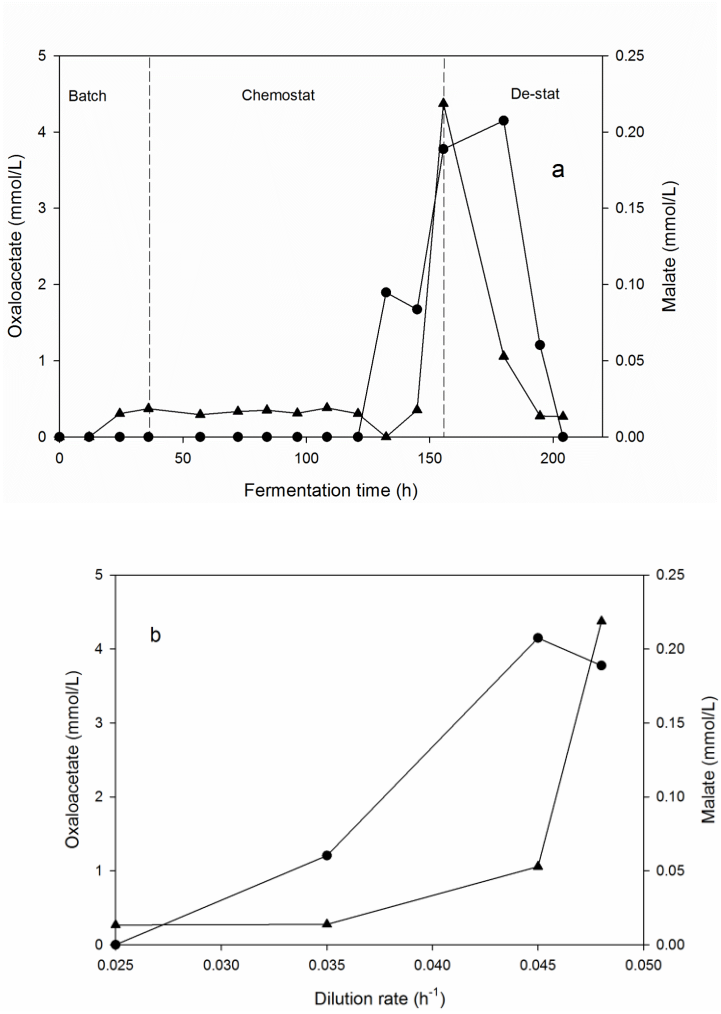

Fig. 4.3. Accumulation of oxaloacetate and malate during A-stat cultivation of *Sc*. A). Time course accumulation of oxaloacetate (-▲-) and malate (-●-) during A-stat cultivation of *Sc.* B) Accumulation of oxaloacetate (-▲-) and malate (-●-) from 0.050 h^{-1} to 0.025 h^{-1} of dilution rate in A-stat cultivation of *S.c*.

Moreover, the role of anaplerotic reactions in primary metabolism of *Streptomycetes* has been widely studied (Dekleva and Strohl, 1988; Hodgson, 2000; Vorisek et al., 1969). Many *Streptomyces* species have showed PEP carboxylase activity for oxaloacetate anaplerotic biosynthesis, e.g., *Streptomyces aureofaciens* (A14), *Streptomyces* C5 and *Streptomyces coelicolor* A3(2) (A21) (Dekleva and Strohl, 1988; Hodgson, 2000; Vorisek et al., 1969). Dekleva and Strohl (1988) observed a minor stimulation of PEP carboxylase by fructose 1,6-bisphosphate and AMP, in *Streptomyces* C5,

whereas oxaloacetate, aspartate, malate, succinate, ATP, citrate and CoASH were reported as severe inhibitors of PEP carboxylase. However, the transition from primary to secondary metabolism led to an increment of PEP carboxylase activity, as a response to the growing demand of TCA intermediates during antibiotic biosynthesis (Dekleva and Strohl, 1988; Hodgson, 2000). Our data showed a transition stage from primary to secondary metabolism at around the 30-36th h of fermentation, concurring with a larger accumulation of CA. Apparently, at this point, PEP carboxylase was active and contributed to the accumulation of oxaloacetate (See Fig. 4.3 A) and the highest CA production (at 36 h of fermentation, Fig. 4.2). Afterward, PEP carboxylase was inhibited by the constant production and accumulation of oxaloacetate and succinate (oxaloacetate: from 36 h of fermentation onwards, Fig. 4.3 A; succinate: from 36 to 120.92 h of fermentation, Fig. 4.4), while CA concentration was ceasing (from 36 h of fermentation onwards, Fig. 4.2).

In the present work, malate and acetate accumulation was also observed during the A-stat cultivation, with acetate being the earliest. Acetyl-CoA, produced either by pyruvate or acetate became accessible to the action of malate synthase that, along with glyoxylate, did produce malate under glycerol and phosphate limitation. The metabolite profiles found in this work showed that malate concentration was increasing with glycerol limitation, mainly between 132.2 and 204 h of fermentation (See Fig. 4.3 A and 4.4). The glyoxylate pathway, a bypass in the TCA cycle, retains two carbon dioxide molecules, and contributes to maintain cell metabolism under limited carbon source availability. Chan and Sim (1998) found a large expression of malate synthase in *Sc* when the strain was exposed to acetate, as a sole carbon source; in contrast, the malate synthase activity was approximately 14-fold lower when glycerol was used. Soh et al. (2001) found that the maximum isocitrate lyase and malate synthase enzymatic activity, under either acetate or glycerol limitation, as the unique carbon source, occurred at the same time and was not associated with biomass accumulation; therefore, it is manifest that the glyoxylate pathway in *Sc* was active under limited carbon source conditions (Soh et al., 2001). Therefore,

based on the malate and acetate accumulation, observed in this work, we argue that the glyoxylate pathway was active under phosphate limitation and glycerol depletion.

Regarding acetate metabolism, it is alternatively related to the formation of N-acetylated clavaminic acid compounds, in the clavam pathway. Crystallographic studies and mass spectrometry analysis have shown a close similarity between *orf14* (acetyl transferase (CBG)) and the GCN5-related acetyltransferase (GNAT) protein (Iqbal et al., 2010; Paradkar, 2013). One important fact was that oxaloacetate was accumulated under either high or limited glycerol concentrations; meanwhile, succinate and acetate were accumulated when glycerol was still available; for the case of malate, it was accumulated with glycerol depletion; all cultures run under phosphate limitation (Fig. 4.3 A and 4.4). Lactate, alpha-ketoglutarate, pyruvate and formate were not detected in this work.

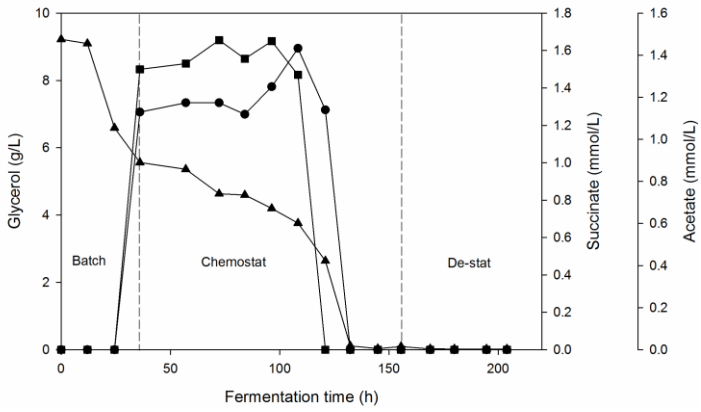

Fig. 4.4. Time course development of glycerol consumption (-▲-), and accumulation of succinate (-●-) and acetate (-■-) in A-stat cultivation in *Sc*.

Coincidentally, when glycerol was below 3.8 g/L and, and the acetate and succinate concentration were progressively decreasing to zero, a slight increment (~1 g/L) on biomass production was observed (from the 108th to the 132th h of fermentation. See Fig. 4.2 and 4.4). Under these circumstances one can argue that both acetate and succinate were eventually co-assimilated by the cell, thus leading to a further biomass precursor production (See also

supplementary material 4). In this regard, Chan and Sim (1998) and Soh et al. (2001) found a relationship between the carbon source (either glycerol or acetate), cell growth and isocitrate lyase activity, where, for both glycerol and acetate, high levels of ICL activity coincided with a decrease in growth. Additionally the authors reported that *Sc* was able to grow on acetate as the sole carbon source.

The role of succinate in anabolic processes of *Sc* is a matter of continuous studies (Dekleva and Strohl, 1988; Hodgson, 2000). Succinate is produced in the TCA cycle; it is also substrate for fumarate biosynthesis. In our experiments, we observed succinate accumulation within the time frame during which CA was accumulated (succinate: from 36 to 120.92 h of fermentation, Fig. 4.4; CA: from 36 h of fermentation onwards, Fig. 4.2); succinate is related to the clavam pathway, where it is released as a byproduct of three intermediate clavam reactions (See Fig. 4.5) (Ozcengiz and Demain, 2013; Townsend, 2002). The enzyme involved in these three reactions is clavaminate synthase, an a-ketoglutarate (a-KG) and a ferrous iron-dependent oxygenase; this enzyme catalyzes the following reactions: (i) deoxiguanidino-proclavaminic acid is hydroxylated to guanidine-proclavaminic acid, (ii) proclavaminic acid to dihydroclavaminic acid, (iii) biosynthesis of clavaminic acid (Krol et al., 1989; Salowe et al., 1991; Solomon et al., 2000; Townsend, 2002; Zhang et al., 2002; Zhou et al., 2001; Zhou et al., 1998). After 36 h of fermentation, CA production declines, and succinate accumulation must decrease accordingly; in contrast, succinate remains invariable for over 100 hours, so a complementary carbon source must be present. Succinate is also released as byproduct by the action of a-KG and a ferrous iron-dependent oxygenase during cephamycin C biosynthesis (Hamed et al., 2013; Ozcengiz and Demain, 2013). Hence, cephamycin C pathway, if active, is a potential source for succinate accumulation. It has been found that *Sc* produces CA and cephamycin C, simultaneously, either in batch or fed-batch mode (Bellão et al., 2013). In fed-batch reactors, fed with glycerol, CA production was higher than that of

cephamycin C; in contrast, cephamycin C was greater than CA production when starch was used (Bellão et al., 2013).

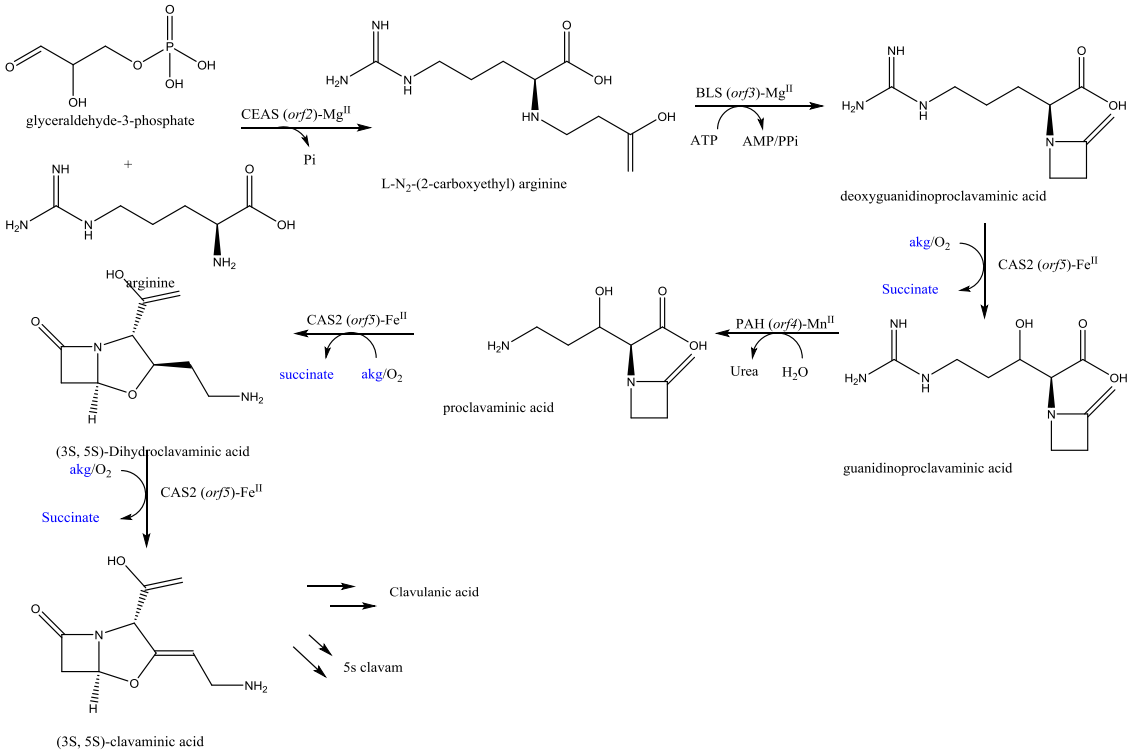

Fig. 4.5. A condensed clavam pathway in *Sc.* Succinate is a byproduct in three reactions catalyzed by clavaminic acid synthase in the presence of an alpha ketoglutarate (akg) dependent oxygenase.

TCA cycle intermediate accumulation has also been observed in *Streptomyces* mutant strains (Colombié et al. 2005; Viollier et al. 2001). Interestingly, the level of accumulation of succinate, oxaloacetate, malate and acetate found in this work - using a wild type strain - were comparable with levels reported in *Streptomyces ambofaciens* and *Streptomyces coelicolor* mutants (Colombié et al. 2005; Viollier et al. 2001). To the best of our knowledge, this is the first report of a strong association of succinate, oxaloacetate, malate and acetate accumulation, with CA production by *Sc*.

4.3.2. Flux Balance Analysis in *Sc* at batch and A-stat stages

FBA was used as a tool for explaining the experimentally proven association between succinate, oxaloacetate, malate and acetate with CA production. For this, a set of simulations was conducted using experimental data from the A-stat cultivation as constraints. Table 4.1 shows a comparison between the experimentally observed dilution rates and the simulated specific growth rates; a good agreement, 10% on average, was observed thus indicating the general validity of the model. Figure 4.6 shows the metabolic flux distribution for the various pathways that the metabolic model did account for.

Table 4.1. Comparison of experimentally observed dilution rates from A-stat cultivation and simulated specific growth rates, using measured fluxes as constraints.

Compounds used as constraints*	**Observed dilution rate D (h^{-1}) and, experimental and simulated specific growth rate μ_{exp}, μ (h^{-1})**							
	Batch stage		**A-stat stage**					
	μ_{exp}	**μ**	**D**	**μ**	**D**	**μ**	**D**	**μ**
	0.063	0.054	0.050	0.050	0.045	0.045	0.035	0.044
Glycerol	-		0.7280		1.1098		0.9679	
O_2	-		1.8481		1.6648		1.6205	
CO_2	-		0.2529		0.0672		0.0228	
Malate	0.0016		0.0016		0.0057		0	
Succinate	0.0140		0		0		0	
Acetate	0.0150		0		0		0	
Oxaloacetate	0.0007		0.0440		0.0291		0	
CA	0.0006		-		-		-	

*Flux units [mmol/(g_{CDW}*h]

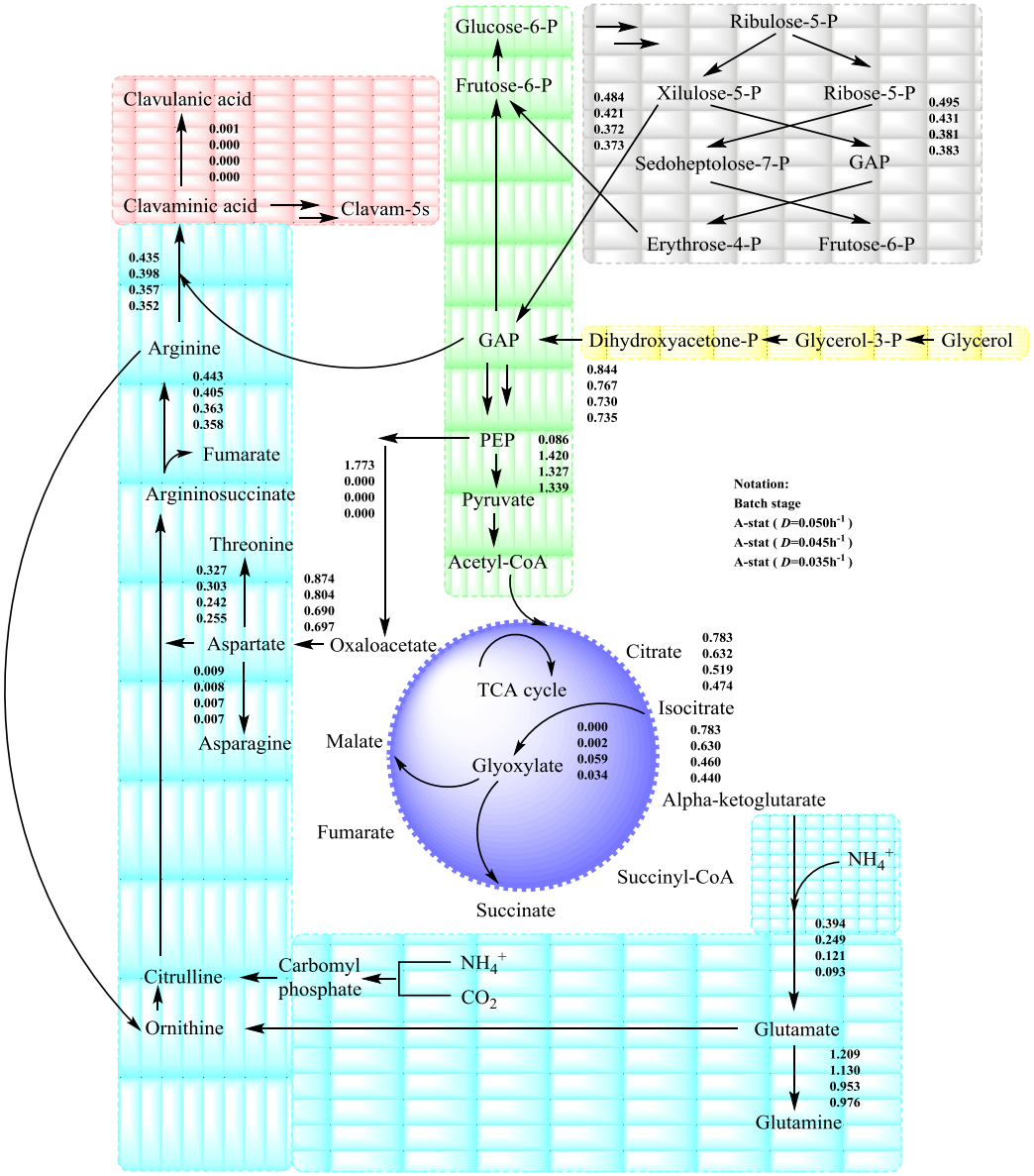

Fig. 4.6. Carbon flux distribution in CA production by *Sc,* at batch and A-stat stages. Units for fluxes were mmol/(g_{CDW}*h). Notation: The flux values correspond to a metabolic flux distribution at batch (36 h of fermentation) and at three selected dilution rates in the A-stat stage (0.05, 0.045 and 0.035 h^{-1}) (top to bottom, respectively).

4.3.2.1. Biomass precursors in A-stat cultivation: amino acid flux profiles

Dilution rates in the chemostat and A-stat mode were nearly the same as the specific growth rate at steady state and quasi steady state, respectively; henceforth, we expected a decreased carbon flux throughout the entire network

of *Sc* when the dilution rates varied from 0.050 h^{-1} to 0.035 h^{-1}. Indeed, fluxes involved in biomass-precursor biosynthesis, were reduced, e.g., the pentose phosphate pathway decreased its overall-flux in a 22.6% on average. A clear example of why biomass synthesis decreased can be seen in the amino acid synthesis, where a decrease in carbon flux was observed (See fluxes of glutamate, glutamine, aspartate, arginine, threonine and asparagine in Fig. 4.6), with the exception of alanine (which increased) and, cysteine and lysine (no presence at all) (See fluxes of alanine, cysteine and lysine in the Supplementary material 5). Ammonia has been reported to induce alanine dehydrogenase (ADH) in *Sc* (Aharonowitz and Friedrich, 1980). In that work, ADH was found in cell free extracts of *Sc*, suggesting it was induced by the presence of ammonia and alanine as nitrogen sources; in contrast, the reductive amination reaction where L-alanine is obtained from pyruvate, was strongly inhibited by alanine, serine and NADPH. Our results suggest that ADH was highly active during the A-stat stage, as the reduced nitrogen assimilation (See the glutamate flux in Fig. 4.6) would allow for a larger availability of ammonia in the medium and the induction of ADH.

According to Monod kinetics and the background of the continuous cultivation theory, one would expect that the glycerol concentration, and assimilation, both decrease with a decreasing dilution rate D (Enfors, 2011). Interestingly, an slight increment in the glycerol exchange reaction was experimentally determined when the dilution rate varied from 0.050 h^{-1} to 0.035 h^{-1} (Table 4.1). Moreover, GAP and arginine have been reported as the main precursors of CA biosynthesis and the starting point for clavam-compounds biosynthesis (Bascarán et al., 1989; Bushell et al., 2006; Khaleeli et al., 1999; Li et al., 2000; Valentine et al., 1993). GAP is a glycolytic intermediate, so its intracellular pool depends greatly on the activity of both glycolysis and gluconeogenesis; accordingly, GAP availability rather than arginine is commonly considered as the bottleneck for CA production (Ives and Bushell, 1997). Our simulation results showed a reduction in the pool of GAP and arginine under the four tested environmental conditions, and an adverse effect on the clavam pathway and CA

biosynthesis (See fluxes of arginine and the reactions where GAP is involved in Fig. 4.6). This instance was consistent with the decline of alpha-ketoglutarate carbon flux (76.4%) towards glutamate, a reaction mediated by glutamate dehydrogenase; these compounds are direct precursors of the urea cycle where arginine is synthesized. Furthermore, the oxidative activity in TCA cycle was limited, thus leading to a lower level of TCA cycle intermediates (39.4% and 43.8%, less flux, for isocitrate and alpha-ketoglutarate, respectively) and an active glyoxylate pathway.

4.3.2.2. FBA at the batch stage: Activation of PEP carboxylase

As previously mentioned, malate and oxaloacetate were reported as severe inhibitors of PEP carboxylase in *Streptomyces* C5 (Dekleva and Strohl, 1988). In the experimental part of this work, malate and oxaloacetate were accumulated with values up to 0.0057 mmol/(g_{CDW}*h^{-1}) and 0.0440 mmol/(g_{CDW}*h^{-1}), respectively (Table 4.1), during the decrease of the dilution rate (from 0.050 h^{-1} to 0.035 h^{-1}). The model suggests that PEP carboxylase was deactivated under these environmental conditions by the inhibitory effect of malate and oxaloacetate. The reaction driven by PEP carboxylase, where oxaloacetate was produced from PEP, was not active since the carbon flux through this irreversible reaction was zero at the three dilution rates evaluated; in contrast, PEP carboxylase was highly active - with a flux value of 1.773 mmol/(g_{CDW}*h) - at the batch stage where CA acquired its highest yield. In *Streptomyces* species, PEP carboxylase has been reported active during the synthesis of antibiotics (Dekleva and Strohl, 1988; Hodgson, 2000).

Likewise, a substantial increment of the flux from PEP towards pyruvate was observed during the four evaluated environmental conditions (See pyruvate in Fig. 4.6). Interestingly, while the metabolic flux mediated by pyruvate kinase incremented, PEP carboxylase was turned off within the A-stage, clearly a tradeoff between pyruvate kinase and PEP carboxylase. Indeed, in the batch stage the highest flux value of PEP carboxylase coincided with the lowest flux value of pyruvate i.e., CA biosynthesis fitted with a high PEP carboxylase enzymatic activity and a reduced activity of pyruvate kinase. Undoubtedly,

oxaloacetate production, via PEP carboxylase, plays an important role in CA biosynthesis. The positive influence of the oxaloacetate amino acid family on CA production has been already studied by means of feeding experiments, using oxaloacetate, aspartate, threonine and arginine as supplement in chemostat cultivation (Bushell et al., 2006). Coincidently, in this work, the accumulation of oxaloacetate and succinate agreed with a larger CA production.

4.3.2.3. FBA at the A-stat stage: Activation of ICL

Regarding the reaction mediated by ICL, the model did predict the experimentally proved activation of the glyoxylate pathway, at the A-stat stage of this work, due to the fact that the irreversible reaction catalyzed by ICL was active (See glyoxylate flux in Fig. 4.6). The activation of ICL was eventually caused by glycerol and phosphate depletion during the A-stat stage. Unexpectedly, malate synthase was off, thus proving the FBA limitations under certain special circumstances e.g., the presence of parallel pathways without any related flux measurement (special case: glyoxylate to malate, glyoxylate to glycine) (Wiechert, 2001). Moreover, at the batch stage, where higher CA titers were experimentally obtained, the glyoxylate shunt was off, allowing the TCA cycle to run in the oxidative direction, providing arginine's precursors such as alpha-ketoglutarate and oxaloacetate. In fact, TCA cycle intermediates showed the highest flux values in batch stage. Despite the noteworthy increase in the carbon flux driven by pyruvate kinase, a moderate decrease of its flux - 5.7% on average - was observed at the A-stat stage. A further decrease of the fluxes in the TCA cycle - within A-stat stage - was also observed.

4.3.2.4. TCA intermediate - CA production metabolic relationships

As previously highlighted, CA concentration was close to zero at the A-stat stage, while at the batch stage CA reached its highest titer. We also have discussed about the proven association between the TCA cycle intermediates and CA production, and the importance of the pools of oxaloacetate-aspartate, alpha-ketoglutarate-glutamate, and their role in the synthesis of the anabolic precursors of CA. In this regard, the analysis will focus on the effect of the

possible physiological flux ratio that eventually would regulate carbon flux distribution in early steps of the clavam pathway. Figure 4.7 shows flux-ratio profiles for some combinations of the above-mentioned metabolites. Increments of flux-ratio of aspartate/glutamate and aspartate/alpha-ketoglutarate were observed.

The flux-ratio for aspartate/glutamate had a substantial increment (237% on average, from batch to $D = 0.035$ h^{-1}), thus showing a clear decreasing trend of the carbon flux in the oxidative direction of the TCA cycle (See Fig. 4.7). This instance was caused likely by glycerol and phosphate depletion, which possibly triggered an activation of glyoxylate pathway within the A-stat stage. The flux-ratio for aspartate/arginine was rather constant since aspartate is a direct precursor of arginine. In mammals, the reaction mediated by argininosuccinate synthetase - where citrulline and aspartate condense to form argininosuccinate - has been reported to be the rate-limiting step under circumstances where the urea cycle runs maximally (Haines et al., 2011, Morris Jr, 1992). Therefore, argininosuccinate synthetase might regulate carbon flux towards the synthesis of arginine, thus rendering an invariable flux-ratio profile of aspartate/arginine. On the contrary, the glutamate/arginine flux-ratio decreased in a 71%. Here, the intracellular flux toward glutamate (a reaction mediated by glutamate dehydrogenase where alpha-ketoglutarate, together with urea, were used as co-substrate), suffered a severe diminution (76.9%), while aspartate metabolic flux ceased around 20.1%. The tendency for the flux-ratio of aspartate/alpha-ketoglutarate arose modestly. The activation of the glyoxylate shunt allows for producing succinate and malate; the latter is used as substrate to generate oxaloacetate, which is a precursor of aspartate. This circumstance let to obtain more aspartate than alpha-ketoglutarate. The non-accumulation of succinate and the absence of CA during the A-stat cultivation mode was an indicative of the potential blocked condition of the clavam pathway. Indeed, the *in silico* results showed an imbalance between aspartate and glutamate fluxes at A-stat stage with a strong negative effect on the arginine biosynthesis (See arginine in Fig. 4.6 and 4.7).

In summary, a clear relationship between aspartate and glutamate with CA production is notorious; this association has an effect on the other TCA cycle intermediates. Consequently, the reactions driven by glutamate dehydrogenase and aspartate aminotransferase could eventually be considered as potential metabolic targets for further genetic modification so as to obtain over-producer *Sc* strains.

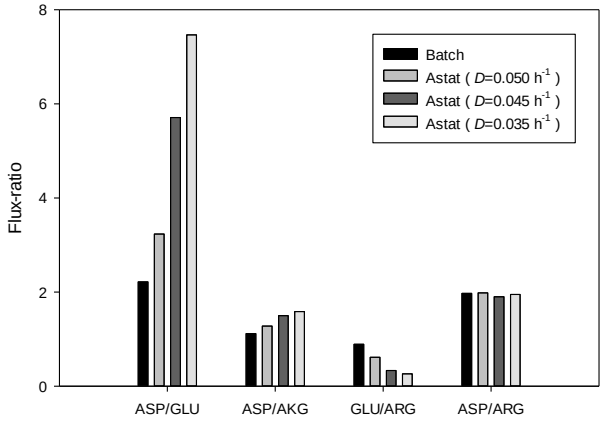

Fig. 4.7. Flux ratio profiles for the intracellular fluxes of aspartate (ASP), glutamate (GLU), alpha-ketoglutarate (AKG) and arginine (ARG). Notation: The flux ratio values correspond to data from a metabolic flux distribution of an A-stat cultivation at batch (36 h of fermentation) and three selected dilution rates within the A-stat stage, 0.05, 0.045 and 0.035 h^{-1}.

4.4. Conclusions

In this work, a strong association between the accumulation of succinate, oxaloacetate, malate and acetate with CA production in *Sc,* was encountered. The activation of glyoxylate pathway, wherein malate is generated by condensation of glyoxylate and acetyl-CoA over action of malate synthase, when the strain was exposed to glycerol and phosphate limitation, was also found. The reaction catalyzed by PEP carboxylase was consistent with oxaloacetate accumulation and the highest CA production. Furthermore, CA biosynthesis coincided with the accumulation of oxaloacetate, succinate and acetate during the batch period, and while achieving steady state; in contrast, when CA was depleted, malate was

accumulated just before starting the A-stat stage and at the point when D decreased to 0.025 h^{-1}. These results demonstrated the close relationship between TCA intermediates and CA production, and could give rise to potential metabolic targets for obtaining a desired CA-overproducer strain; the reactions conducted by glutamate dehydrogenase and aspartate aminotransferase are potential candidates for this purpose. The genome scale model showed a good agreement between the observed D and simulated specific growth rates, and the model, was capable of representing the metabolic patterns found in this work, indicating its general validity.

Acknowledgments

H.R.M. thanks the German Academic Exchange service (DAAD) for financial support. H.R.M. thanks Prof. Enfors and Victor Lopez-Agudelo for the valuable discussion about *in silico* A-stat simulation. H.R.M also thanks Prof. Dr. Rainer Breitling (University of Manchester, England) for providing a base genome scale model of *Sc,* reported by Medema et al. (2010).

4.5. Supplementary material

Supplementary material 1

Table S4.1: *In silico* medium containing the same composition of the experimental medium.

***In silico* medium composition**		
'EX_h(e)'	h[e] <=>	Hydrogen
'EX_k(e)'	k[e] <=>	Potassium
'EX_glu_L(e)'	glu_L[e] <=>	L-Glutamate
'EX_pi(e)'	pi[e] <=>	Phosphate
'EX_na1(e)'	na1[e] <=>	Sodium
'EX_cit(e)'	cit[e] <=>	Citrate
'EX_cu2(e)'	cu2[e] <=>	Copper
'EX_fe2(e)'	fe2[e] <=>	Iron
'EX_glc_D(e)'	glc_D[e] <=>	Glucose
'EX_h2o(e)'	h2o[e] <=>	Water
'EX_glyc(e)'	glyc[e] <=>	Glycerol
'EX_mg2(e)'	mg2[e] <=>	Magnesium
'EX_mn2(e)'	mn2[e] <=>	Manganese
'EX_nh4(e)'	nh4[e] <=>	Ammonium
'EX_so4(e)'	so4[e] <=>	Sulfate
'EX_o2(e)'	o2[e] <=>	Oxygen

Supplementary material 2

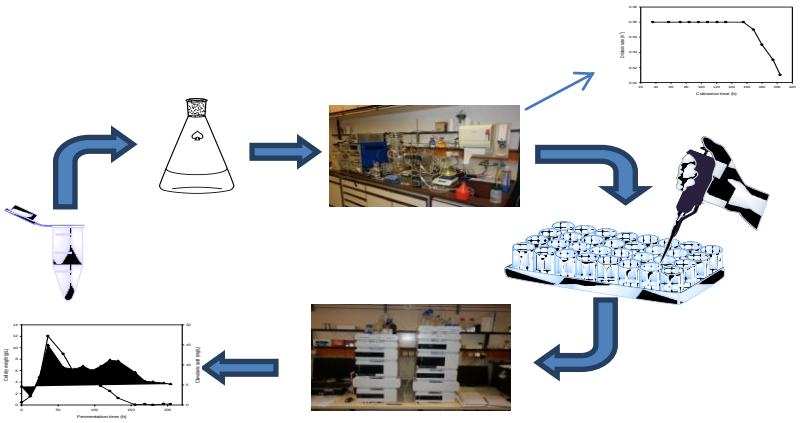

Fig. S4.1. Scheme for A-stat cultivations in *Streptomyces clavuligerus*.

Supplementary material 3

CA has been reported to be unstable in synthetic buffer solutions (Ramirez-Malule et al., 2016) and fed batch cultivations (Roubos et al., 2002). If *Sc* either halts or decreases CA production, the continuous feeding will severely affect the concentration of CA. Nonetheless, if CA is produced at the same rate as the feeding conditions, its concentration must remain invariable despite the continuous feeding.

Due to its unstable nature CA concentration decreases once *Sc* halts CA biosynthesis, at the end of the batch phase. Actually there are three scenarios: (i) CA is still produced after the batch phase with no further degradation, (ii) a simultaneous production and degradation of CA is present, (iii) *Sc* stops CA biosynthesis after the batch phase; CA present is further degraded.

The dilution effect of CA, caused by continuous feeding, was simulated assuming that *Sc* stopped CA production at the end of batch phase and CA was no further degraded in the continuous mode (see the model below). The results are shown in the figure below. Experimental CA concentrations were higher than the *in silico* ones, which might be

caused by CA production during the chemostat stage. However, with this analysis one cannot differentiate if scenario (i) or (ii) was actually present.

Model description: I did a product mass balance, in this case CA, in a continuous culture. The general mass balance equation is the following:

$$accumulation\ within\ system\ =$$

$$(flow\ in\ through\ system\ boundaries) + (generation\ within\ system)$$

$$-(flow\ out\ through\ system\ boundaries) - (consumption\ within\ system)$$

Assumptions:

Flow in through system boundaries = 0

Generation within system = 0,

Consumption within system ("degradation") = 0,

Therefore, the final equation is the following:

$$accumulation\ within\ system\ = -(flow\ out\ through\ system\ boundaries)$$

$$\frac{dCA}{dt} = -\frac{F}{V} * CA$$

But, $D = \frac{F}{V}$, where D is dilution rate.

$$\therefore\ \frac{dCA}{dt} = -D * CA$$

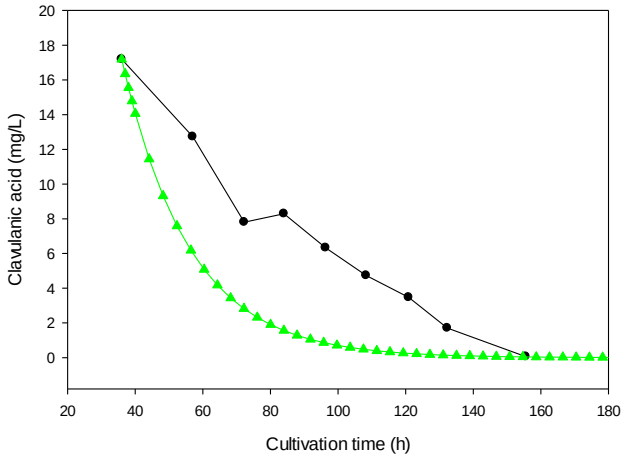

Fig. S4.2. Comparison between the experimentally observed clavulanic acid concentration in A-stat cultivation and the *in silico* results. Note: (-▲-) and (-●-) indicates *in silico* and experimental clavulanic acid concentration as a function of cultivation time, respectively.

Supplementary material 4

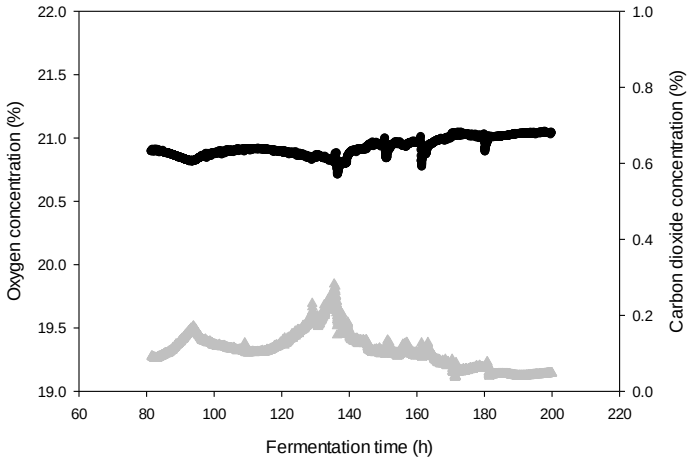

Fig. S4.3. Oxygen (black circles) and carbon dioxide (gray triangles) concentration as a function of fermentation time.

Profiles for oxygen and carbon dioxide concentration during the continuous fermentation mode of *Sc* were rather constant, except for a small change around t = 120 h, possibly caused by co-assimilation of acetate and succinate. This circumstance coincided with a slight increment in biomass synthesis.

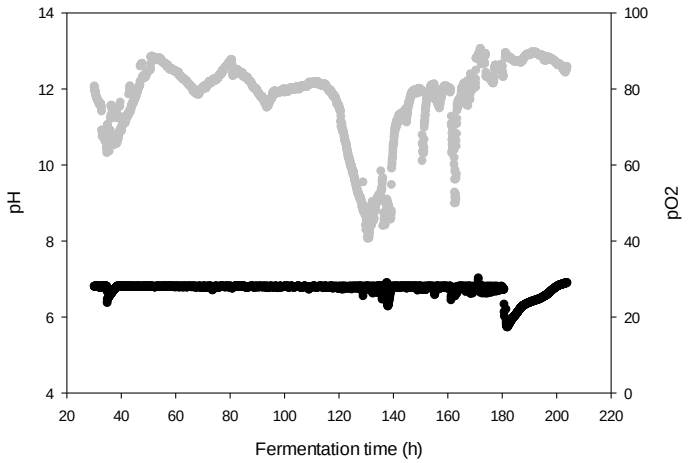

Fig. S4.4. pH (black circle) and pO_2 (gray triangle) profiles along the fermentation time.

pH was rather constant along the fermentation time while pO_2 had a similar behavior but with a slight decrement about 120 h. This instance was likely caused by an increment of biomass synthesis and due to the co-assimilation of acetate and succinate.

Supplementary material 5

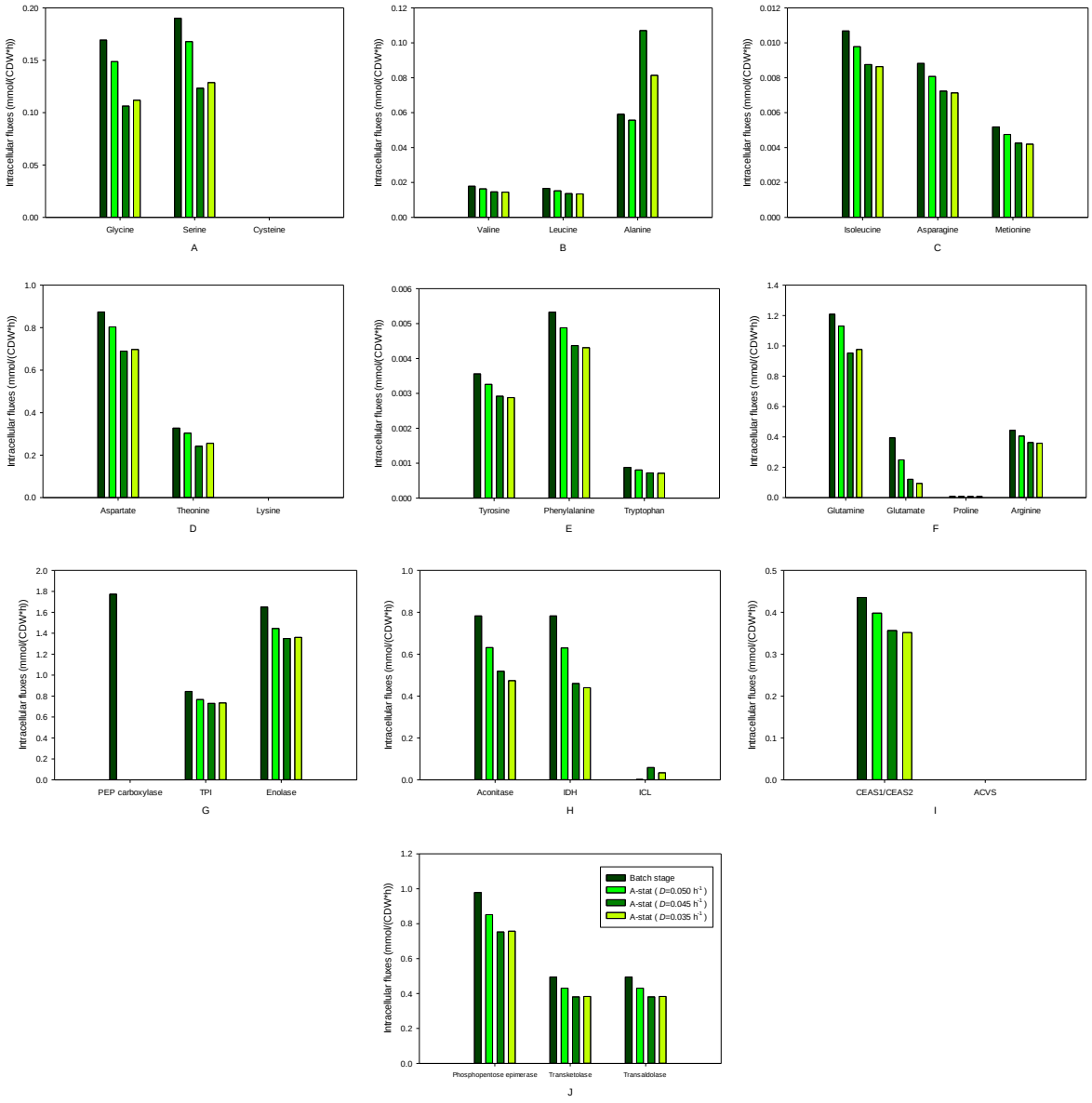

Fig. S4.5. A selected group of intracellular fluxes through metabolic network of *Sc* at batch and A-stat stages. A, the 3-phosphoglycerate-family amino acids. B, the pyruvate-family amino acids. C and D, the oxaloacetate-family amino acids. E, the PEP and erythrose-4-phophate family amino acids. F, The alpha-ketoglutarate-family amino acids. G, glycolysis pathway. H, TCA cycle. I, Clavam pathway and cephamycyn C biosynthesis. J, pentose phosphate pathway. Flux units [mmol/(g_{CDW}*h]

Notation:

TPI: triose-phosphate isomerase

IDH: isocitrate dehydrogenase

ICL: isocitrate lyase

CEAS1/CEAS2: N^2-(2-carboxy-ethyl) arginine synthase

ACVS: δ-(L-α-aminoadipyl)-L-cysteinyl-D-valine synthetase

Published as: **Ramirez-Malule, H**., Restrepo, A., Cardona, W., Junne, S., Neubauer, P., Rios-Estepa, R., 2016. Inversion of the stereochemical configuration (3S,5S)-clavaminic acid into (3R,5R)-clavulanic acid: A computationally-assisted approach based on experimental evidence. J. Theor. Biol. 395, 40–50. doi:10.1016/j.jtbi.2016.01.028

CHAPTER 5

5. Inversion of the stereochemical configuration (3S, 5S)-clavaminic acid into (3R, 5R)-clavulanic acid: A computationally-assisted approach based on experimental evidence

HIGHLIGHTS

- An accumulation of acetate was experimentally observed when CA was synthesized by *Streptomyces clavuligerus*.
- A possible reaction mechanism for acetate incorporation into the N-acetyl-glycyl-clavaminic chemical structure was proposed.
- A computational-based approach was used to asses a proposed two stages reaction mechanism, for which the enzyme-driven reaction is considered to occur just for the second step; in contrast, the first step, was thermodynamically feasible.
- A novel double epimerization for the inversion of the stereochemical configuration (3S, 5S)-clavaminic acid into (3R, 5R)-clavulanic acid, using proline racemase, was proposed.

Abstract

Clavulanic acid (CA), a potent inhibitor of β-lactamase enzymes, is produced in *Streptomyces clavuligerus* (*Sc*) fermentation processes, for which low yields are commonly obtained. Improved knowledge of the clavam biosynthetic pathway, especially the steps involved in the inversion of 3S-5S into 3R-5R stereochemical configuration, would help to eventually identify bottlenecks in the pathway. In this work we study the role of acetate in the CA biosynthesis by a combined continuous-culture

and computational simulation approach. From this we derived a new model for the synthesis of N-acetyl-glycyl-clavaminic acid (NAG-clavam) by *Sc*.

Sc cultures were kept at a dilution rate of 0.05 h^{-1} for over four residence times(τ) with constant biomass concentration. An accumulation of acetate was observed when CA was synthesized; acetate concentration was rather constant with an average of 1.39 mmol/L. Acetylated compounds, such as NAG-clavam and N-acetyl-clavaminic acid, have been reported in the clavam pathway. Although the acetyl group is present in the β-lactam intermediate NAG-clavam, it is unknown how this group is incorporated to the molecule. Hence, under the consideration of the experimentally proven accumulation of acetate during CA biosynthesis, and the fact that an acetyl group is present in the NAG-clavam structure, a computational evaluation of the tentative formation of NAG-clavam was performed for the purpose of providing further understanding. The calculations suggest that for the proposed reaction mechanism, the reaction proceeds until completion of the first step, without the direct action of an enzyme, where acetate and ATP are involved. For this step, the computed activation energy was ≅ 2.82 kcal/mol while the reaction energy was ≅ 2.38 kcal/mol. As this is an endothermic chemical process with a relatively small activation energy, the reaction rate should be considerably high. The calculations offered in this work should not be considered as a definite characterization of the potential energy surface for the reaction between acetate and ATP, but rather as a first approximation that provides valuable insight about the reaction mechanism. Finally, a complete route for the inversion of the stereochemical configuration from (3S, 5S)-clavaminic acid into (3R, 5R)-clavulanic acid is proposed, including a novel alternative for the double epimerization using proline racemase and NAG-clavam formation.

Keywords: Clavulanic acid, acetate, accumulation, N-acetyl-glycyl-clavaminic acid, reaction mechanism, potential energy surface.

5.1. Introduction

Clavulanic acid (CA) is a potent β-lactamase inhibitor produced by *Streptomyces clavuligerus* (*Sc*) (Brown et al., 1976; Llarrull et al., 2010). CA is used in

combination with β-lactam antibiotics to treat infections caused by β-lactamase-producing pathogens (Elander, 2003; Ozcengiz and Demain, 2013). CA biosynthesis is preceded by the condensation of a C-5 precursor, arginine, and a C-3 precursor, glyceraldehyde-3-phosphate (GAP), thus leading to the so-called clavam pathway.

The clavam pathway, where CA is synthesized, can be divided into the so-called "early" and "late" steps. The "early" steps are widely accepted; in contrast, some steps of the "late" fraction of the pathway remain unclear or even unknown. The clavam biosynthetic pathway starts with the condensation of arginine and GAP, wherein *L*-N^2-(2-carboxy-ethyl) arginine is obtained by the action of the enzyme N^2-(2-carboxy-ethyl) arginine synthase (CEAS1/CEAS2), in a thiamin diphosphate-dependent reaction (Arulanantham et al., 2006; Khaleeli et al., 1999; Ozcengiz and Demain, 2013). Next, the (3S, 5S)-clavaminic acid intermediate is synthesized in five continuous reactions; these reactions have been characterized, and their enzymes identified. β-lactam synthetase (BLS1/BLS2) is responsible for the deoxyguanidinoproclavaminic acid formation, whereas proclavaminic acid is produced by proclavaminate amidino hydrolase (PAH1/PAH2) (Bachmann et al., 1998; Wu et al., 1995). Finally, three of these reactions are catalyzed by clavaminic acid synthase with an alpha ketoglutarate-dependent oxygenase, yielding clavaminic acid (Zhang et al., 2002). At this point, the carbon flux splits into two different ways leading to CA and 5S clavam-compound biosynthesis (Fig. 5.1).

The reaction mechanism under which (3S, 5S)-clavaminic acid is converted into the intermediate (3R, 5R)-clavaldehyde is still not clearly understood (Arulanantham et al., 2006). Although compounds such as N-acetyl-clavaminic acid and NAG-clavam have been encountered in an uncharacterized - non CA producer - mutant strain of *Sc,* called *dcl-8,* their provenances remain unknown (Elson et al., 1988). Jensen et al, (2004) demonstrated that NAG-clavam accumulation was caused by the mutation of either *orf15* or *orf16* in *Sc*; N-glycyl-clavaminic acid was also detected, as a mixture with clavaminic acid, by HPLC and mass spectrometric analysis (Jensen et al., 2004). Despite the fact that

NAG-clavam, N-glycyl-clavaminic acid and N-acetyl-clavaminic acid have been detected in *Sc* cultures, only the origin of N-glycyl-clavaminic acid is clearly known (Arulanantham et al., 2006).

An expansion of the knowledge of the "late" steps of the clavam pathway, especially the steps of inversion of 3S-5S into the 3R-5R stereochemical configuration, would favor understanding of the CA biosynthesis route and eventually identify the bottleneck(s) which are responsible for the low titers.

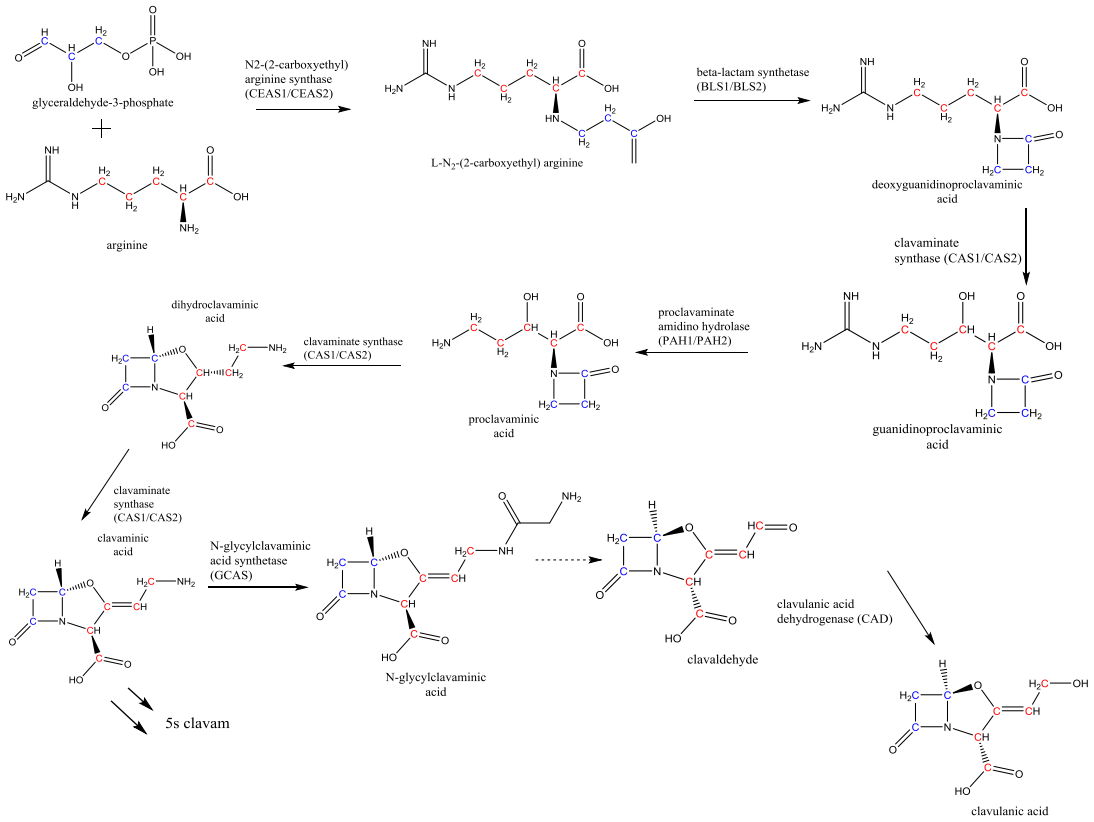

Fig. 5.1. Condensed clavam biosynthetic pathway. Color Code: red and blue C correspond to carbon atoms from arginine and glyceraldehyde-3-phosphate, respectively.

The intricacies of chemical transformations and the associated description of molecular evolution, in the form of reaction mechanisms, are particularly suited for high level computation using the sophisticated tools of quantum mechanics; a

limited sample of studies is listed in the bibliography (Cardona et al., 2013; Cramer, 2004; Gonzalez et al., 1996; Hase et al., 1999; Jaramillo et al., 2010; Leach, 2001; Orrego et al., 2009). A comprehensive picture of the state of the art of the use of computations in studying reaction mechanisms is provided in the references within those works, especially the works by Cramer, Leach and Hase. Cardona et al. (2013) used computer calculations for a better understanding of previously reported experimental measurements of antileishmanial activity and cytotoxicity of a set of 43 compounds, where β-unsaturated lactone rings, as Michael acceptors, had a correlation with biological activity. Although there are reports in biological system using computer calculations, as far as we know this type of studies in the clavam pathway are still missing.

In this work, we present data from an initial non stationary phase of a chemostat culture of *Sc* DSM No 41826 in a 0.5 L reactor using a chemically defined medium. Acetate was accumulated during CA production; a computational analysis proposes a possible reaction mechanism that explains how this is linked with the NAG-clavam formation.

5.2. Materials and methods

5.2.1. Microorganism

Streptomyces clavuligerus DSM No 41826 was used throughout this work. Stock cultures were stored at -80°C in a glycerol solution (16.7% v/v).

5.2.2. Culture media and experimental conditions

In the present work, the seed and production medium described by Roubos et al. (2002) was used. The seed medium had the following composition (in g/L): glycerol 15, soy peptone 15, sodium chloride 3, calcium carbonate 1 at an initial pH of 6.8. Antifoam 204 (Sigma Inc., St. Louis, MO) was added at a concentration up to 1:1000 v/v whenever needed.

The production medium composition was (in g/L): glycerol 9.3, K_2HPO_4 0.8, $(NH_4)_2SO_4$ 1.26, monosodium glutamate 9.8, $FeSO_4*7H_2O$ 0.18, $MgSO_4*7H_2O$ 0.72, MOPS 10.5 and trace element solution 1.44 [mL]. The composition of the trace element solution was (in g/L): H_2SO_4 (96%) 20.4, citrate*$1H_2O$ 50, $ZnSO_4*7H_2O$ 16.75, $CuSO_4*5H_2O$ 2.5, $MnCl_2*4H_2O$ 1.5, H_3BO_3 2 and $Na_2MoO_4*2H_2O$ 2. Antifoam 204 was added into the production medium at a concentration of 1:1000 v/v. The reactor medium had the same composition as the production medium, whereas the feed, containing no MOPS, had the same composition as the production medium, except for K_2HPO_4, which was added at a concentration of 0.58 g/L.

Cryotube cell suspensions (1.2 mL) were inoculated into 50 mL of seed medium in a 250 mL UltraYield© shake flask (Thomson Instrument Company, Oceanside, CA). Cells were grown for 26 h in a rotary shaker incubator at 200 rpm at 28 °C. 250 mL UltraYield© shake flasks were filled with 45 mL of production medium and inoculated with 5 mL of cultivated seed broth. Cells were grown for 20 h. The preculture was inoculated at 10% v/v into the reactor medium.

Culture samples (2 mL) were withdrawn at approximately 12 h intervals. Samples were centrifuged at 15,000 rpm and 4 °C for 10 min; supernatants were used for CA, acetate and glycerol quantification, via HPLC-DAD and HPLC-RID. Wet biomass was washed with 0.9% NaCl and centrifuged. Finally, test tubes were dried over night at 75 °C for dry cell weight determination.

Chemostat cultivation was conducted in a 0.5 L bioreactor, with a working volume of 0.3 L, equipped with pH and DO sensors, cooling bath for temperature control and exhaust gas device. The strain was grown at 28 °C, with magnetic stirring, 2 vvm of aeration rate and a constant pH of 6.8, automatically controlled by addition of HCl (1 M). Air supply was started after 5 h of fermentation in order to maintain CO_2 availability as co-substrate, and to induce the anaplerotic reaction (carboxylation of phosphoenolpyruvate to produce oxaloacetate). After

36 h of batch fermentation, the dilution rate (D) was set to 0.05 h^{-1}, based on pre-experimental work.

5.2.3. Analytical methods

CA was determined by high performance liquid chromatography (HPLC) using a developed method based on Foulstone and Reading (1982). Potassium clavulanate vetranal (Sigma-Aldrich) was used for calibration purposes. Samples were derivatized with imidazole and analyzed in an Agilent 1200 Series HPLC system (Foulstone and Reading, 1982); data analysis was carried out by Agilent Chemstation software; temperature was set at 30 °C; a Zorbax Eclipse XDB-C-18 reverse phase column $(5\ \mu m, 4.6 \times 150\ mm)$, C-18 cartridge of precolumn (Phenomenex®, Aschaffenburg, Germany), 1mL/min flow rate and diode array detector (DAD), were used. The mobile phase consisted of solvent A (KH_2PO_4 50 mM, pH 3.2) and solvent B (methanol HPLC grade) used in a gradient mode as follows: linear gradient from 6% to 10% solvent B for 20 min, linear gradient from 10% to 76% solvent B for 22 min, 76% solvent B for 10 min and linear gradient to 6% solvent B for 1 min. The clavulanate-imidazole complex was detected at 311 nm.

Glycerol was determined by HPLC-RID. The Agilent technology 1200 series HPLC system was operated at 15 °C with a HyperREZ XP carbohydrate H^+ column (thermo scientific) 300*7.7 mm, 8 µm, 0.5ml/min flow rate and refractive index detector (RID). The isocratic mode was used with sulfuric acid (5mM) as the mobile phase. This method was also used for acetate determination (Junne et al., 2011).

5.2.4. Description of the calculations

Several degrees of sophistication are available for the application of quantum mechanics to the electronic structure of atoms and molecules (Szabo and Ostlund, 1989). These all involve solving the time-independent Schrödinger equation.

$$H\Psi = E\Psi \quad (1)$$

This is an Eigen-value based equation, comprising the molecular Hamiltonian equation (H) acting on the molecular wave functions (Ψ) to recover the very same function multiplied by the energy (E) of the molecular system. In atomic units, under the Born–Oppenheimer approximation, for a system containing *n* electrons and *N* nuclei, the molecular Hamiltonian equation becomes:

$$H = -\frac{1}{2}\sum_{i=1}^{n}\nabla_i^2 - \sum_{i=1}^{n}\sum_{A=1}^{N}\frac{Z_A}{r_{iA}} + \sum_{i=1}^{n}\sum_{j>i}^{n}\frac{1}{r_{ij}} \quad (2)$$

Here, r defines distances between particles. The first term measures the kinetic energy of the electrons, the second term describes the collective interaction between all electrons with all nuclei, while the third term corresponds to the electric repulsion among all electron pairs. With this Hamiltonian equation, Schrodinger's equation (1) becomes a second order differential equation in partial derivatives with non separable variables. Unfortunately, this sort of equations do not possess known analytical solutions, thus, approximation methods have to be used. In this work, PM3 (Parameterized Model number 3) was used for all calculations (Stewart, 1991, 1989a, 1989b). Due to the impossibility of analytically solving equation 1, PM3 uses experimental data to parameterize the molecular Hamiltonian 2, thus, PM3 belongs to the large family of semi-empirical methods.

5.3. Results and discussion

In the present work, acetate accumulation and its incorporation into the CA biosynthesis by *Sc* was studied in the initial, rather non stationary phase of a chemostat cultivation. The culture was grown under phosphate limitation, in which CA production was observed to be highly favored (Bushell et al., 2006; Ives and Bushell, 1997; Kirk et al., 2000). After the first 36 h of fermentation (batch mode), the culture was kept at a dilution rate of 0.05 h^{-1} for over 4 residence times (τ); biomass concentration was rather constant. The maximum cell dry weight was obtained at t=36 h, reaching 10.44 g/L. After 57 hours of cultivation, the biomass concentration rendered an average of 6.69 g/L (Fig. 5.2).

After 132 h of cultivation glycerol depletion was nearly complete and afterwards remained below 0.1 g/L (Fig. 5.2). After 3τ, the CO_2 production and O_2 uptake were constant until the end of the experiment, indicating steady-state conditions in the very late phase of the observation period. This condition can be reinforced, if one takes into account the narrow difference, less than 12%, detected between the observed dilution rate and the specific growth rate. Thus, as shown in Fig. 5.2, transient conditions were achieved concerning the glycerol availability, while the culture was adopting itself to the continuous process mode.

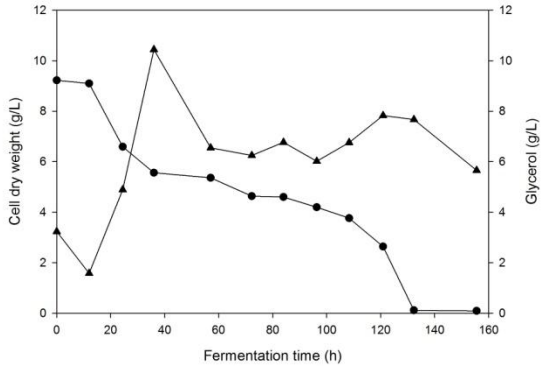

Fig. 5.2. Continuous cultivation of *Sc* indicating cell dry weight (-▲-) and glycerol consumption (-●-), as a function of fermentation time.

The highest CA concentration of 17.2 mg/L was obtained at 36 h of fermentation, (Fig. 5.3). A clear decline in the concentration of CA was observed after this time. CA degradation has been already reported (Roubos et al., 2002). The authors found that the degradation rate constant (k_d) was increased at a high concentration of ammonia (>15 mM) and glycerol (>7 g/L) in fed-batch cultivation. Additionally, Roubos and co-workers reported that the CA degradation was probably caused by presence of an enzyme induced by high concentration of ammonia and glycerol. The results of the present work are in good agreement with those found by Roubos et al. (2002), specifically regarding the magnitude of CA degradation as a function of the substrate availability. In this context, CA degradation can be further explained by the formation of other β-lactam compounds from the clavaminic acid branch point. Therefore, the

metabolic flux towards CA biosynthesis would be decreased due to the diverted carbon flux towards the so-called 5S clavam pathway, thus diminishing CA titers.

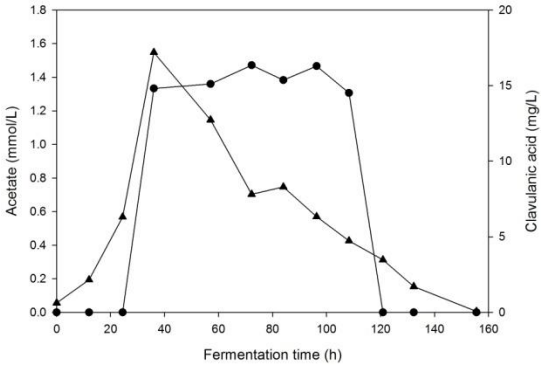

Fig. 5.3. Continuous cultivation of *Sc*. The dynamic change of acetate (-●-) and CA (-▲-) as a function of fermentation time.

Accumulation of acetate has been reported for batch fermentation of *Streptomyces ambofaciens*, when glucose was used as carbon source (Colombié et al., 2005) and, in mutants of *Streptomyces coelicolor* (Viollier et al., 2001). Viollier et al. (2001), using glucose as carbon source, reported the accumulation of pyruvate, succinate, fumarate, malate, citrate and acetate in *citA* (BZ2) and bald mutants (*bldA*, *bldB*, *bldG*, *bldH*, *bldJ*), with an unbalanced glycolitic and TCA flux. In this work, an accumulation of acetate was observed within the time frame, during which CA was accumulated (Fig. 5.3). Furthermore, acetate concentration was approximately constant, with an average of 1.39 mmol/L, between 36 and 108 h. Interestingly, during this time period, CA continuously declined, indicating that synthesis of acetate and CA coincide. After 100 h of fermentation, a re-assimilation of acetate occurred, thus leading to a drop in its concentration (Fig. 5.2 and 5.3), probably due to accelerated growth. Chan and Sim (1998) and Soh et al. (2001) reported that *Sc* was able to grow on acetate as the sole carbon source, and additionally a relationship between carbon source (either glycerol or acetate), growth and isocitrate lyase activity, was found (Chan and Sim, 1998; Soh et al., 2001).

Although the acetyl group is present in β-lactam intermediate compounds, such as NAG-clavam, it is still unknown how it is incorporated (Arulanantham et al., 2006). In addition, the acetylation of N-glycyl-clavaminic acid, by action of the *orf14* to form N-acetyl-glycyl-clavaminic and the future conversion to N-acetyl-clavaminic acid by *orf16* protein has been proposed (Paradkar, 2013). Based on our experimental data, one can argue that acetate is presumably linked to CA biosynthesis.

Iqbal et al. (2010) demonstrated that *orf14* is a member of a tandem GCN5-related acetyltransferase (GNAT) protein, where the *C*-terminal domain of acetyl transferase possesses probably acyl transfer activity and the *N*-terminal GNAT domain can bind to a single acetyl-CoA molecule (Iqbal et al., 2010). Thus, GNAT might be connected with the synthesis of N-acetylated clavaminic acid compounds. However, other alternatives for acetylation processes must be explored. As an example, the biosynthesis of N-glycyl-clavaminic acid is mediated by N-glycyl-clavaminic acid synthetase, a member of the ATP-grasp fold superfamily (Arulanantham et al., 2006; Fawaz et al., 2011). Excluding the case of the kinases, the reaction mechanism for the ATP-grasp superfamily consists of a two-step process (Fig. 5.4) (Fawaz et al., 2011). For a complete reaction the enzymes require ATP, carboxylic acid and nucleophilic substrates. First, the carboxylic acid substrate reacts with ATP, producing a reactive acylphosphate intermediate. Isotopic studies have shown the presence of this intermediate, which involves transferring a labeled oxygen atom coming from the carboxylic acid substrate to an inorganic substrate (Healy et al., 2000; Mullins et al., 1991, 1990). For the second part of the reaction, and for most of the carboxylic acid substrate, used in the first partial reaction, a direct nucleophilic attack on the carbonyl carbon of acylphosphate intermediate occurs (Fig. 5.4), thus leading to a tetrahedral intermediate (Fawaz et al., 2011).

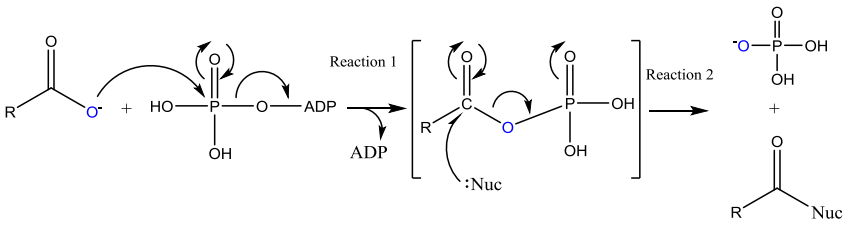

Fig. 5.4. Overall proposed mechanism for a catalyzed reaction by ATP-grasp superfamily enzymes. Color Code: Blue "O" corresponds to a labeled oxygen atom.

Based on this mechanism and the characteristic nature of N-glycyl-clavaminic acid as a nucleophilic substrate, and acetate as a carboxylic acid substrate, one can argue the acetate incorporation in the NAG-clavam formation would take place by means of an analogous mechanism.

The reaction mechanism reported here, involves the first step of the entire chemical transformation, namely, the reaction between acetate and ATP (in Fig. 5.4, replace R by methyl group). Our calculations suggest that the reaction cannot proceed further without the catalytic action of an enzyme. The use of an enzyme to complete the two steps of the reaction described above, has been documented (Healy et al., 2000; Mullins et al., 1990). Both studies report that an enzyme is required for the first part of the reaction. In contrast, we apply a computational-based approach to asses the proposed two step reaction mechanism, in a way that the enzyme-driven reaction is considered just for the second part of the reaction.

As stated above, the reaction can only complete the first step without the direct action of an enzyme. The structure for the transition state, using an ATP model that contains only phosphate groups is shown in Fig. 5.5.

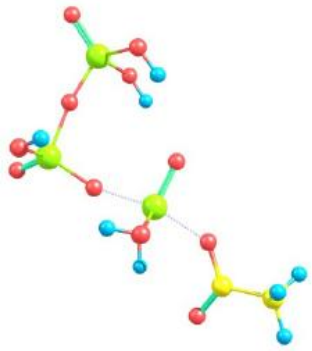

Fig. 5.5. Transition-state structure of an ATP model that only includes phosphate groups. P atoms in green, O atoms in red, H atoms in blue, C atoms in yellow.

The potential energy surface corresponding to the intrinsic reaction coordinate (IRC), which defines the minimum energy path connecting the reactants and products via the transition state, is shown in Fig. 5.6. The computed activation energy is ≅ 2.82 kcal/mol while the reaction energy is ≅ 2.38 kcal/mol. As it is clearly seen, this is an endothermic process with a relatively small activation energy. Thus, the reaction rate should be considerably high. The transition state happens late in the reaction coordinate and thus, according to Hammond's postulate, should structurally resemble the products.

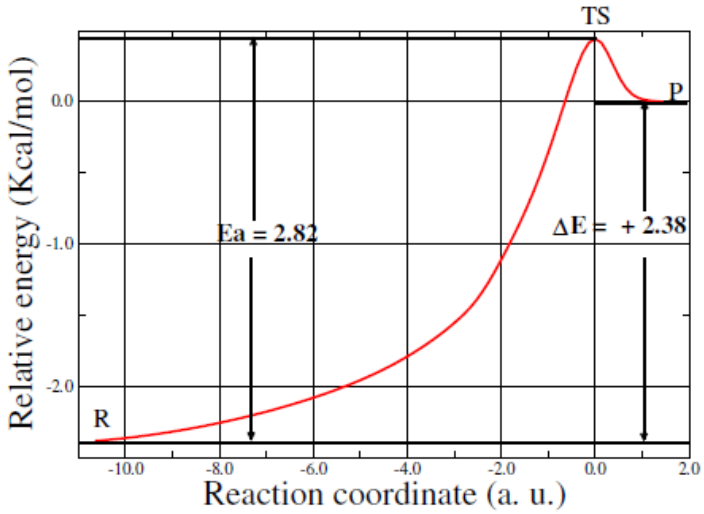

Fig. 5.6. Intrinsic reaction path for the first step in the reaction between ATP and acetate.

Furthermore, Fulston and co-workers detected the unstable intermediate (3R, 5R)-clavaldehyde, which, in the presence of the NADPH-dependent clavulanic acid dehydrogenase (CAD), produces (3R, 5R)-clavulanic acid (Fulston et al., 2001). In that work, the CAD, responsible for the formation of the allylic alcohol group of CA, was isolated and its gene encoded in the CA biosynthetic gene cluster. The authors proposed a biochemical mechanism for the stereochemical inversion, based on spontaneous racemization of benzyl clavulanate-9-aldehyde, where an ester or a thioester of clavulanate-9-aldehyde might be an intermediate that undergoes a similar inversion of (3S, 5S)-clavaminic acid to (3R, 5R)-clavulanic acid (Fig. 5.7a) (Fulston et al., 2001). However, based on the N-glycyl-clavaminic acid biosynthesis, the inversion of the stereochemical configuration could eventually occur in a different way, due to structural and chemical differences between an ester or a thioester of clavulanate-9-aldehyde and N-glycyl-clavaminic acid, specifically in the substituent of the carboxylic acid and amino groups (Fig. 5.7b).

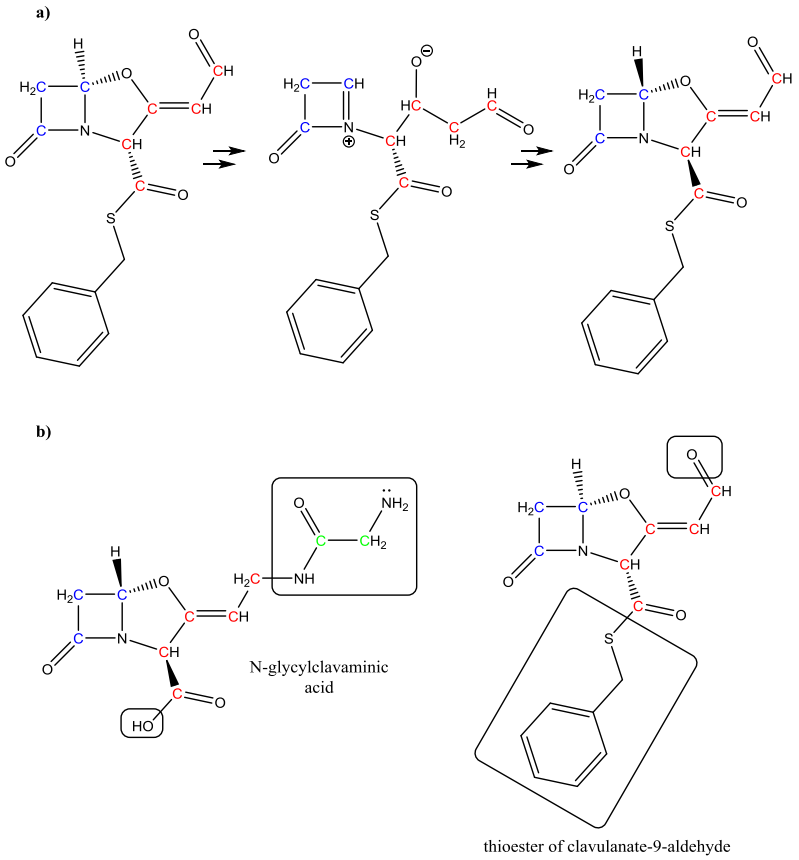

Fig. 5.7. A proposed racemization mechanism of β-lactam intermediates. a) A proposed mechanism based on spontaneous racemization of benzyl clavulanate-9-aldehyde, for the stereochemical inversion of (3S, 5S)-clavaminic acid to (3R, 5R)-clavulanic acid, during CA biosynthesis (adapted from Fulston et al. 2001). b) Structural-chemical differences between an ester (replace S by O) or a thioester of clavulanate-9-aldehyde and N-glycyl-clavaminic acid. Color Code: red, blue and green C correspond to a carbon atom from arginine, glyceraldehyde-3-phosphate and glycine, respectively.

An incorporation of $^{18}O_2$-derived oxygen at the C-9 position of CA, and on the oxazolidine ring, was reported by Townsend and Krol (1988) when cultures of *Sc* were exposed to an $^{18}O_2$-containing atmosphere (Hamed et al., 2013; Townsend and Krol, 1988).

Li et al. (2000) reported the probable involvement of *orf10* in the oxidative steps between (3S, 5S)-clavaminic acid and (3R, 5R)-clavaldehyde (Li et al., 2000; Mellado et al., 2002). Moreover, Bycroft and co-workers reported the loss of the C-8-hydrogen (C-4-hydrogen of ornithine) during CA production from clavaminic

acid (Bycroft et al., 1988; Hamed et al., 2013). Finally, an admissible mechanism for the double epimerization of (3S, 5S)-clavaminic acid to (3R, 5R)-clavulanic acid was proposed by Elson (1988) (Fig. 5.8). Even a more recent report proposed three mechanism of epimerization in which *orf12* is involved (Valegård et al., 2013). The authors found that *orf12* have similar functionality to the esterase VIII superfamily, and its C-terminal domain showed low-level esterase activity over 3'-*O*-acetyl cephalosporins and thioester substrate. These results, among others, constitute well supported experimental and theoretical evidence for the reaction mechanisms during CA formation. Yet, all of them lack a thermodynamic feasibility analysis, which could be considered, for instance, by a computational approach.

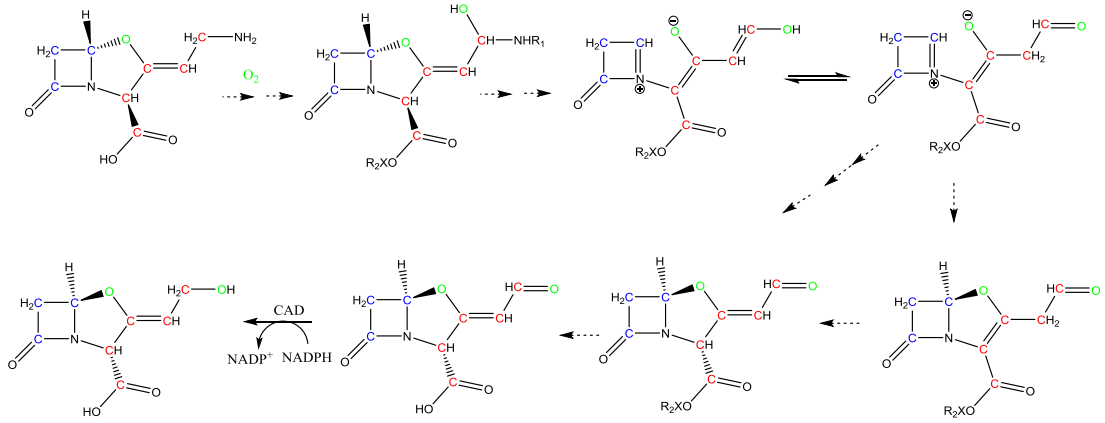

Fig. 5.8. Proposed mechanism for the double epimerization of clavaminic acid during CA production (Elson, 1988).

The structural similarity between proline and the bicyclic β-lactam ring is evident (Fig. 5.9). A special case is the proximity of the nitrogen atom to the carboxylic acid group.

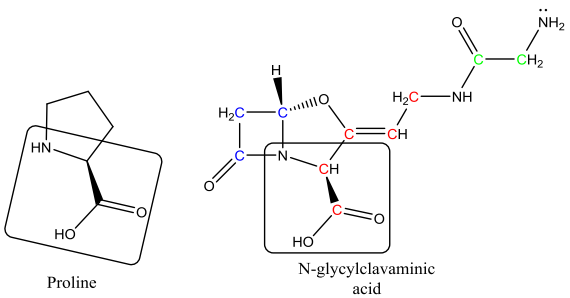

Fig. 5.9. Structural similarities between proline and the bicyclic β-lactam ring.

Proline racemase catalyzes the interconversion of D- and L-proline, where one form of the enzyme binds to L-proline and the other binds to D-proline. The reaction consists mainly of a two-base mechanism. In the first part of the reaction, one base on the enzyme removes the substrate α-hydrogen as a proton; in the second one, the conjugate acid of another base donates a proton to the opposite side of the α-carbon (Cardinale and Abeles, 1968; Rudnickt and Abeles, 1975). Thus, the two-base mechanism could eventually be an alternative for the epimerization process during CA biosynthesis using proline racemase.

Bearing in mind all the above mentioned arguments, here we propose a mechanism for the stereochemical inversion of (3S, 5S)-clavaminic acid to (3R, 5R)-clavulanic acid as follows:

Stage 1: N-glycyl-clavaminic acid formation in the presence of *orf17,* ATP, and glycine. The *orf17* protein is a member of the ATP-grasp fold superfamily; the known mechanism for N-glycyl-clavaminic acid formation considers the attack of the carboxylic acid substrate (glycine) to the phosphorus in the phosphate group, forming a reactive acylphosphate intermediate, while ADP is liberated. In the second part of the reaction, the nucleophile (clavaminic acid) attacks the carbonyl carbon, leading to a tetrahedral intermediate that contains a substituent attached to the central carbon that can act as a leaving group. The intermediate collapses and releases phosphate as the leaving group.

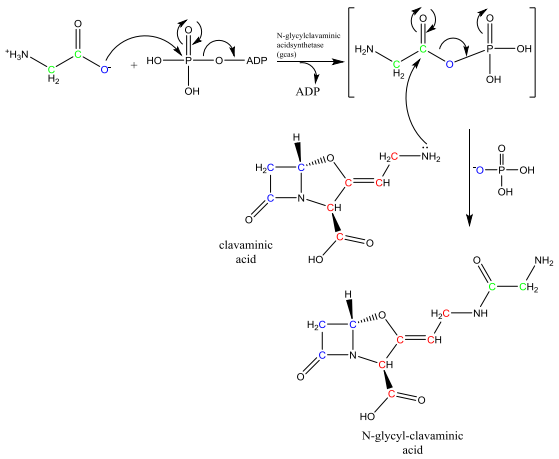

Fig. 5.10. N-glycyl-clavaminic acid formation in the presence of the *orf17* protein, ATP, and glycine.

Stage 2: Acetate incorporation during NAG-clavam formation. From our experimental work, we propose that acetate is a direct precursor due to its nature as a carboxylic acid substrate, its accumulation during CA production, and the presence of the acetyl group in the NAG-clavam structure. The reaction proceeds as described in stage 1; yet, the carboxylic acid and nucleophilic substrates are acetate and N-glycyl-clavaminic acid, respectively.

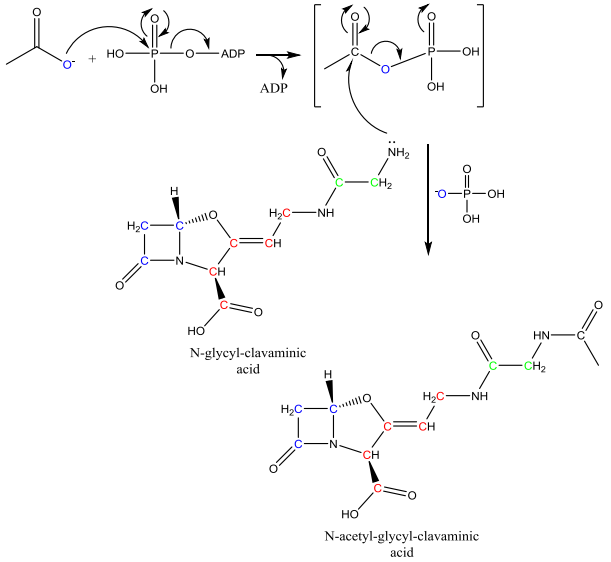

Fig. 5.11. A proposed mechanism for acetate incorporation during NAG-clavam formation.

Stage 3: N-acetyl-clavaminic acid formation with release of acetamide: the *orf16* protein is probably involved in this reaction, but the step still remains unclear (Paradkar, 2013). Then, an incorporation of molecular oxygen (O_2-derived oxygen at C-9) into the allylic hydroxy group of CA could occur (Hamed et al., 2013; Townsend and Krol, 1988).

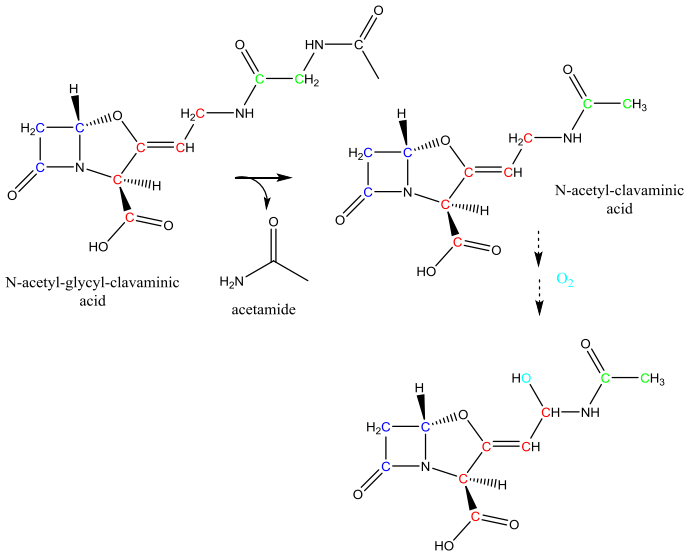

Fig. 5.12. Reaction steps for N-acetyl-clavaminic acid formation and the incorporation of molecular oxygen into the allylic hydroxy group of CA.

Stage 4: Mechanism for double epimerization by proline racemase. In the first step of this reaction, one base of the enzyme (deprotonated Cys (a thiolate RS-)) removes the substrate α-hydrogen as a proton. Then, the conjugate acid of another base (protonated Cys (a thiol RSH)) donates a proton to the opposite side of the α-carbon. This mechanism of action of proline racemase was adapted from Rudnickt and Abeles (1975).

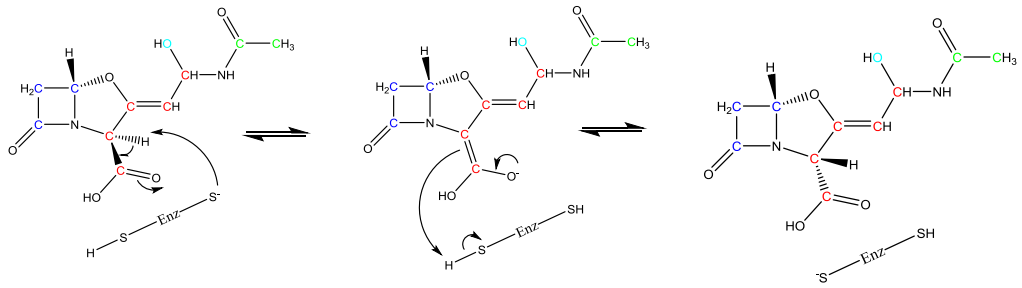

Fig. 5.13. A proposed mechanism for a double epimerization process, by action of proline racemase, during CA production.

Stage 5: Stereochemical inversion

The reaction proceeds as in stage 4, however, the inversion of stereochemistry occurs on the next chiral center (5S carbon between the oxygen and the nitrogen in the bicyclic β-lactam ring).

Stage 6: The structure obtained in stage 5 suffers a removal of acetamide (unclear step), thus resulting in the unstable intermediate (3R, 5R)-clavaldehyde. From there the CA biosynthesis directly proceeds, in the presence of the NADPH-dependent dehydrogenase by the conversion of (3R, 5R)-clavaldehyde into CA in a simple reduction step (the aldehyde group present in (3R, 5R)-clavaldehyde is reduced to alcohol group, by action of CAD, to form CA). It is worth mentioning that (3R, 5R)-clavaldehyde has the same stereochemistry as CA.

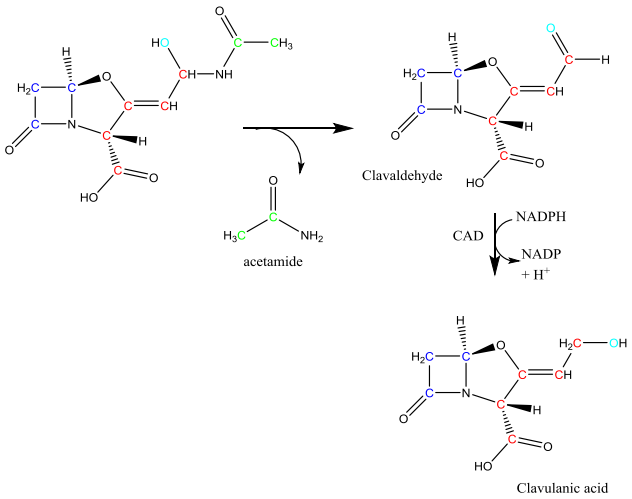

Fig. 5.14. The formation of the unstable (3R, 5R)-clavaldehyde, and the subsequent CA biosynthesis.

5.4. Conclusions

The clavam biosynthetic pathway is crucial for CA biosynthesis in *Sc*, however, some steps in the pathway remain unclear. In this work, we propose and computationally assess a reaction mechanism for the acetate incorporation during the formation of NAG-clavam, which is a postulated new step in the clavam pathway. The reaction takes place in two steps; yet, it can only complete the first one, which involves acetate and ATP, without the direct action of an enzyme, while an enzyme is required for the second step of the reaction. Nonetheless, the calculations performed in this work should not be considered as a definite characterization of the potential energy surface for the reaction between acetate and ATP, but rather as a first approximation that provides valuable insight in the reaction mechanism. Further calculations, including a more realistic environment, either with explicit consideration of solvent molecules or using a continuum model to mimic the solvent, are in progress.

Clearly, the computer simulation of chemical systems is a powerful tool to obtain detailed information about reaction mechanisms that are still unclear in metabolic

networks or those who lack experimental evidence data and/or suitable experimental methods. In the case of *Sc* metabolism, evidence of acetate participation in the clavam pathway would, in the end, help to improve genome scale metabolic reconstructions of *Sc,* for which upgraded and cured metabolic networks might be obtained. In doing so, patterns for carbon flux distribution in the cell would eventually change, to represent more realistic cellular phenotypes.

We also propose a complete route for the inversion of the stereochemical configuration of (3S, 5S)-clavaminic acid into (3R, 5R)-clavulanic acid, including a novel alternative of double epimerization using proline racemase, due to the structural-chemical similarities between proline and bicyclic β-lactam ring (special case: proximity of nitrogen atom to the carboxylic acid group). This alternative reaction does not require rupture of the bicyclic β-lactam ring; in contrast, other proposed mechanisms consist of the formation of an iminium ion as intermediate, after oxazolidine ring opening, to form (3R, 5R)-clavaldehyde by oxazolidine ring closure.

Acknowledgments

H.R.M. thanks the German Academic Exchange Service (DAAD) for financial support.

CHAPTER 6

6. Theoretical analysis of the ^{13}C-labeled compound distribution profile in the clavulanic acid biosynthetic pathway in *Streptomyces clavuligerus*: A perspective for an isotopic labeling study

Abstract

Streptomyces clavuligerus (Sc) produces clavulanic acid (CA), a potent inhibitor of β-lactamase enzymes. Mostly, due to unknown causes, CA production is low in fermentation. By the help of ^{13}C metabolic flux analysis (^{13}C-MFA), which indirectly allows identifying bottlenecks in the network, one can propose strategies for genetic modifications aim at increasing product yields. In this work, a theoretical approximation of the fate of carbon labeled glycerol in *Sc* metabolism is presented. For the purpose of knowing what are the theoretical incorporations of labeled carbons, along the CA metabolic pathway, we used either [U-^{13}C] glycerol or [2,3,4-^{13}C] arginine as labeled precursor. The theoretical synthesis of labeled carbon through the glycolytic, gluconeogenesis, tricarboxylic acid cycle, urea cycle and clavam pathway was proposed. As the metabolic activity progressed, labeled CA was encountered. In conclusion, three and one CA isotopomers from [U-^{13}C] glycerol and [2,3,4-^{13}C] arginine were proposed, respectively. A complete overview of the entire carbon labeling distribution of CA biosynthesis in *Sc*, was discussed.

6.1. Introduction

Many pathogens have shown resistance to β-lactam antibiotics due to its ability to synthesize β-lactamases (Brown et al., 1976). β-lactamase activity is responsible for the hydrolysis of β-lactam rings, rendering the β-lactam antibiotics ineffective (Llarrull et al., 2010). Clavulanic acid (CA) is produced in submerged culture by *Streptomyces clavuligerus (Sc);* despite its weak antibacterial activity, it is a powerful inhibitor of β-lactamase enzymes (Baggaley et al., 1997) with some important application already available in the market (Elander, 2003).

Although the fermentative process has been widely studied, yields still remain low (around 1 g/L on average) (Bushell et al., 2006; Roubos, 2002; Roubos et al., 2002; Teodoro et al., 2010). Flux Balance Analysis (FBA) is a powerful metabolic engineering tool for quantifying metabolic fluxes in a specific pathway (Stephanopoulos et al., 1998; Villadsen et al., 2011). Knowing flux distribution is a starting point for strain improvement by means of identifying metabolic targets susceptible of genetic modifications (Wiechert, 2001). Nevertheless its proved applications, the traditional FBA have limitations and fails when the pathway under consideration presents parallel metabolic fluxes, metabolic cycles, reversible reaction steps and split pathways where cofactors are not balanced. As an alternative, the ^{13}C metabolic flux analysis technique (^{13}C-MFA), an extension of FBA (Krömer et al., 2009; Wiechert, 2001), provides a reliable framework for treating such situations. The ^{13}C-MFA approach uses compounds that possess in their structure, labeled carbons (^{13}C) which would subsequently be incorporated into the metabolic network by means of feeding experiments. The ^{13}C-labeled compounds that appear during fermentations are linked with the initial labeled precursor (for instance [U-^{13}C] glucose or [U-^{13}C] glycerol) and these enrichments along with the upper and lower boundaries of rates and the stoichiometric matrix can eventually be used as constraints for ^{13}C metabolic modeling purposes (Krömer et al., 2009). Due to scarce CA production studies using labeled compound as substrate (Bycroft et al., 1988; Elson and Oliver, 1978; Elson et al., 1982; Stirling and Elson, 1979; Townsend and Krol, 1988), one can explore theoretically, as a first approximation, the fate of carbon labeled in *Sc* metabolism and find the isotopomers of key compounds such as CA and amino acids that eventually would match future isotopic labeled experimental studies.

In this work, we present a theoretical approach of incorporation of ^{13}C-labeled compounds in the CA biosynthetic pathway in *Sc*, using, separately, [U-^{13}C] glycerol and [2,3,4-^{13}C] arginine as labeled precursors. A theoretical proposal for measurements of CA isotopomers, by means of the gas chromatography-mass spectrometry technique, was also discussed. This chapter was aim at showing

that further studies in this direction must be carried out for a better understanding the *Sc* metabolism.

6.2. The metabolic network of *Sc*

For this purpose, the metabolic network for CA biosynthesis in *Sc* was obtained using information from open scientific literature (Bushell et al., 2006; Roubos, 2002), and from public databases (e.g. http://www.enzyme-database.org/, http://www.genome.jp/kegg/). The following metabolic pathways were initially considered: glycolysis, gluconeogenesis, pentose phosphate, tricarboxylic acid cycle (TCA cycle), urea cycle and the clavam pathway (Fig. 6.1). It was considered that the entire pathway was fed with a suitable combination of labeled and unlabeled glycerol as unique carbon source. Only one anaplerotic reaction was considered, wherein the oxaloacetate was obtained by the carboxylation of phosphoenolpyruvate (PEP) over the action of the enzyme PEP carboxylase (Hodgson, 2000). Although the urea cycle is unusual in most prokaryotes, several authors have reported the activity of several of its enzymes (Bascarán et al., 1989; Dela Fuente et al., 1996). In fact, arginine has been found to be a major precursor for CA biosynthesis (Bascarán et al., 1989; Khaleeli et al., 1999; Li and Townsend, 2006; Valentine et al., 1993). The clavam pathway was crucial for CA, clavam-2-carboxylate and alanylclavam isotopomers proposed in this work.

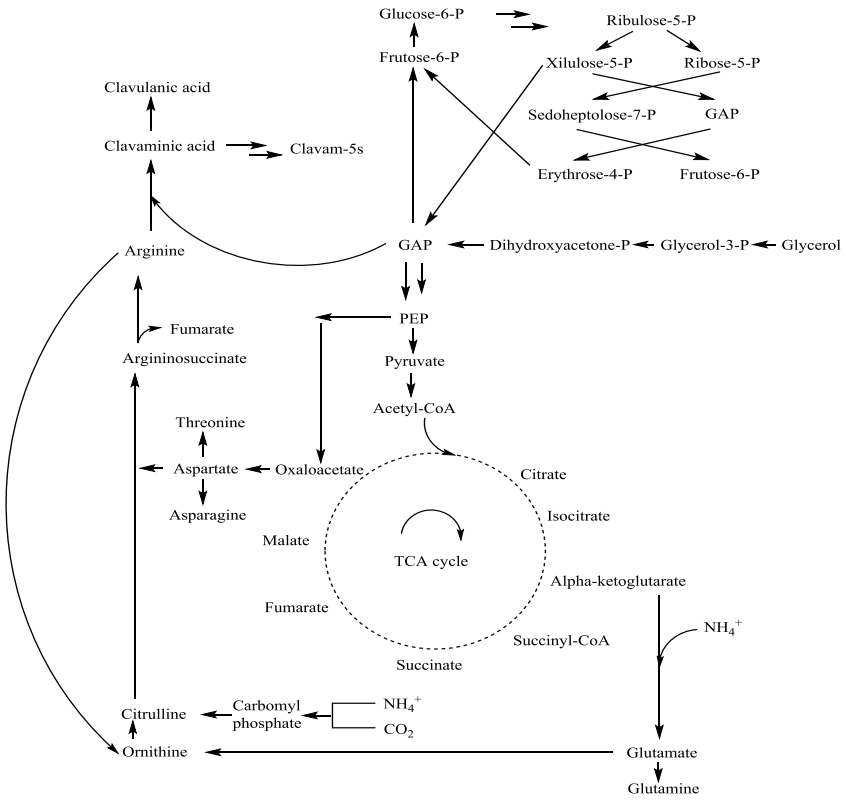

Fig. 6.1. Condensed scheme of the CA biosynthetic pathway in *Sc.*

6.2.1. Incorporation of labeled substrates into the metabolic pathway

The methodology used for the estimation of the isotopic distribution consisted of the analysis of each reaction throughout the entire metabolic network. Knowing how the substrates are transformed into products in each reaction, i.e. which bonds are broken and which are created, as well as the location of atoms in the new component, it is then possible to infer the origin of atoms in each single product in all reactions. Based on knowledge of the different reactions in a metabolic pathway, it is possible to predict the origin of each carbon in major secondary metabolites, produced by the bacterium.

The selection of an appropriate ^{13}C tracer precursor for a specific biological system, the kind of metabolic network model (either dynamic or stationary) and measurement of isotopic compounds either by GC-MS or NMR need to be

studied in detail before performing a labeling experiment. Therefore, it is of primal importance to decide which technique is going to be used hand in hand with the labeled precursor selection in order to generate sufficient information for proper simulation of the metabolic model. Currently, there is a possibility either of using a tracer or multiple tracers for labelling experiments; labeled carbons either in one or more positions can also be used as it generates a wide range of possibilities. However, the optimal tracers can be chosen either by *in silico* simulation, flux estimation and statistical analysis using software already available e.g., METRAN (Antoniewicz et al., 2006).

[U-^{13}C] glycerol and labeled arginine (with labeled carbons at carbon positions 2, 3 and 4) were considered as precursors for the theoretical analysis of incorporation of ^{13}C-labeled compound on CA biosynthetic pathway in *Sc.* We assumed that initially all compounds were unlabeled because the medium came from a culture of *Sc* with unlabeled precursors and subsequently the ^{13}C-labeled compound appeared when the [U-^{13}C] glycerol and labeled arginine were used.

6.3. [U-^{13}C] glycerol as precursor in CA biosynthesis

Glycerol is catabolized through the glycolysis and gluconeogenesis pathways. Once [U-^{13}C] glycerol is up taken, it is processed to glyceraldehyde-3-phosphate (GAP) (a major glycolytic intermediate) keeping unmodified the three labeled carbons in its structure since it is derived from [U-^{13}C] glycerol. Then, gluconeogenesis turns on for glucose biosynthesis. Besides GAP, dihydroxyacetone phosphate (DHAP) is also obtained. Subsequently, the condensation of GAP and DHAP produces a hybrid of fructose 1,6 bisphosphate by the action of the enzyme aldolase (Alefounder et al., 1989); therefore, it is possible to predict the presence of three glucose isotopomers. For the hybrid of fructose 1,6 bisphosphate three labeling distribution can be eventually obtained: either uniformly labeled carbons or labeled at the first three carbons, or even at the last three carbons (Fig. 6.2). Instead, the starting point for glycolysis is GAP derived from labeled and unlabeled glycerol. As the metabolic activity

progresses, labeled and unlabeled pyruvate as well as acetyl-CoA are encountered (Fig. 6.2 and 6.3).

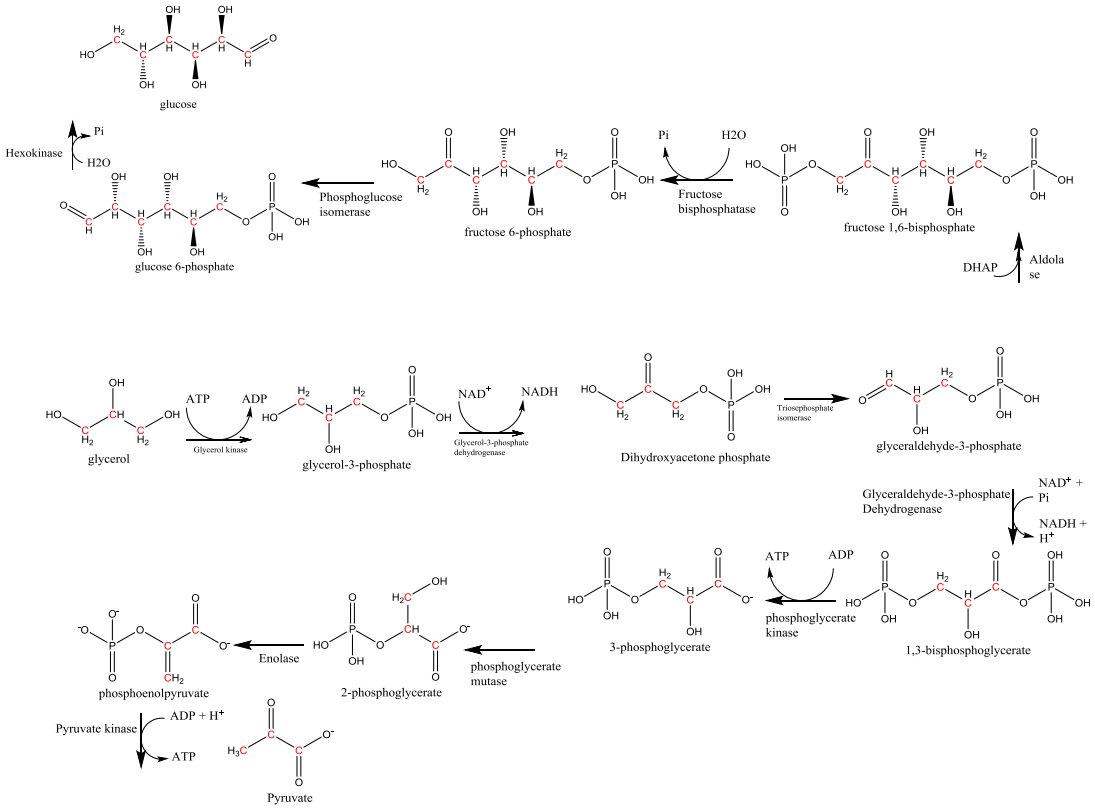

Fig. 6.2. Isotopomer distribution in the glycolysis and gluconeogenesis pathways. Color Code: red C corresponds to a labeled carbon atom.

Once the labeled acetyl-CoA reaches the TCA cycle, the condensation of an unlabeled oxaloacetate molecule with an entirely carbon-labeled acetyl unit form a citrate molecule. A further isomerization of citrate into isocitrate is carried out by a dehydration step leaving unmodified the labeling distribution. Indeed, the result is an exchange of a hydroxyl group and a hydrogen atom. However, due to the characteristic symmetrical condition in the plane of citrate, two possibilities must be taken into account for *cis*-aconitate as the double bond can appear at the first carbon position, either on the right or on the left side in the citrate structure; Potter and Heidelberger (1949) demonstrated that the two -CH_2COOH groups of citrate do not behave identically as they have different

reactivities, thus leading to only one possibility for *cis*-aconitate wherein the double bond is in the -CH_2COOH group coming from oxaloacetate (Fig. 6.3) (Barry, 1997; Ogston, 1948; Potter and Heidelberger, 1949). Consequently, one labeling possibility for isocitrate is encountered, keeping two labeled carbons in its structure. The conversion of isocitrate into alpha ketoglutarate is the first oxidative decarboxylation reaction; at this point, the missed carbon dioxide molecule come from the unlabeled oxaloacetate, thus ending up in an alpha ketoglutarate molecule with two labeled carbons from acetyl-CoA. Alpha ketoglutarate plays an important role in CA biosynthesis, as it is a precursor for important intermediates in the urea cycle, e.g., ornithine and arginine (Chen et al., 2003). Following the TCA cycle, there is a second oxidative decarboxylation that allows the formation of succinyl-CoA from alpha ketoglutarate. In this step, one unlabeled carbon dioxide molecule is lost, thus producing one succinyl-CoA molecule with 2 labeled carbons in its structure. Similarly, the labeling possibility for succinate and fumarate can be uncovered, having into consideration that both molecules are symmetrical and two labeling alternatives must appear from fumarate. Unlike to what happens with the -CH_2COOH arms of citrate, the -CH_2COOH groups of succinate are indistinguishable by the enzyme succinate dehydrogenase.

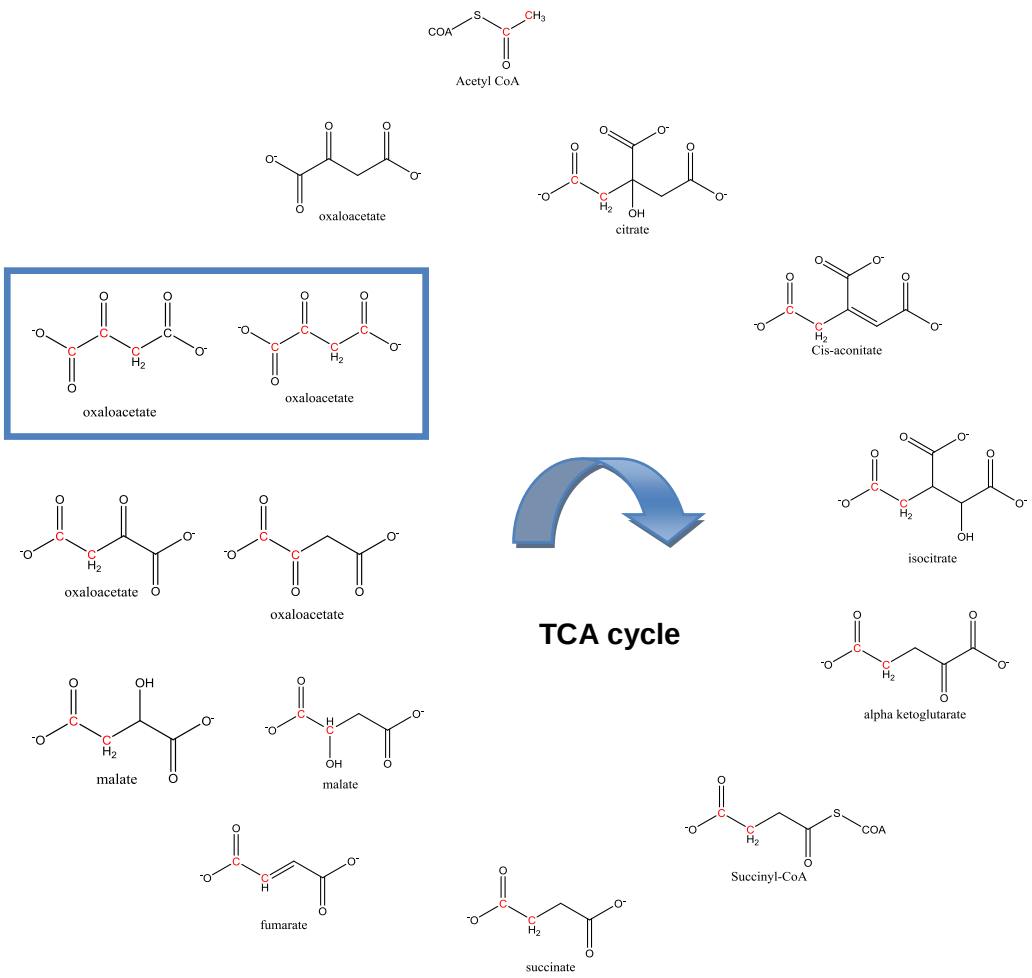

Fig. 6.3. Isotopomer distribution in the TCA cycle. The two structures inside the blue rectangle are generated by the carboxylation of PEP to oxaloacetate either with unlabeled or labeled carbon dioxide. Color Code: red C corresponds to a labeled carbon atom.

In the case of the hydration step of fumarate to malate, wherein the fumarate molecule is symmetrical, the enzyme fumarase catalyzes a stereospecific trans addition of a hydroxyl group and a hydrogen atom (Berg et al., 2002), leading to two labeling conditions for malate, one with $-^{13}CH_2-$ and the other with $-^{13}CH\text{-}OH$ (Fig. 6.3). Consequently, two labeling possibilities are found for oxaloacetate; since an anaplerotic reaction is being considered in the metabolic network, hence, additional possibilities for labeling are generated. Therefore, oxaloacetate can be obtained by carboxylation of labeled PEP, but, in the cytoplasmic environment, unlabeled and labeled carbon dioxide (coming from the decarboxylation of pyruvate into acetyl-CoA) are still available which

facilitates two more labeling possibilities. Finally, four oxaloacetate isotopomers are proposed to coming out from the first loop of the TCA cycle (Fig. 6.3). In the remaining loops of the TCA, further unlabeled and labeled carbon dioxide are available in the medium because the later molecule is produced from oxaloacetate isotopomers in the oxidative decarboxylation steps. Note that the two carbons coming from acetyl-CoA do not leave as CO_2 on the first loop of the TCA cycle but they rather are incorporated into new oxaloacetate; yet they are not oxidized until subsequent turns of the cycle, and the two –COOH groups of oxaloacetate are released as CO_2 during all cycles.

Transamination reactions play an important role in amino acid biosynthesis, e.g., the conversion of oxaloacetate into aspartate, where glutamate is an amino donor and later on it is converted into alpha ketoglutarate (see appendix A for aspartate, threonine and asparagine isotopomers). Though the reaction between carbamoyl phosphate and ornithine which produces citrulline takes place in the mitochondria, the remaining reactions of the urea cycle are localized within the cytosol. The condensation of citrulline and aspartate produces argininosuccinate that subsequently splits into arginine and fumarate (Haines et al., 2011). Furthermore, ornithine and urea are generated by the hydrolysis of arginine. The important fact is that the carbon fragment of fumarate comes from aspartate and therefore, from oxaloacetate as well (Fig. 6.4). In summary, the oxaloacetate isotopomers are not crucial for CA biosynthesis since the carbon fragment is lost as fumarate; in contrast, one arginine isotopomer has been proposed in the urea cycle, taking into consideration that it was originated from alpha ketoglutarate (see appendix B).

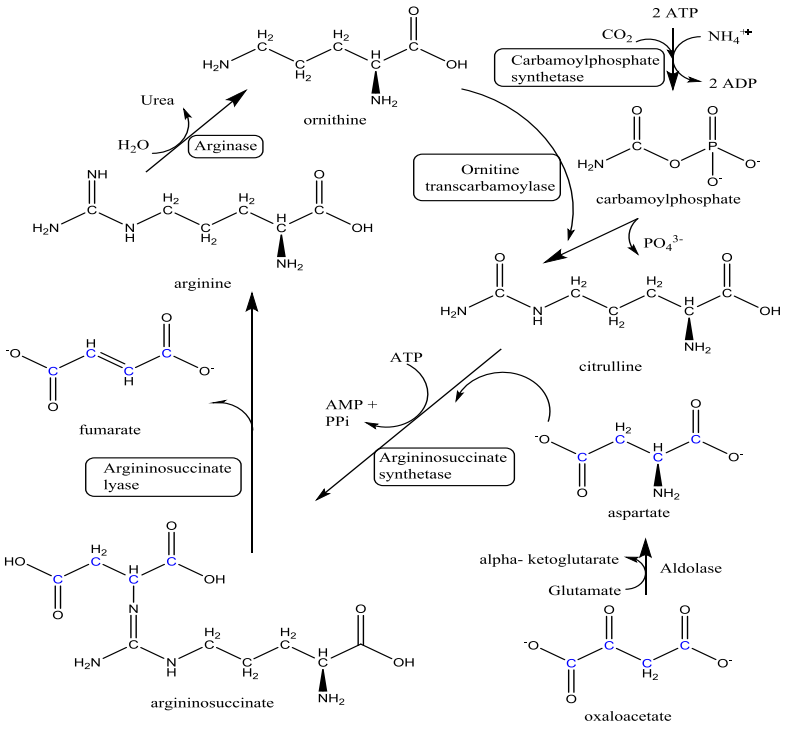

Fig. 6.4. Urea cycle. Note that the carbon fragment of fumarate comes from oxaloacetate. Color Code: blue C corresponds to carbon atoms from oxaloacetate.

The biosynthesis of CA starts with the condensation of arginine and GAP followed by five reactions until clavaminic acid is synthesized. This group of reactions is usually known as “early steps”. At this point, a bifurcation occurs and the metabolic flux splits to bring about carbon for CA biosynthesis and the 5S clavam pathway (“later steps”) (Fulston et al., 2001; Jensen et al., 2004; Ozcengiz and Demain, 2013; Townsend, 2002; Zelyas et al., 2008) (Fig. 6.5). Since CA has 8 carbons in its structure, a C5 unit from arginine and a C3 unit from GAP are used as precursors. Indeed, the C3 unit from GAP is incorporated into the β-lactam ring of CA and the C5 unit in the rest of the structure. Based on the information on GAP and arginine isotopomers, we argue that three CA isotopomers from labeled glycerol are obtained (see appendix C). The same can also be stated for the case of clavam-2-carboxylate. AlanyLclavam biosynthesis is a special case since unlabeled and labeled glycine would participate in the pathway (Fig. 6.5).

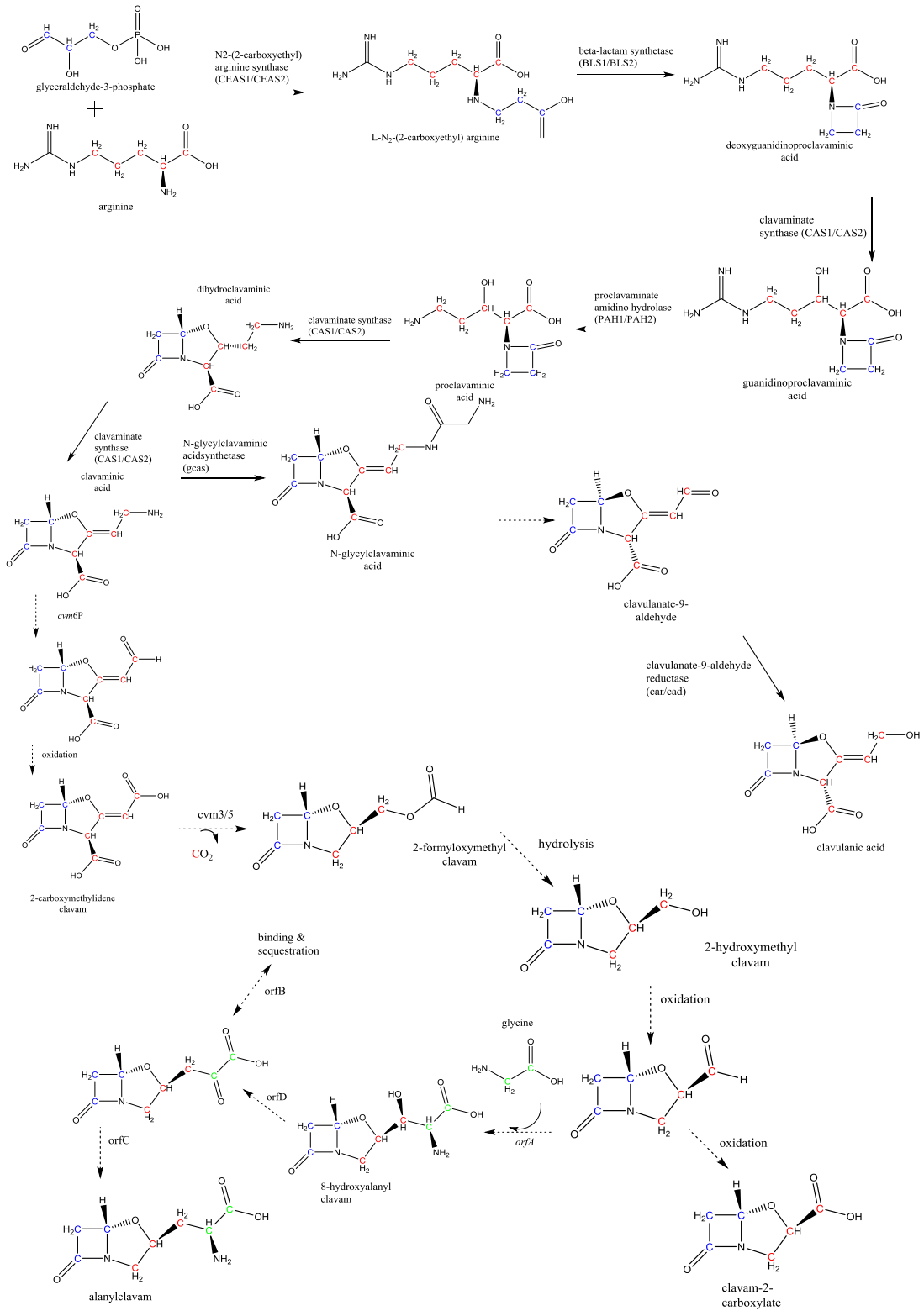

Fig. 6.5. Clavam pathway. Color Code: red, blue and green C corresponds to a labeled carbon atom.

For glycine biosynthesis, the glycolytic-intermediate 3-phosphoglycerate is used (Berg et al., 2002), keeping unmodified the three labeled carbons in its structure since it is derived from [U-^{13}C] glycerol. In the transition of serine into glycine, the labeled carbon bonded to hydroxyl group of glycine is transferred to THF. Therefore, glycine with two labeled carbon in its structure was found (Fig. 6.6). Taking into consideration the chance of finding unlabeled glycine, seven alanyclavam isotopomers can be expected (see appendix D).

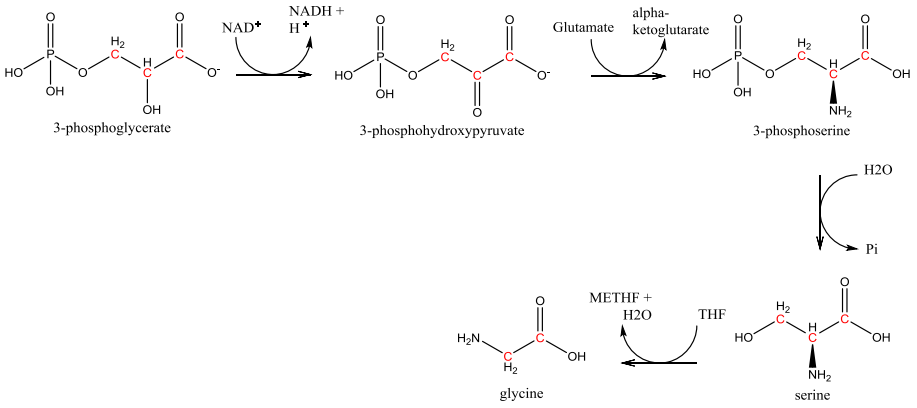

Fig. 6.6. Glycine biosynthesis. In the transition of serine into glycine, the labeled carbon bonded to hydroxyl group of glycine is transferred to THF.

6.4. [2,3,4-^{13}C] Arginine as precursor in CA biosynthesis

Amino acids can be experimentally quantified by a derivatization reaction with the reagent N-methyl-N-(*tert*-butyldimethylsilyl)trifluoroacetamide (MTBSTFA) (Stenerson, 2011). In this case, the active hydrogen of polar functional groups (–OH and –NH2) of amino acid are replaced by *tert*-butyl dimethysilyl (TBDMS) and derivatized amino acid are formed. Theoretically, expected mass fragments are present when a methyl or a *tert*-butyl group of TBDMS substituent is lost, as well as (TBDMS + CO) and (TBDMS + COO) yielding the fragment $(M-15)^+$, $(M-57)^+$, $(M-85)^+$ and $(M-159)^+$, respectively (Chaves Das Neves and Vasconcelos, 1987; Christensen and Nielsen, 1999; Dauner and Sauer, 2000; Fischer and Sauer, 2003). Knowing that CA, clavam-2-carboxylate and alanyclavam have a carboxyl group and/or an amino group in their structures, it is possible to

measure these compounds by GC-MS using MTBSTFA, when labeled substrates are used. Moreover, arginine with labeled carbons at positions 2, 3 and 4 on its structure, is proposed since none of the labeled carbons are lost after the fragmentation of the derivatized molecule, during the MS analysis. Therefore, one CA, one clavam-2-carboxylate and one alanyclavam isotopomers from [2,3,4-^{13}C] arginine are proposed to be attained (Fig. 6.7).

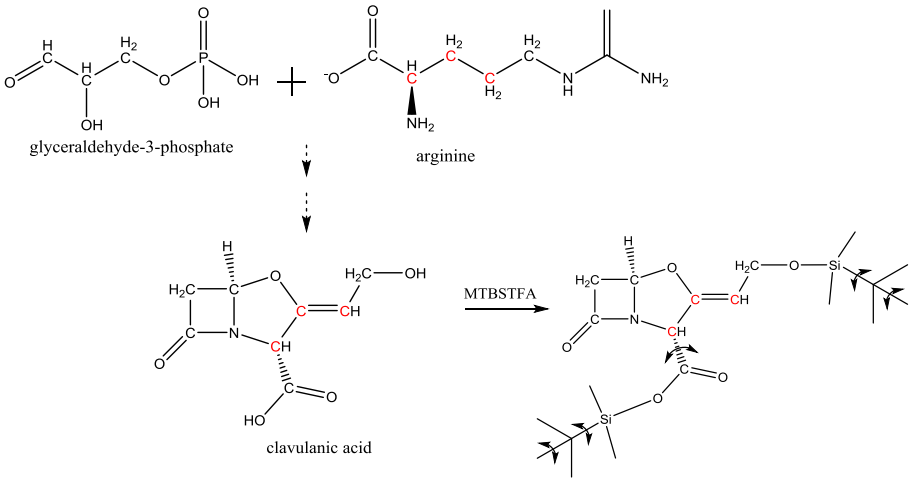

Fig. 6.7. CA isotopomers using [2,3,4-^{13}C] arginine. CA kept the labeled carbon atoms from arginine. The arrow representing the theoretical expected fragmentation sites: $(M-15)^+$, $(M-57)^+$, and $(M-159)^+$.

6.5. Conclusions

In this work, a complete theoretical overview of the entire labeling distribution on CA biosynthesis in *Sc* was presented. The theoretical approach allowed to obtain the incorporations of ^{13}C-labelling occurrences in CA, clavam-2-carboxylate and alanyclavam biosynthesis in *Sc,* using either [U-^{13}C] glycerol or [2,3,4-^{13}C] arginine, as labeled precursors (Table 6.1). Quantitative determination of CA, clavam-2-carboxylate and alanyclavam isotopomers are crucial for metabolic flux analysis studies, since they pose as constraints for the metabolic model.

Table 6.1. Complete overview of the entire labeling distribution in CA biosynthesis in *Sc.*

Compounds	The possible incorporations of ^{13}C-labelled	
	[U-^{13}C] glycerol	[2,3,4-^{13}C] arginine
Clavulanic acid	3	1
Clavam-2-carboxylate	3	1
Alanyclavam	7	1
Oxaloacetate, aspartate, threonine and asparagine	4	-
Alpha ketoglutarate glutamate, glutamine, ornithine and arginine	1	-

Nonetheless, the isotopomer distribution offered in this work should not be considered as a definite result, but rather as a first approximation that provides valuable insight about CA isotopomers that eventually could match future labeled studies in *Sc.*

Finally, the results shown in this work and the scarce information about CA production studies using labeled compound as substrate, create a propitious environment for future research involving metabolic models that takes into consideration the label distribution of ^{13}C-glycerol metabolism in *Sc.*

Acknowledgments

H.R.M. thanks the German Academic Exchange service (DAAD) for financial support. H.R.M. thanks Robert Spann and Sergej Trippel for the valuable discussion about ^{13}C incorporation in biological samples and its quantification, by GC-MS, in amino acids. H.R.M also thanks Prof. Felipe Otalvaro for all valuable suggestions.

6.6. Appendix

Appendix A

Isotopomer distributions of aspartate, threonine and asparagine, taking into consideration that they came from oxaloacetate. Note that four oxaloacetate isotopomers have been proposed but only one possibility was showed. Color Code: red C correspond to a labeled carbon atom.

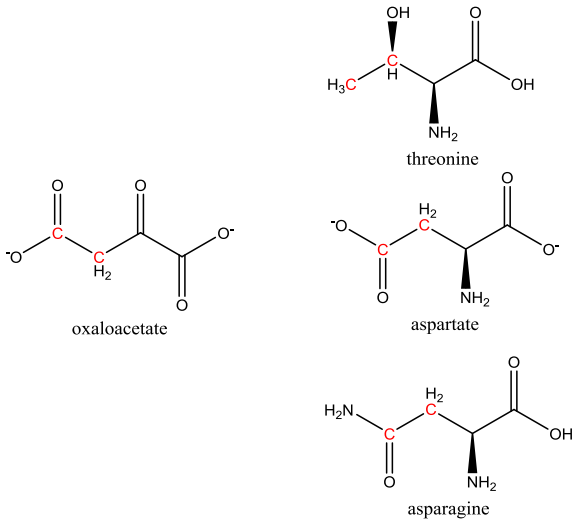

Appendix B

Isotopomer distribution of glutamate, glutamine, ornithine and arginine, taking into consideration that they were originated from alpha ketoglutarate. Color Code: red C correspond to a labeled carbon atom.

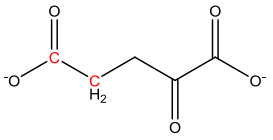

alpha ketoglutarate

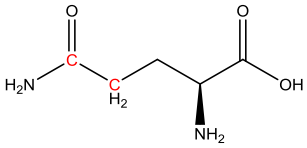

glutamine

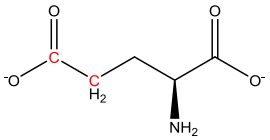

glutamate

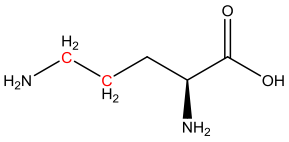

ornithine

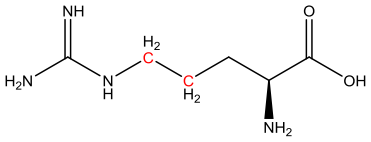

arginine

Appendix C

CA isotopomers based on the information of GAP and arginine isotopomers. Note that three CA isotopomers have been proposed, but only one option was showed. Color Code: red and blue C corresponds to a labeled carbon atom. A Similar procedure was done for clavam-2-carbolylate.

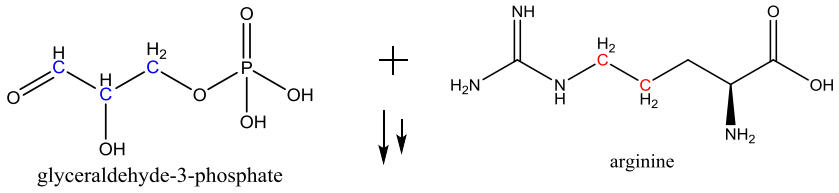

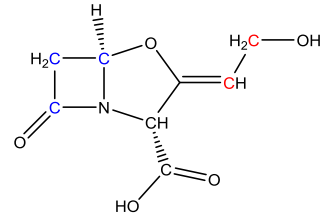

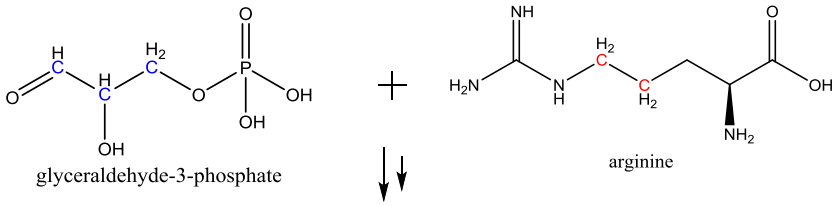

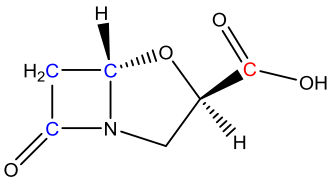

Appendix D

Alanyclavam isotopomers based on the information of GAP, arginine and glycine isotopomers, taking into consideration that glycine is coming from the glycolytic-intermediate 3-phosphoglycerate. Note that seven alanyclavam isotopomers were proposed but only one alternative was showed here. Color Code: red, blue and green C corresponds to a labeled Carbon atom.

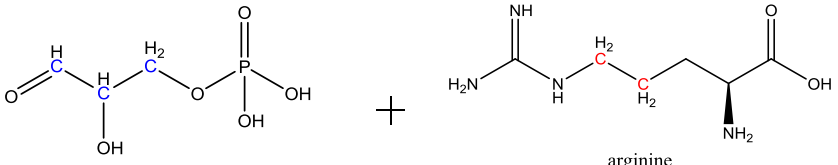

glyceraldehyde-3-phosphate

arginine

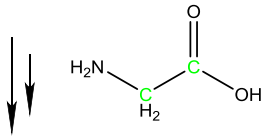

glycine

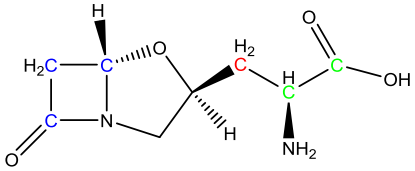

Alanyclavam

7. Conclusions and future work

In this work, a successful combination of constraint-based modeling and experimental testing was used as a strategy for improving the understanding of clavulanic acid (CA) biosynthesis in *Streptomyces clavuligerus* (*Sc*).

To generate more reliable data for CA quantification, an improved HPLC-DAD method, was successful developed and validated; the method involves a gradient elution approach for treating samples from fermentation broths of *Sc*. The proposed gradient elution configuration avoided overlapping of new peaks with the CA peak, a case commonly found in isocratic elution. This method can be used for fermentation samples taken from complex and chemically defined media

Second, a genome scale metabolic model for *Sc* was also successfully developed and validated. The model represents the complexity of *Sc* metabolism; it also can be used for *in silico* simulations of metabolic activities in phylogenetically related organisms. By using the model and a sensitivity analysis, a trade-off between succinate, acetate and oxaloacetate secretion, and CA production and biomass synthesis was identified. Moreover, a ratio lower than 2 between arginine synthesis (CA precursor – C5) and the net flux of glyceraldehyde-3-phosphate (GAP) (CA precursor – C3) was a necessary condition for CA biosynthesis.

The next step was to generate experimental data for CA production, by means of chemostat and accelerostat (A-stat) cultivations of *Sc*, under diverse environmental conditions. Here, a combined flux balance analysis and an A-stat approach showed a strong association between the accumulation of succinate, oxaloacetate, malate and acetate with CA production, thus confirming model predictions. To the best of our knowledge, this is the first work showing such an association in CA biosynthesis. Furthermore, the activation of glyoxylate pathway when the strain was exposed to glycerol and phosphate limitation was also found. The reaction catalyzed by PEP carboxylase was consistent with oxaloacetate accumulation and the highest CA production. Besides, the simultaneous CA and acetate production gave rise to propose

a reaction mechanism for the acetylation of N-glycyl-clavaminic acid to form N-acetyl-glycyl-clavaminic acid, which is a postulated new step in the clavam pathway. Further, a complete route for the inversion of the stereochemical configuration of (3S, 5S)-clavaminic acid into (3R, 5R)-clavulanic acid, including a novel alternative of double epimerization using proline racemase with non-rupture of the bicyclic β-lactam ring, was also proposed.

So as to complete this contribution to the understanding of *Sc* metabolism, further studies must be performed: to identify clavam intermediate in the later steps of the clavam pathway and to identify mechanisms involved in CA degradation. Recently, chromatographic methods that consider quantification of molecules with labeled carbon within their structures have been developed. Besides, there are various sequencing techniques such as pyrosequencing, 454, SOLID and Illumina, which are used for a wide range of applications (Faure and Joly, 2015; Liu et al., 2012; Luo et al., 2012). The availability of transcriptome data, obtained under diverse environmental condition, may further constraint genome scale metabolic models. However, studies for CA production using these techniques are still scarce.

For the purpose of refining the proposed model further studies on transcriptional analysis must be performed and used as constraints for metabolic modeling. Moreover, dynamic FBA approaches along with single or multiple isotope tracers for ^{13}C Metabolic Flux Analysis, either under steady state or unsteady-state conditions, would render complementary information for elucidating the complexity of *Sc* metabolism.

8. References

Alefounder, P.R., Baldwin, S. a, Perham, R.N., Short, N.J., 1989. Cloning, sequence analysis and over-expression of the gene for the class II fructose 1,6-bisphosphate aldolase of *Escherichia coli*. Biochem. J. 257, 529–34.

Antoniewicz, M.R., Kelleher, J.K., Stephanopoulos, G., 2006. Determination of confidence intervals of metabolic fluxes estimated from stable isotope measurements. Metab. Eng. 8, 324–37.

Arulanantham, H., Kershaw, N.J., Hewitson, K.S., Hughes, C.E., Thirkettle, J.E., Schofield, C.J., 2006. ORF17 from the clavulanic acid biosynthesis gene cluster catalyzes the ATP-dependent formation of N-glycyl-clavaminic acid. J. Biol. Chem. 281, 279–87.

Bachmann, B., Li, R., Townsend, C., 1998. βeta-lactam synthetase: a new biosynthetic enzyme. Proc. Natl. Acad. Sci. U. S. A. 95, 9082–6.

Baggaley, K.H., Brown, A.G., Schofield, C.J., 1997. Chemistry and biosynthesis of clavulanic acid and other clavams. Nat. Prod. Rep. 309–333.

Barry, J., 1997. Enzymes and symmetrical molecules. Trends Biochem. Sci. 22, 227–230.

Bascarán, V., Hardisson, C., Braña, a F., 1989. Regulation of nitrogen catabolic enzymes in *Streptomyces clavuligerus*. J. Gen. Microbiol. 135, 2465–74.

Bell, S.L., Palsson, B.Ø., 2005. Phenotype phase plane analysis using interior point methods. Comput. Chem. Eng. 29, 481–486.

Bellão, C., Antonio, T., Araujo, M.L.G.C., Badino, A.C., 2013. Production of clavulanic acid and cephamycin c by *Streptomyces clavuligerus* under different fed-batch conditions. Brazilian J. Chem. Eng. 30, 257–266. doi:10.1007/BF00327805

Berg, J.M., Tymoczko, J.L., Stryer, L., 2002. Biochemistry, Fifth. ed.

Bird, A.E., Bellis, J.M., Gasson, B.C., 1982. Spectrophotometric assay of clavulanic acid by reaction with lmidazole. Analyst 107, 1241–1245.

Brown, A.., Butterworth, D., Cole, M., Hanscomb, G., Hood, J.., Reading, C., Rolinson, G.., 1976. Naturally occurring β-lactamase inhibitors with actibacterial activity. J. Antibiot. (Tokyo). 29, 668–669.

Burgard, A.P., Pharkya, P., Maranas, C.D., 2003. OptKnock: A bilevel programming framework for identifying gene knockout strategies for microbial strain optimization. Biotechnol. Bioeng. 84, 647–657.

Bushell, M.E., Kirk, S., Zhao, H.-J., Avignone-Rossa, C.A., 2006. Manipulation of the physiology of clavulanic acid biosynthesis with the aid of metabolic flux analysis. Enzyme Microb. Technol. 39, 149–157.

Bycroft, B.W., Pensore, A., Gillett, J., Elson, S.W., 1988. The incorporation of DL-[4-$^{2}H_2$, 5-^{13}C] ornithine into clavulanic acid and N-acetylgiycylclavaminic acid. J. Chem. Soc. Chem. Commun. 980–981.

Cardinale, G.L., Abeles, R.H., 1968. Purification and mechanism of action of proline Racemase. Biochemistry 7, 3970–3978.

Cardona, W., Guerra, D., Restrepo, A., 2013. Reactivity of δ-substituted α,β-unsaturated cyclic lactones with antileishmanial activity. Mol. Simul. 40, 477–484.

Chan, M., Sim, T., 1998. Malate synthase from *Streptomyces clavuligerus* NRRL3585 : cloning, molecular characterization and its control by acetate. Microbiology 144, 3229–3237.

Chaves Das Neves, H.J., Vasconcelos, A.M.P., 1987. Capillary gas chromatography of amino acids, including asparagine and glutamine: sensitive gas chromatographic-mass spectrometric and selected ion monitoring gas chromatographic-mass spectrometric detection of the N,O(s)-*tert*.-butyldimethylsilyl derivatives. J. chomatography 392, 249–258.

Chen, K.-C., Lin, Y.-H., Wu, J.-Y., Hwang, S.-C.J., 2003. Enhancement of clavulanic acid production in *Streptomyces clavuligerus* with ornithine feeding. Enzyme Microb. Technol. 32, 152–156.

Christensen, B., Nielsen, J., 1999. Isotopomer analysis using GC-MS. Metab. Eng. 1, 282–90.

Colombié, V., Bideaux, C., Goma, G., Uribelarrea, J.L., 2005. Effects of glucose limitation on biomass and spiramycin production by *Streptomyces ambofaciens*. Bioprocess Biosyst. Eng. 28, 55–61.

Cramer, C.J., 2004. Essentials of computational chemistry, Second. ed. Wiley.

Dauner, M., Sauer, U., 2000. GC-MS analysis of amino acids rapidly provides rich information for isotopomer balancing. Biotechnol. Prog. 16, 642–9.

Deckwer, W.-D., Mayer, A.F., 1996. Simultaneous production and decomposition of clavulanic acid during *Streptomyces clavuligerus* cultivations. Appl. Microbiol. Biotechnol. 45, 41–46.

Dela Fuente, J., Martin, J.F., Liras, P., 1996. New type of hexameric ornithine carbamoyltransferase with arginase activity in the cephamycin producers *Streptomyces clavuligerus* and *Nocardia lactamdurans*. Biochem. J. 179, 173–179.

Dubala, A., Nagarajan, J.S.K., Vimal, C.S., George, R., 2015. Simultaneous liquid chromatography-mass spectrometry quantification of cefixime and clavulanic acid in human plasma. J. Chromatogr. Sci. 53, 694–701.

Dubala, A., Nagarajan, J.S.K., Vimal, C.S., George, R., 2013. Simultaneous quantification of cefpodoxime proxetil and clavulanic acid in human plasma by LC-MS using solid phase extraction with application to pharmacokinetic studies. J. Chromatogr. B. Analyt. Technol. Biomed. Life Sci. 921-922, 49–55.

Eckers, C., Chalkleya, R., Haskinsa, N., Edwardsb, J., Elsonc, S., 1996. Investigation into the use of derivatization with lmidazole for the detection of clavam compounds by liquid chromatography-mass spectrometry. Anal. Commun. 33, 215–218.

Edwards, J.S., Ramakrishna, R., Palsson, B.O., 2002. Characterizing the metabolic phenotype: A phenotype phase plane analysis. Biotechnol. Bioeng. 77, 27–36.

Elander, R.P., 2003. Industrial production of β-lactam antibiotics. Appl. Microbiol. Biotechnol. 61, 385–392.

Elson, S., Gillett, J., Nicholson, N.H., Tyler, J.W., 1988. N-Acyl derivatives of clavaminic acid produced by a mutant of *Streptomyces clavuligerus*. J. Am. Chem. Soc. Chem. communitations 979–980.

Elson, S.W., 1988. The biosynthesis of clavulanic acid, in: recent advances in the chemistry of β-lactam antibiotics: The proceedings of the fourth international symposium, organised by the fine chemicals and medicinals group of the industrial division of the royal society of chemistry. p. 303.

Elson, S.W., Oliver, R.S., 1978. Studies on the biosynthesis of clavulanic acid. I. Incorporation of ^{13}C-labelled precursors. J. Antibiot. (Tokyo). 31, 586–592.

Elson, S.W., Oliver, R.S., Bycroft, B.W., Faruk., E.A., 1982. Studies on the biosynthesis of clavulanic acid. III. Incorporation of DL-(3, 4-13C2) glutamic acid. J. Antibiot.

Enfors, S., 2011. Fermentation Process Engineering.

Faure, D., Joly, D., 2015. Next-generation sequencing as a powerful motor for advances in the biological and environmental sciences. Genetica 143, 129–132.

Fawaz, M., Topper, M., Firestine, S., 2011. The ATP-Grasp Enzymes. Bioorg. Chem. 39, 185–191.

Fischer, E., Sauer, U., 2003. Metabolic flux profiling of *Escherichia coli* mutants in central carbon metabolism using GC-MS. Eur. J. Biochem. 270, 880–891.

Foroutan, S.M., Zarghi, A., Shafaati, A., Khoddam, A., Movahed, H., 2007. Simultaneous determination of amoxicillin and clavulanic acid in human plasma by isocratic reversed-phase HPLC using UV detection. J. Pharm. Biomed. Anal. 45, 531–534.

Foulstone, M., Reading, C., 1982. Assay of amoxicillin and clavulanic acid, the components of Augmentin, in biological fluids with high-performance liquid chromatography. Antimicrob. Agents Chemother. 22, 753–762.

Fulston, M., Davison, M., Elson, S.W., Tyler, J.W., Woroniecki, S.R., 2001. Clavulanic acid biosynthesis; the final steps. J. Chem. Soc. Perkin Trans. 1 1, 1122–1130.

Garcia Sanchez, C., Vargas Garcia, C., Torres, R., 2012. Predictive potential of flux balance analysis of *Saccharomyces cerevisiae* using as optimization function combinations of cell compartmental objectives. PLoS One 7, e43006.

Gianchandani, E.P., Chavali, A.K., Papin, J. a, 2010. The application of flux balance analysis in systems biology. Wiley Interdiscip. Rev. Syst. Biol. Med. 2, 372–82.

Giraudeau, P., Massou, S., Robin, Y., Cahoreau, E., Portais, J.C., Akoka, S., 2011. Ultrafast quantitative 2D NMR: an efficient tool for the measurement of specific isotopic enrichments in complex biological mixtures. Anal Chem 83, 3112–3119.

GlaxoSmithKline, 2015. GSK announces first quarter 2015 results, sets out prospects for newly shaped Group and expectations for improvements in performance 2016-2020. Press release.

Gonzalez, C., Restrepo, A., Márquez, M., Wiberg, K., 1996. Ab initio study of the stability of the ylide-like intermediate methyleneoxonium in the reaction between singlet methylene and water. J. Phys. Chem. A 118, 5408–5411.

Grafahrend-Belau, E., Schreiber, F., Koschützki, D., Junker, B.H., 2009. Flux balance analysis of barley seeds: a computational approach to study systemic properties of central metabolism. Plant Physiol. 149, 585–98.

Haines, R.J., Pendleton, L.C., Eichler, D.C., 2011. Argininosuccinate synthase: at the center of arginine metabolism. Int. J. Biochem. Mol. Biol. 2, 8–23.

Hamed, R.B., Gomez-Castellanos, J.R., Henry, L., Ducho, C., McDonough, M.A., Schofield, C.J., 2013. The enzymes of β-lactam biosynthesis. Nat. Prod. Rep. 30, 21–107.

Hase, W., Francisco, J., Steinfeld, J., 1999. Chemical kinetics and dynamics, Second. ed. Prentice Hall.

Healy, V.L., Mullins, L.S., Li, X., Hall, S.E., Raushel, F.M., Walsh, C.T., 2000. D-Ala-D-X ligases: evaluation of D-alanyl phosphate intermediate by MIX, PIX and rapid quench studies. Chem. Biol. 7, 505–14.

Hodgson, D. a, 2000. Primary metabolism and its control in streptomycetes: a most unusual group of bacteria. Adv. Microb. Physiol. 42, 47–238.

Hoizey, G., Lamiable, D., Frances, C., Trenque, T., Kaltenbach, M., Denis, J., 2002. Simultaneous determination of amoxicillin and clavulanic acid in human plasma by HPLC with UV detection. J. Pharm. Biomed. Anal. 30, 661–666.

Holzhütter, H.G., 2004. The principle of flux minimization and its application to estimate stationary fluxes in metabolic networks. Eur. J. Biochem. 271, 2905–2922.

ICH, 2005. ICH harmonised tripartite guideline validation of analytical procedures : 1994.

Iqbal, A., Arunlanantham, H., Brown, T., Chowdhury, R., Clifton, I.J., Kershaw, N.J., Hewitson, K.S., McDonough, M.A., Schofield, C.J., 2010. Crystallographic and mass spectrometric analyses of a tandem GNAT protein from the clavulanic acid biosynthesis pathway. Proteins 78, 1398–407.

Ives, P.R., Bushell, M.E., 1997. Manipulation of the physiology of clavulanic acid production in *Streptomyces clavuligerus*. Microbiology 143, 3573–9.

Jaramillo, C., Guerra, D., Moreno, L.F., Restrepo, A., 2010. Competitive substituent effects on the reactivity of aromatic rings. J. Phys. Chem. A 114, 6033–6038.

Jensen, S.E., Paradkar, A.S., Mosher, R.H., Anders, C., Beatty, P.H., Brumlik, M.J., Griffin, A., Barton, B., 2004. Five additional genes are involved in clavulanic acid biosynthesis in *Streptomyces clavuligerus*. Antimicrob. Agents Chemother. 48, 192–202.

Junne, S., Klingner, A., Kabisch, J., Schweder, T., Neubauer, P., 2011. A two-compartment bioreactor system made of commercial parts for bioprocess scale-down studies: impact of oscillations on *Bacillus subtilis* fed-batch cultivations. Biotechnol. J. 6, 1009–17.

Khaleeli, N., Li, R., Townsend, C. a., 1999. Origin of the β-lactam carbons in clavulanic acid from an unusual thiamine pyrophosphate-mediated reaction. J. Am. Chem. Soc. 121, 9223–9224.

Kirk, S., Avignone-rossa, C.A., Bushell, M.E., 2000. Growth limiting substrate affects antibiotic production and associated metabolic fluxes in *Streptomyces clavuligerus*. Biotechnol. Lett. 22, 1803–1809.

Krömer, J., Quek, L., Nielsen, L., 2009. ^{13}C-fluxomics : a tool for measuring metabolic phenotypes. Aust. Biochem. 40, 17–20.

Leach, R., 2001. Molecular Modelling. Principles and Applications.

Li, R., Khaleeli, N., Townsend, C. a, 2000. Expansion of the clavulanic acid gene cluster: identification and in vivo functional analysis of three new genes required for biosynthesis of clavulanic acid by *Streptomyces clavuligerus*. J. Bacteriol. 182, 4087–95.

Li, R., Townsend, C. a, 2006. Rational strain improvement for enhanced clavulanic acid production by genetic engineering of the glycolytic pathway in *Streptomyces clavuligerus*. Metab. Eng. 8, 240–52.

Liras, P., Martín, J.F., 2005. Assay methods for detection and quantification of antimicrobial metabolites produced by *Streptomyces clavuligerus*. Method Biotechnol. 18, 149–163.

Liu, L., Li, Y., Li, S., Hu, N., He, Y., Pong, R., Lin, D., Lu, L., Law, M., 2012. Comparison of next-generation sequencing systems. J. Biomed. Biotechnol. 2012.

Llarrull, L.I., Testero, S. a, Fisher, J.F., Mobashery, S., 2010. The future of the β-lactams. Curr. Opin. Microbiol. 13, 551–557.

Luo, C., Tsementzi, D., Kyrpides, N., Read, T., Konstantinidis, K.T., 2012. Direct comparisons of Illumina vs. Roche 454 sequencing technologies on the same microbial community DNA sample. PLoS One 7.

Malmberg, L.H., Hu, W.S., 1991. Kinetic analysis of cephalosporin biosynthesis in *Streptomyces clavuligerus*. Biotechnol. Bioeng. 38, 941–947.

Martín, J., Méndez, R., 1988. High-performance liquid chromatographic determination of clavulanic acid in human serum and urine using a pre-column reaction with 1, 2, 4-triazole. J. Liq. Chromatogr. 11, 1697–1705.

Medema, M.H., Trefzer, A., Kovalchuk, A., van den Berg, M., Müller, U., Heijne, W., Wu, L., Alam, M.T., Ronning, C.M., Nierman, W.C., Bovenberg, R. a L., Breitling, R., Takano, E., 2010. The sequence of a 1.8-mb bacterial linear plasmid reveals a rich evolutionary reservoir of secondary metabolic pathways. Genome Biol. Evol. 2, 212–24.

Mellado, E., Lorenzana, L.M., Rodríguez-Sáiz, M., Díez, B., Liras, P., Barredo, J.L., 2002. The clavulanic acid biosynthetic cluster of *Streptomyces clavuligerus*: genetic organization of the region upstream of the car gene. Microbiology 148, 1427–38.

Meng, F., Chen, X., Zeng, Y., Zhong, D., 2005. Sensitive liquid chromatography-tandem mass spectrometry method for the determination of cefixime in human plasma: application to a pharmacokinetic study. J. Chromatogr. B. Analyt. Technol. Biomed. Life Sci. 819, 277–282.

Mullins, L.S., Lusty, C.J., Raushel, F.M., 1991. Alterations in the energetics of the carbamoyl phosphate synthetase reaction by site-directed modification of the essential sulfhydryl group. J. Biol. Chem. 266, 8236–40.

Mullins, L.S., Zawadzkeg, E., Walsh, T., Raushelall, M., 1990. Kinetic evidence for the formation of d-alanyl phosphate in the mechanism of D-Alanyl-D-alanine ligase*. J. Biol. Chem. 265, 8993–8998.

Neto, A.B., Hirata, D.B., Filho, L.C.M.C., Bellão, C., Júnior, A.C.B., Hokka, C.O., 2005. A study on clavulanic acid production by *Streptomyces clavuligerus* in batch , fed-batch and continuous processeS. Brazilian J. Chem. Eng. 22, 557–563.

Ogston, A., 1948. Interpretation of experiment on metabolic processes, using isotopic tracer elements. Nature 162, 963–963.

Orrego, J., Cano, H., Restrepo, A., 2009. Quantum mechanical study of the gas-phase reactions between a series of substituted singlet carbenes and water. J. Phys. Chem. A 113, 6517–6523.

Ozcengiz, G., Demain, A.L., 2013. Recent advances in the biosynthesis of penicillins, cephalosporins and clavams and its regulation. Biotechnol. Adv. 31, 287–311.

Palsson, B., 2005. Systems Biology: Properties of reconstructed networks. cambridge University Press.

Paradkar, A., 2013. Clavulanic acid production by *Streptomyces clavuligerus*: biogenesis, regulation and strain improvement. J. Antibiot. (Tokyo). 66, 411–20.

Potter, V.R., Heidelberger, C., 1949. Biosynthesis of “asymmetry” citric acid: a substantiation of the ogston concept. Nature 164, 180–180.

Ramirez-Malule, H., Junne, S., López, C., Zapata, J., Sáez, A., Neubauer, P., Rios-Estepa, R., 2016. An improved HPLC-DAD method for clavulanic acid quantification in fermentation broths of *Streptomyces clavuligerus*. J. Pharm. Biomed. Anal. 120, 241–247.

Reyns, T., Baere, S. De, Croubels, S., Backer, P. De, 2006. Determination of clavulanic acid in calf plasma by liquid chromatography tandem mass spectrometry. J. mass Spectrom. 41, 1414–1420.

Reznik, E., Mehta, P., Segrè, D., 2013. Flux imbalance analysis and the sensitivity of cellular growth to changes in metabolite pools. PLoS Comput. Biol. 9, e1003195.

Rosa, J.C., Baptista Neto, A., Hokka, C.O., Badino, A.C., 2005. Influence of dissolved oxygen and shear conditions on clavulanic acid production by *Streptomyces clavuligerus*. Bioprocess Biosyst. Eng. 27, 99–104.

Roubos, J.A., 2002. Bioprocesses modeling and optimization fed-batch clavulanic acid production by *Streptomyces clavuligerus*. Technische Universiteit Delft.

Roubos, J.A., Krabben, P., Laat, W.T.A.M. De, Heijnen, J.J., 2002. Clavulanic acid degradation in *Streptomyces clavuligerus* fed-batch cultivations. Biotechnol. Prog. 18, 451–457.

Rudnickt, G., Abeles, R.H., 1975. Reaction mechanism and structure of the active site of proline racemase. Biochemistry 14, 4515–4522.

Sánchez, C., Quintero, J.C., Ochoa, S., 2015. Flux balance analysis in the production of clavulanic acid by *Streptomyces clavuligerus*. Biotechnol. Prog. 31, 1226–1236.

Saudagar, P.S., Singhal, R.S., 2007. Optimization of nutritional requirements and feeding strategies for clavulanic acid production by *Streptomyces clavuligerus*. Bioresour. Technol. 98, 2010–7. doi:10.1016/j.biortech.2006.08.003

Saudagar, P.S., Survase, S.A., Singhal, R.S., 2008. Clavulanic acid: A review. Biotechnol. Adv. 26, 335–351.

Schellenberger, J., Que, R., Fleming, R.M.T., Thiele, I., Orth, J.D., Feist, A.M., Zielinski, D.C., Bordbar, A., Lewis, N.E., Rahmanian, S., Kang, J., Hyduke, D.R., Palsson, B.Ø., 2011. Quantitative prediction of cellular metabolism with constraint-based models: the COBRA Toolbox v2.0. Nat. Protoc. 6, 1290–307.

Schellinger, A.P., Carr, P.W., 2006. Isocratic and gradient elution chromatography: a comparison in terms of speed, retention reproducibility and quantitation. J. Chromatogr. A 1109, 253–266.

Schuetz, R., Kuepfer, L., Sauer, U., 2007. Systematic evaluation of objective functions for predicting intracellular fluxes in *Escherichia coli*. Mol. Syst. Biol. 3, 119.

Shah, A.J., Adlard, M.W., Stride, J.D., 1990. A sensitive assay for clavulanic acid and sulbactam in biological fluids by high-performance liquid chromatography and precolumn derivatization. J. Pharm. Biomed. Anal. 8, 437–443.

Soh, B.S., Loke, P., Sim, T., 2001. Cloning, heterologous expression and purification of an isocitrate lyase from *Streptomyces clavuligerus* NRRL 3585. Biochim. Biophys. Acta 1522, 112–117.

Stenerson, K., 2011. GC-MS analysis of amino acids. Sigma Aldrich report. US 25, 1–3.

Stephanopoulos, G., Aristidou, A., Nielsen, J., 1998. Metabolic engineering. Principles and methodologies. Academic press.

Stewart, J., 1991. Optimization of parameters for semiempirical methods. III Extension of PM3 to Be, Mg, Zn, Ga, Ge, As, Se, Cd, In, Sn, Sb, Te, Hg, Tl, Pb, and Bi. J. Comput. Chem. 12, 320–341.

Stewart, J., 1989a. Optimization of parameters for semiempirical methods I. Method. J. Comput. Chem. 10, 209–220.

Stewart, J., 1989b. Optimization of Parameters for Semiempirical Methods 2. Applications. J. Comput. Chem. 10, 221–264.

Stirling, I., Elson, S.W., 1979. Studies on the biosynthesis of clavulanic acid. II. Chemical degradations of ^{14}C-labelled clavulanic acid. J. Antibiot.

Szabo, A., Ostlund, N., 1989. Modern quantum chemistry. McGraw–Hill.

Teodoro, J.C., Araujo, M.L.G.C., Hokka, C.O., Badino, A.C., 2010. Influence of glycerol and ornithine feeding on clavulanic acid production by *Streptomyces clavuligerus*. Brazilian J. Chem. Eng. 27, 499–506.

Townsend, C. a, 2002. New reactions in clavulanic acid biosynthesis. Curr. Opin. Chem. Biol. 6, 583–9.

Townsend, C. a., Krol, W.J., 1988. The role of molecular oxygen in clavulanic acid biosynthesis: evidence for a bacterial oxidative deamination. J. Am. Chem. Soc. Chem. communitations 1234–1236.

Tsou, T., Wu, J., Young, C., Wang, T., 1997. Simultaneous determination of amoxycillin and clavulanic acid in pharmaceutical products by HPLC with β-cyclodextrin stationary phase. J. Pharm. Biomed. Anal. 15, 1197–1205.

Valegård, K., Iqbal, A., Kershaw, N.J., Ivison, D., Généreux, C., Dubus, A., Blikstad, C., Demetriades, M., Hopkinson, R.J., Lloyd, A.J., Roper, D.I., Schofield, C.J., Andersson, I., McDonough, M.A., 2013. Structural and mechanistic studies of the orf12 gene product from the clavulanic acid biosynthesis pathway. Acta Crystallogr. Sect. D Biol. Crystallogr. 69, 1567–1579.

Valentine, B.P., Bailey, C.R., Doherty, A., Morris, J., Elson, S.W., Baggaley, K.H., Nicholson, N.H., 1993. Evidence that arginine is a later metabolic intermediate than ornithine in the biosynthesis of clavulanic acid by *Streptomyces clavuligerus*. J. Chem. Soc. Chem. Commun. 1210–1211.

Van Boeckel, T.P., Gandra, S., Ashok, A., Caudron, Q., Grenfell, B.T., Levin, S.A., Laxminarayan, R., 2014. Global antibiotic consumption 2000 to 2010: an analysis of national pharmaceutical sales data. Lancet Infect. Dis. 14, 742–750.

Villadsen, J., Nielsen, J., Lidén, G., 2011. Bioreaction engineering principles.

Viollier, P.H., Minas, W., Dale, G.E., Folcher, M., Thompson, C.J., 2001. Role of acid metabolism in *Streptomyces coelicolor* morphological differentiation and antibiotic biosynthesis. J. Bacteriol. 183, 3184–3192.

Wiechert, W., 2001. ^{13}C metabolic flux analysis. Metab. Eng. 3, 195–206.

World Health Organization, 2015. WHO. Antimicrobial resistance factsheet [www document]. URL http://www.who.int/mediacentre/factsheets/fs194/en/ (accessed 11.14.15).

Wu, T.K., Busby, R.W., Houston, T.A., Mcilwaine, D.B., Egan, L.A., Townsend, C.A., Wu, T., Busby, R.W., Houston, T.A., Ilwaine, D.B.M.C., Egan, L.A., Townsend, C.A., 1995. Identification, cloning, sequencing, and overexpression of the gene encoding proclavaminate amidino hydrolase and characterization of protein function in clavulanic acid biosynthesis. J. Bacteriol. 177, 3714–3720.

Yoon, K.-H., Lee, S.-Y., Kim, W., Park, J.-S., Kim, H.-J., 2004. Simultaneous determination of amoxicillin and clavulanic acid in human plasma by HPLC-ESI mass spectrometry. J. Chromatogr. B. Analyt. Technol. Biomed. Life Sci. 813, 121–127.

Yousofshahi, M., Ullah, E., Stern, R., Hassoun, S., 2013. MC^3: a steady-state model and constraint consistency checker for biochemical networks. BMC Syst. Biol. 7, 129.

Yuan, Y., Hoon Yang, T., Heinzle, E., 2010. ^{13}C metabolic flux analysis for larger scale cultivation using gas chromatography-combustion-isotope ratio mass spectrometry. Metab. Eng. 12, 392–400.

Zelyas, N.J., Cai, H., Kwong, T., Jensen, S.E., 2008. Alanylclavam biosynthetic genes are clustered together with one group of clavulanic acid biosynthetic genes in *Streptomyces clavuligerus*. J. Bacteriol. 190, 7957–65.

Zhang, Z., Ren, J.S., Harlos, K., McKinnon, C.H., Clifton, I.J., Schofield, C.J., 2002. Crystal structure of a clavaminate synthase-Fe(II)-2-oxoglutarate-substrate-NO complex: evidence for metal centered rearrangements. FEBS Lett. 517, 7–12.